

**NUMERICAL SIMULATION OF FLUID
FLOW PAST SELF-PROPELLED BODY**

Surattana Sungnul

**A Thesis Submitted in Partial Fulfillment of the Requirements
for the Degree of Doctor of Philosophy in Applied Mathematics**

Suranaree University of Technology

Academic Year 2005

ISBN 974-533-554-1

การจำลองเชิงตัวเลขของของไหลที่ไหลผ่านวัตถุที่
เคลื่อนที่ได้ด้วยตัวเอง

นางสุรัตนา สังข์หนู

วิทยานิพนธ์นี้เป็นส่วนหนึ่งของการศึกษาตามหลักสูตรปริญญาวิทยาศาสตรดุษฎีบัณฑิต

สาขาวิชาคณิตศาสตร์ประยุกต์

มหาวิทยาลัยเทคโนโลยีสุรนารี

ปีการศึกษา 2548

ISBN 974-533-554-1

NUMERICAL SIMULATION OF FLUID FLOW PAST SELF-PROPELLED BODY


Suranaree University of Technology has approved this thesis submitted in partial fulfillment of the requirements for the Degree of Doctor of Philosophy.

Thesis Examining Committee



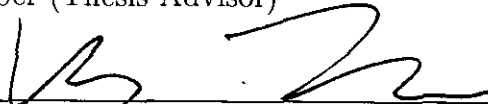
(Assoc. Prof. Dr. Prapasri Asawakun)

Chairperson



(Assoc. Prof. Dr. Nikolay Moshkin)

Member (Thesis Advisor)



(Dr. Vejapong Juttijudata)

Member



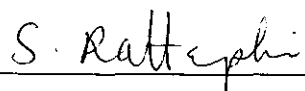
(Prof. Dr. Sergey Meleshko)

Member



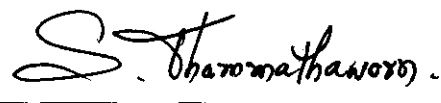
(Asst. Prof. Dr. Ekachai Juntasaro)

Member



(Assoc. Prof. Dr. Saowanee Rattanaphani)

Vice Rector for Academic Affairs



(Assoc. Prof. Dr. Sompong Thammathaworn)

Dean of Institute of Science

สุรัตนา สังข์หนูน : การจำลองเชิงตัวเลขของของไหลที่ไหลผ่านวัตถุที่เคลื่อนที่ได้ด้วยตัวเอง (NUMERICAL SIMULATION OF FLUID FLOW PAST SELF-PROPELLED BODY) อาจารย์ที่ปรึกษา: รองศาสตราจารย์ ดร.นิโคลัน มอสกิน, 100 หน้า. ISBN 974-533-554-1

งานวิจัยนี้ศึกษาการเคลื่อนที่ของของไหลที่ไหลผ่านวัตถุทรงกระบอกแข็งเกร็ง 2 อัน ซึ่งมีรัศมีเท่ากัน และหมุนในทิศตรงกันข้าม ด้วยอัตราเร็วเชิงมุมเท่ากัน โดยทำการศึกษาการเคลื่อนที่ทั้งแบบที่วัตถุสามารถเคลื่อนที่ได้ด้วยตัวเองโดยไม่อาศัยแรงจากภายนอกในการขับเคลื่อน และวัตถุที่ไม่สามารถเคลื่อนที่ได้ด้วยตัวเองโดยอาศัยแรงจากภายนอกในการขับเคลื่อน พารามิเตอร์ที่มีผลต่อการเคลื่อนที่ที่ศึกษาในงานวิจัยนี้ประกอบไปด้วยเลขเรย์โนลด์ ระยะห่างระหว่างทรงกระบอก และ อัตราการหมุนของทรงกระบอก ช่วงของพารามิเตอร์ที่ทำการศึกษาคือ $5 \leq Re \leq 40$, $0.5 \leq g \leq 2.5$ และ $0 \leq \alpha \leq 2.5$ กระบวนการวิจัยเริ่มจากสร้างแบบจำลองทางคณิตศาสตร์เพื่ออธิบายการเคลื่อนที่ หลังจากนั้นแปลงระบบพิกัดฉากเป็นระบบพิกัดทรงกระบอกสองขั้ว วิธีการคำนวณเชิงตัวเลขใช้วิธีผลต่างอันดับในการหาคำตอบประมาณด้วยหลักการของวิธีการแยก สุดท้ายทำการเปรียบเทียบผลลัพธ์เชิงพลศาสตร์ระหว่างการไหลผ่านวัตถุที่เคลื่อนที่ได้ด้วยตัวเอง กับวัตถุที่ไม่สามารถเคลื่อนที่ได้ด้วยตัวเอง เช่น สัมประสิทธิ์แรงต้าน และสัมประสิทธิ์แรงยก

สาขาวิชาคณิตศาสตร์
ปีการศึกษา 2548

ลายมือชื่อนักศึกษา Surattana Sangnun

ลายมือชื่ออาจารย์ที่ปรึกษา [Signature]

SURATTANA SUNGNUL : NUMERICAL SIMULATION OF FLUID
FLOW PAST SELF-PROPELLED BODY. THESIS ADVISOR : ASSOC.
PROF. NIKOLAY MOSHKIN, Ph.D. 100 PP. ISBN 974-533-554-1


NUMERICAL SIMULATION/ FLUID FLOW/ VISCOUS INCOMPRESSIBLE
FLUID SELF-PROPELLED BODY, FINITE-DIFFERENCE.

In this research, we interested in the self-propulsion of a rigid body. The shape of the body is constant during the motion, and the thrust is produced because of the motion of the body boundary. The combined body which consists of two rotating circular cylinders of equal radii is an example where the self-propelled motion is due to a non-zero velocity of the boundary. We study the self-motion of rotating cylinders and also flow over two towed rotating cylinders. Different rotation of cylinders can be considered as a propulsion device for controlling the motion of the body. In the present study, we have numerically investigated steady viscous incompressible fluid flow over two rotating circular cylinders in a side-by-side arrangement at moderate Reynolds numbers, $1 \leq Re \leq 40$, with gap spacing between cylinder surfaces, $0.5D \leq g \leq 14D$, and the rate of rotation, $0 \leq \alpha \leq 2.5$, ($Re = DU_\infty/\nu$, $\alpha = \omega D/2U_\infty$, D is diameter of cylinder, ω is angular velocity of cylinder, U_∞ is velocity of stream flow, ν is the coefficient of kinematic viscosity). First, we construct a mathematical formulation to describe the self-propelled motion and transform the problem to cylindrical bipolar coordinate. Secondly, we derive a finite difference scheme for the approximate solution which is based on the splitting method. Finally, we compare the basic hydrodynamic characteristics of flow past towed and self-propelled two rotating circular cylinders.

School of Mathematics

Academic Year 2005

Student's Signature Surattana Sungnul

Advisor's Signature 

ACKNOWLEDGEMENTS

I am profoundly grateful to my thesis advisor Assoc. Prof. Dr. Nikolay Moshkin for his support, patient help and offering many useful suggestions.

I would like to acknowledge all the lecturers who taught and helped me during the course of studies at Suranaree University of Technology. They are Assoc. Prof. Dr. Prapasri Asawakun, Prof. Dr. Sergey Meleshko, Asst. Prof. Dr. Eckart Schulz and Prof. Dr. Boris Kvasov.

I also would like to express my appreciation to Asst. Prof. Dr. Ekachai Juntasaro, Dr. Vejapong Juttijudata and Dr. Elvin James Moore for their valuable discussions and comments.

I would like to express my appreciation to the following for their sincere help. These include Dr. Jessada Tanthanuch, Dr. Kanthima Thailert, Mr. Boonlert Srihirun, Miss Wannapa Ruangthanakorn and all of my friends at Suranaree University of Technology.

I acknowledge the financial support of the Ministry of University Affairs of Thailand (MUA). I am indebted to King Mongkut's Institute of Technology North Bangkok for grants to support my studies throughout.

Finally, I am deeply grateful to my parents, and my husband, Jirarath for support, understanding encouragement, and love.

Surattana Sungnul

CONTENTS

	Page
ABSTRACT IN THAI	I
ABSTRACT IN ENGLISH	II
ACKNOWLEDGEMENTS	III
CONTENTS	IV
LIST OF TABLES	V
LIST OF FIGURES	VI
 CHAPTER	
I INTRODUCTION	1
1.1 General Context	1
1.2 Governing Equations of Continuum Motion	3
1.3 Previous Research	6
1.4 Objectives and Overview of the Thesis	9
II MATHEMATICAL FORMULATION OF PROBLEM	11
2.1 Motion of Rigid Body in a Viscous Incompressible Fluid	11
2.2 Viscous Incompressible Fluid Flow Past Two Circular Cylinders.	14
III NUMERICAL METHODS	18
3.1 Discretization of the Solution Domain	18
3.2 Discretization of the Governing Equation	19
3.2.1 The Projection Method in Time	20
3.2.2 Discretization in Space	22
3.3 Force Computation	31

CONTENTS (Continued)

	Page
IV VALIDATION OF NUMERICAL ALGORITHM	33
4.1 Flow Past Two Nonrotating Circular Cylinders (Large Gap Spacing)	33
4.2 Flow Past Two Rotating Circular Cylinders (Large Gap Spacing)	39
4.3 Flow Past Two Nonrotating Circular Cylinders (Small Gap Spacing, $g = 1$)	42
4.4 Results of Validation	45
V SIMULATION RESULTS	46
5.1 Wake Patterns Depending on the Reynolds Number and Rate of Rotation	46
5.2 Wake Pattern Depending on Gap Spacing and Rate of Rotation .	54
VI CONCLUSIONS	68
REFERENCES	71
APPENDICES	
APPENDIX A TRANSFORMATION OF GOVERNING EQUATIONS TO CYLINDRICAL BIPOLAR COORDINATES	78
A.1 Definitions of Main Tensor Operations in the Curvilinear Coordinate System	78
A.2 The Cylindrical Bipolar Coordinate System . .	82
APPENDIX B THE METHOD OF STABILIZING CORRECTIONS	89
B.1 The Elimination Method for Three-Point Equations (Samarskij (1989))	91
B.2 The Cyclic Elimination Method (Samarskij (1989))	94

CONTENTS (Continued)

	Page
CURRICULUM VITAE	99

LIST OF TABLES

Table		Page
4.1	Length of wake bubble	39
4.2	Validation of the numerical algorithm; comparison study for flow over two side-by-side circular cylinders at $g = 14$ with flow over a single cylinder	40
4.3	Sequence of grid; Drag and lift coefficient at $Re = 20$ and $g = 14$	40
4.4	Hydrodynamic parameters of flow over a rotating circular cylinder at $Re = 20$ with $g = 14$	42
4.5	Sequence of grid; Drag and lift coefficient at $Re = 20$ and $g = 14$, $\alpha = 1.0$	42
5.1	Drag and lift coefficient of flow over two rotating circular cylinders at $Re = 10, 20$ and 40 with $g = 1$	48
5.2	Drag and lift coefficient of flow over two rotating circular cylinder at $Re = 20$ with $g = 0.5, 1, 1.5$	55

LIST OF FIGURES

Figure		Page
2.1	Physical coordinates.	16
3.1	Sketch of the meshes in physical and computational domains. . .	19
3.2	The flow chart of the numerical algorithm.	23
3.3	Staggered arrangement of v_ξ, v_η and p	24
3.4	Grid construction	30
4.1	Variations of the drag and lift coefficients with g at $Re = 20$. . .	34
4.2	Pressure distribution at the surface of a circular cylinder (right), $Re = 40, g = 14$	35
4.3	Observed lengths of the region of close streamlines behind a circular cylinder	35
4.4	Streamline patterns of flow over two circular cylinders (near left cylinder) at $Re = 5, 10, 20$ and 40 with $g = 14D$	36
4.5	Pressure patterns of flow over two circular cylinders (near left cylinder) at $Re = 5, 10, 20$ and 40 with $g = 14D$	37
4.6	Vorticity patterns of flow over two circular cylinders (near left cylinder) at $Re = 5, 10, 20$ and 40 with $g = 14D$	38
4.7	Variations of the drag and lift coefficients with g at $Re = 20$ and $\alpha = 1.0$	41
4.8	Streamline patterns of flow over two rotating circular cylinders at $Re = 20, g = 14$, and $\alpha = 0.1, 0.5, 1.0, 2.0$	43
4.9	Pressure patterns of flow over two rotating circular cylinders at $Re = 20, g = 14$, and $\alpha = 0.1, 0.5, 1.0, 2.0$	44

LIST OF FIGURES (Continued)

Figure		Page
5.1	Drag and lift coefficients at $Re = 10(a) - (b)$, $20(c) - (d)$, $40(e) - (f)$ and $g = 1$, $\alpha \in [0.5, 2.5]$	49
5.2	Streamline patterns of flow over two circular cylinders at $Re = 10$, $g = 1$, and $\alpha = 0.5, 1.0, 1.65, 2.0$	51
5.3	Streamline patterns of flow over two circular cylinders at $Re = 20$, $g = 1$, and $\alpha = 0.5, 1.5, 1.74, 2.0$	52
5.4	Streamline patterns of flow over two circular cylinders at $Re = 40$, $g = 1$, and $\alpha = 1.0, 1.5, 1.755, 2.0$	53
5.5	Comparison of drag and lift coefficients for different gap spacing $g = 0.5(a) - (b)$, $1.0(c) - (d)$, $1.5(e) - (f)$ and $\alpha \in [0.5, 2.5]$ at $Re = 20$	56
5.6	Streamline patterns of flow over two circular cylinders at $Re = 20$, $\alpha = 0.5$ and $g = 0.5; 1.0; 1.5$	57
5.7	Streamline patterns of flow over two circular cylinders at $Re = 20$, $\alpha = 1.0$ and $g = 0.5; 1.0; 1.5$	58
5.8	Streamline patterns of flow over two circular cylinders at $Re = 20$, $\alpha = 1.5$ and $g = 0.5; 1.0; 1.5$	59
5.9	Streamline patterns of flow over two circular cylinders at $Re = 20$, $\alpha = 2.0$ and $g = 0.5; 1.0; 1.5$	60
5.10	Pressure patterns of flow over two circular cylinders at $Re = 20$, $\alpha = 0.5$ and $g = 0.5; 1.0; 1.5$	62
5.11	Pressure patterns of flow over two circular cylinders at $Re = 20$, $\alpha = 1.0$ and $g = 0.5; 1.0; 1.5$	63

LIST OF FIGURES (Continued)

Figure		Page
5.12	Pressure patterns of flow over two circular cylinders at $Re = 20$, $\alpha = 1.5$ and $g = 0.5; 1.0; 1.5$	64
5.13	Pressure patterns of flow over two circular cylinders at $Re = 20$, $\alpha = 2.0$ and $g = 0.5; 1.0; 1.5$	65
5.14	Streamline patterns of self-motion at $Re = 20$, $\alpha = \alpha_{crit}$ and $g = 0.5; 1.0; 1.5$	66
5.15	Pressure patterns of self-motion at $Re = 20$, $\alpha = \alpha_{crit}$ and $g =$ $0.5; 1.0; 1.5$	67
A.1	Geometrical sketch of the cylindrical bipolar coordinates.	84

CHAPTER I

INTRODUCTION

1.1 General Context

Fluid flows past a bluff body have long drawn great interest in the field of fluid mechanics because of their academic and engineering importance. Flow over a single circular cylinder has yet to be accepted as a building-block problem for understanding the fluid dynamics in the bluff-body wake. Because of this, various analytical, numerical and experimental investigations have been carried out and flow results are now available in the literature providing information for various Reynolds numbers. A detailed survey on nonrotating circular cylinder flows can be found in a book by Zdravkovich (1997). However, most flows over bluff-bodies of engineering interest involve geometries that are too complex to be reasonably modeled by such a simple configuration as a single cylinder. Parametric studies have been performed by several researchers to understand the dynamics of flow over two nonrotating circular cylinders. Zdravkovich (1977, 1987) has reviewed the problem of flow interference when two cylinders are placed in a steady current. He observed that, “. . .when more than one bluff body are placed in a fluid flow, the resulting forces and vortex shedding pattern may be completely different from those formed on a single body at the same Reynolds number . . .”. A variety of flow patterns may be discerned as the spacing between two circular cylinders is changed. In many engineering applications, such as off-shore structures, heat exchangers, power transmission lines and chimneys, multiple cylindrical structures are often found.

Results on the flow past rotating cylinders are scarce. A survey of work on the flow past rotating cylinder has been provided by Stojkovic *et al.* (2002). For such flows the results depend not only on the Reynolds number but also on a parameter representing the rotational velocity of the cylinder wall. The rotation of a cylinder in a viscous uniform flow is expected to modify the wake flow pattern and may reduce drag and lift forces. The basic rationale behind the rotational effect is that as a cylinder rotates, the flow is accelerated on one side of the cylinder and decelerated on the other side. Hence, the pressure on the accelerated side becomes smaller than that on the decelerated side, resulting in a lift force. Such a phenomenon is referred to as the Magnus effect.

Owing to difficulties arising from the analytical treatment of viscous flows around rotating cylinders, investigations are mainly restricted to experimental and numerical studies in order to provide reliable information on this phenomenon. As mentioned above, many experimental studies are available on the flow around stationary cylinders (e.g. Zdravkovich (1997)). However, for a rotating cylinder and especially for force measurements (lift and drag) in the lower Reynolds number range, there is only a limited amount of reliable data exist. A few numerical investigations have been devoted to the laminar flow around a rotating cylinder.

The problem of steady flow past two rotating circular cylinders in a viscous fluid has long attracted mathematicians, because it is impossible, in general, to obtain a solution of Stokes' equations of slow viscous flow in which the fluid velocity vanishes at infinity (Jeffery (1922)). This is Jeffery's paradox. It has been shown numerically that in the case of steady motion of two rotating cylinders there is no overall force or torque acting upon them. It was ascertained that the pair of rotating cylinders is a self-propelled body.

There are two different types of stationary motion of bodies in a fluid.

The first type is a towed body. In the stationary motion regime external forces must affect the body. The second type is a self-propelled body. Self-propelled means that a body moves because of the interaction between its boundary and the surrounding fluid and without the action of an external force. To realize such a motion regime, the body must have its own source of energy, i.e., the energy spent against the drag forces. In pure motion by self-propulsion the total net force and torque, external to the system body-fluid, acting on the body are zero. The forward force (thrust) that makes the body move is generated by the body itself and the motion is due to the interaction of the body's external surface and the fluid in which it is immersed. The hydrodynamic mechanism of self-propulsion is different. The problem of the flow past a self-propelled body has a natural origin (self-propulsion is executed by marine animals, ships and airplanes). Though the problem of fluid flow past a self propelled body has a natural origin and though it is of practical importance, the number of works concerning it is very limited.

1.2 Governing Equations of Continuum Motion

We assume the fluid to be a continuum, a point of which is a very small portion of the real fluid. The small volume, a point in our mathematical description, will be called a fluid particle or element of fluid.

Let Ω be a region in 2-D or 3-D space filled with a fluid. Let $\vec{X} = (X^1, X^2, X^3)$, $\vec{X} \in \Omega$ be the coordinates of the fluid particle at time $t = 0$. Let $\vec{x} = (x^1, x^2, x^3)$, $\vec{x} \in \Omega$ be the coordinates of a given fluid particle at time t . Then the fluid motion is, by definition, a function

$$\vec{x} = \varphi(\vec{X}, t) \quad (\text{or } x^i = \varphi^i(\vec{X}, t)) \quad (1.1)$$

such that:

a) φ is invertible,

b) φ and φ^{-1} are smooth enough so that the main operations of calculus may be performed on them,

c) $\vec{X} = \varphi(\vec{X}, 0), \varphi(\vec{X}, t_1 + t_2) = \varphi(\varphi(\vec{X}, t_1), t_2)$.

If \vec{X} is fixed and t is changed, then equation (1.1) determines a trajectory of a fluid particle which is initially placed at point \vec{X} . On the other hand, if t is fixed, then equation (1.1) determines the transformation of the fluid domain at time $t = 0$ to the fluid domain at time $t = t_1$.

Generally two descriptions are used for fluid flow analysis. They are the *Lagrangian* and *Eulerian* descriptions. The Lagrangian method describes the motion of each particle of the flow field in a separate discrete manner. For example, the velocity of the n th particle of an aggregate of particles moving in space can be specified by the scalar equations

$$(v_x)_n = f_n(t)$$

$$(v_y)_n = g_n(t)$$

$$(v_z)_n = h_n(t)$$

where v_x, v_y, v_z are the velocity components in the x, y and z directions, respectively. They are independent of space coordinates, and are functions of time only. Usually, the particles are denoted by the space point they occupy at some initial time t_0 . Thus, $\rho(x_0, t)$ refers to the density at time t of a particle which was at location x_0 at time t_0 . This approach of identifying material points and following them along is also called the particle or material description. It is usually preferred in the description of low density fields, and for moving solids, such as in describing the motion of a projectile and so on. However, in a deformable system such as a fluid, there are an infinite number of elements whose motion is to be described; in such a case, the Lagrangian approach becomes unmanageable.

Instead, we can use spatial coordinates which help in identifying the particles in a flow. The velocity of all particles in a flow can be expressed in the following manner:

$$v_x = f(x, y, z, t)$$

$$v_y = g(x, y, z, t)$$

$$v_z = h(x, y, z, t)$$

This is called the *Eulerian* or *Field approach*. If properties and flow characteristics at each position in space remain invariant with time, the flow is called *steady flow*. A time-dependent flow is called *unsteady flow*.

Fluids obey the general laws of continuum mechanics: conservation of mass, linear momentum and energy. In the Eulerian representation of the flow, we represent the density $\rho(\vec{x}, t)$ as a function of the position \vec{x} and time t . The conservation of mass is expressed by the continuity equation

$$\frac{\partial \rho}{\partial t} + \text{div}(\rho \vec{v}) = 0. \quad (1.2)$$

If we assume that the fluid is incompressible and homogeneous, then the density is constant in space and time: $\rho(\vec{x}, t) \equiv \rho_0$. Then the continuity equation (1.2) becomes

$$\text{div} \vec{v} = 0. \quad (1.3)$$

The momentum equation, which is based on Newton's second law, represents the balance between various forces acting on a fluid element. The forces are

- a) The force due to rate of change of momentum, generally referred to as the inertia force
- b) Body forces such as buoyancy force, magnetic force, and electrostatic force
- c) Pressure force

d) Viscous forces (causing shear stress).

For a fluid element under equilibrium,

$$\textit{Inertia force} + \textit{body force} + \textit{pressure force} + \textit{viscous force} = 0.$$

or

$$\rho \left(\frac{\partial \vec{v}}{\partial t} + (\vec{v} \cdot \nabla) \vec{v} \right) + f = -\nabla p + \mu \Delta \vec{v}, \quad (1.4)$$

where μ is called the coefficient of dynamic viscosity.

Equations (1.3) and (1.4) govern the motion of a viscous incompressible fluid, they are called “the Navier-Stokes equations for viscous incompressible flow”

1.3 Previous Research

The problem of flow past two rotating circular cylinders in a viscous fluid has long attracted mathematicians and engineers. This flow shows some analytical peculiarities regarding the implementation of near-field and far-field boundary conditions. It might be for this reason that the flow has attracted much interest from theoretical fluid dynamicists. It is impossible, in general, to obtain solutions of Stokes’ equations of slow viscous steady flow in which the fluid velocity vanishes at infinity (Jeffery, 1922). If the cylinders are outside one another, Jeffery found that it is impossible, in general, to make the fluid velocity vanish at infinity. He illustrated this by a detailed treatment of the case of equal cylinders, rotating with equal speeds in an opposite sense. This is the Jeffery paradox. To resolve this paradox, Smith (1991) obtained an asymptotic solution of the Stokes equations for the stream function which is valid at large distances from the cylinders. This asymptotic expansion involved many unknown coefficients of the Fourier series and there was no obvious way of obtaining these coefficients. Elliott *et al.* (1995) established the boundary element method by using the asymptotic expansions

given by Smith and showed numerically that the combined bodies have no overall force or torque acting upon them. Watson (1995) pointed out that the pressure field given by Smith's asymptotic form is not single-valued and proposed that an additional term to Jeffery's Fourier series is necessary. However, he did not derive the force, since the outer flow which is governed by the Navier-Stokes equations was not obtained.

In 1973 the problem of flow past rotating cylinders was considered by Senitskii (1973). The problem was studied using a boundary layer approach for the case of large distance between the center of cylinders. In the work of Senitskii (1975) the first terms of an asymptotic expansion by inverse degree of Reynolds number were obtained. Using an asymptotic expansion by degree of a small parameter, which is the ratio of cylinder radius to distance between axes of cylinders, the problem of stationary flow past rotating cylinders was solved approximately by Senitskii (1975a, 1975b). It was ascertained that in the approximation considered the pair of rotating cylinders is a self-propelled body. In connection with the problem of determining the energy required for a body to move in a liquid the motion of a pair of rotating cylinders in a liquid has also been investigated experimentally (Senitskii (1980, 1981)).

In pure motion by self-propulsion the total net force and torque, external to the system body-fluid, acting on the body are zero. The forward force (thrust) that makes the body move is generated by the body itself and the motion is due to the interaction of the body's external surface and the fluid in which it is immersed. The hydrodynamic mechanism of self-propulsion is different for macroscopic and microscopic bodies. Large objects which propel themselves make use of inertia in the surrounding fluid. Their thrust can be produced by muscular action and change of shape, as in animal locomotion, or can be provided by

mechanical propulsion systems, as in an airplane, rocket or submarine (Milne-Thomson (1952)).

Though the problem of a self-propelled body has a natural origin and though it is of practical importance, the number of works concerning it is very limited. Let us briefly refer to the literature on the mathematical analysis and numerical simulation of motion by self-propulsion of a rigid body in an infinite Navier-Stokes fluid. In (Finn (1965), Pukhnacev (1989, 1990)) the asymptotic properties of steady flow past a self-propelled body moving with purely translational velocity are investigated. The existence of such solutions was first established for very particular shapes, like balls and cylinders in (Sennitskii (1978, 1984, 1990)) and for a symmetric body around an axis in Galdi (1997). Considering the general form of rigid body motion, with the rotation of the body taken into account, Galdi (1999) gave a detailed study which proved the existence of steady self-propelled solutions for a body with arbitrary geometry for the cases of zero and nonzero Reynolds number. In (Silvestre (2002a, 2002b)) the existence of a weak solution to the general unsteady nonlinear problem and the attainability of steady purely translational self-propelled motion for a symmetric body was proved. Using a method consistent with asymptotic decomposition for a low Reynolds number, Sennitskii (1978, 1984, 1990) investigated the flow past a circular cylinder with a moving boundary and of flow past a ball with a liquid-permeable boundary and obtained asymptotic formulas for the velocity at great distance from the body. It was noted that the velocity perturbation at large distance from a self-moving body showed more rapid decay than that from a towed one. In Lugovtsov (1971), examples of flat potential viscous flow past a self-moving “body” whose boundary consisted of two symmetrical coupled components were studied. On each boundary, the normal velocity components were

equal to zero and the tangential components were constant.

A numerical solution to the problem of momentumless flow past an extended ellipsoid of rotation was obtained by Izteleulov (1985). A propelling model has a self-consistent distribution of volume force located in a small region behind the body. Simulation of the problem of conductive incompressible viscous flow past a body in an electromagnetic field was considered in Shatrov and Yakovlev (1985), Kxonichev and Yakovlev (1985). In the work of Moshkin *et al.* (1989) and Moshkin(1991), two particular cases of self-motion were studied by numerical solution of the Navier-Stokes equations. In one case, there was a surface behind (downstream of) the ball. The liquid flows through this surface and obtained thereby an additional momentum. In the other case the ball surface was permeable. On one of its parts, between two cones with the divergence semi-angles Θ_1, Θ_2 and a mutual axis $\Theta = \pi$, the liquid is sucked in, and on the other part, ‘cut’ by a cone $\Theta_3 \leq \Theta \leq \pi$, the same quantity of the liquid returned to the flow. Nakanishi *et al.* (1999) applied the vortex method to a low Reynolds number unsteady flow generated by two circular cylinders of equal radii set rotating abruptly with equal angular velocities in a flow initially at rest. Elliot *et al.* (1995) developed the boundary element method by using the asymptotic expansions and showed numerically that the combined bodies (two cylinders) have no overall force or torque acting upon them.

1.4 Objectives and Overview of the Thesis

In this research, we interested in the self-propulsion of a rigid body. The shape of the body is constant during the motion, and the thrust is produced because the body boundary moves. The motion of the body is therefore completely determined by its geometry and by the distribution of the velocity on its boundary.

In fact, the combined body, which consists of two rotating circular cylinders, is an example where self-propelled motion is due to a non-zero velocity of the boundary. We study not only self-motion of rotating cylinders but also flow past two towed rotating cylinders. Different rotation of cylinders can be considered as a propulsion device for controlling the motion of the body.

The main objectives of the research work presented in the thesis are

1. to develop and validate a numerical algorithm to simulate viscous incompressible fluid flow past two rotating and nonrotating circular cylinders,
2. to obtain a consistent set of data for the drag and lift forces for moderate rate of cylinder rotation for which, to the author's knowledge, no data are available in the literature,
3. to highlight and discuss the difference between uniform flow past towed and self-propelled bodies using the example of flow past two rotating circular cylinders.

The mathematical formulation of the problem of rigid body motion in a viscous liquid is described in Chapter II, which aims in defining the differences between steady towed and self-propelled body motion. The problem of fluid flow past two rotating circular cylinders is recast in terms of cylindrical bipolar coordinate system. Chapter III presents a numerical algorithm based on a projection method. In Chapter IV, we present the results of validation of our numerical algorithm by a comparison with available numerical and experimental data. The results of various numerical experiments are reported and discussed in Chapter V. Finally some general comments, a summary of the achievements of this work and some ideas on how this research could be continued are provided in Chapter VI.

CHAPTER II

MATHEMATICAL FORMULATION OF PROBLEM

2.1 Motion of Rigid Body in a Viscous Incompressible Fluid

To better explain our results, let us first give a mathematical formulation of the problem in the general case. We represent a rigid body by a compact set \mathcal{B} that is moving in a viscous fluid \mathcal{L} which occupies the region $\mathcal{D} = \mathcal{R}^3/\mathcal{B}$ exterior to the body. The motion of $\{\mathcal{B}, \mathcal{L}\}$ is described by the following coupled system of equations and boundary conditions

$$\rho \frac{D\vec{v}}{Dt} = \operatorname{div} T(\vec{v}, p), \text{ in } \mathcal{D} \times (0, T), \quad (2.1)$$

$$\operatorname{div} \vec{v} = 0, \text{ in } \mathcal{D} \times (0, T), \quad (2.2)$$

$$\vec{v} = \vec{v}_* \quad \text{at } \Sigma \times (0, T), \quad (2.3)$$

$$\lim_{\vec{x} \rightarrow \infty} (\vec{v}(\vec{x}, t) + \vec{V}(\vec{x}, t)) = 0, \text{ for } t \in (0, T), \quad (2.4)$$

$$m \frac{d\vec{\zeta}}{dt} = - \int_{\Sigma} T(\vec{v}, p) \cdot \vec{n} \, d\sigma, \text{ in } (0, T), \quad (2.5)$$

$$I \frac{d\vec{\omega}}{dt} = - \int_{\Sigma} [\vec{x} \times T(\vec{v}, p)] \cdot \vec{n} \, d\sigma, \text{ in } (0, T), \quad (2.6)$$

$$\vec{v}(\vec{x}, 0) = v_0(\vec{x}), \quad \vec{x} \in \mathcal{D}, \quad (2.7)$$

$$\vec{\zeta}(0) = \zeta_0, \quad \vec{\omega}(0) = \omega_0. \quad (2.8)$$

The quantities $\vec{v} = \vec{v}(\vec{x}, t)$ and $p = p(\vec{x}, t)$ represent the velocity and pressure associated with each particle of \mathcal{L} and $T(\vec{v}, p)$ is the stress tensor, defined by

$$T_{ij}(\vec{v}, p) = \mu \left\{ \frac{\partial v_i}{\partial x_j} + \frac{\partial v_j}{\partial x_i} \right\} - p\delta_{ij}, \quad i, j = 1, 2, 3, \quad (2.9)$$

where μ is the coefficient of dynamic viscosity. The field $\vec{V}(\vec{x}, t) = \vec{\zeta}(t) + \vec{\omega}(t) \times \vec{x}$ represents the velocity of \mathcal{B} , $\vec{\zeta}(t)$ and $\vec{\omega}(t)$ are velocity of center mass and vector of angular velocity of the body, respectively. In equations (2.5) and (2.6) the positive constant m is the mass of \mathcal{B} and I is its inertia tensor. Recall that

$$I_{ij} = \int_B \rho_B(\vec{x})(|\vec{x}|^2\delta_{ij} - x_i x_j) dx,$$

and I is symmetric and positive definite (Danielson (1997)). Here ρ_B is the mass density of the body \mathcal{B} . The distribution of velocity \vec{v}_* on Σ represents the thrust, responsible for the motion of the body. The two equations (2.5) and (2.6) are consequences of Newton's laws of conservation of linear and angular momentum, respectively, for the body \mathcal{B} . Let us consider three possible cases.

a) If $\{\mathcal{B}, \mathcal{L}\}$ performs a steady motion then the left hand side of equations (2.5) and (2.6) are equal to zero. This is the case of steady self-propelled motion. One of the basic questions for this type of problem is the following one: in which way can we choose the field \vec{v}_* in order that \mathcal{B} moves with a (constant) rigid motion velocity $\vec{V} = -\vec{\zeta} - \vec{\omega} \times x$, where $\vec{\zeta} \neq 0$ (so that \mathcal{B} does not move). Equations (2.5) and (2.6) with zero left hand side express the fact that the total external force and torque on \mathcal{B} are identically zero, that is that \mathcal{B} is a self-propelled body. In this case a suitable distribution of velocity field \vec{v}_* at Σ are additional unknown quantities.

b) In the case of a towed body the motion of \mathcal{B} is due to external forces. The field $\vec{V}(\vec{x}, t) = \vec{\zeta}(t) + \vec{\omega}(t) \times \vec{x}$ is a known function of (\vec{x}, t) and the velocity \vec{v}_* on Σ is also a given function. In this case we use integrals in the right hand

side of equations (2.5) and (2.6) to find the external drag force and torque on \mathcal{B} . In the simplest case, where $\vec{V}(\vec{x}, t) = \varsigma - \text{const}$ and $v_* = 0$ on Σ the problem is fluid flow past the towed body. The direction of stream flow coincides with the direction of the vector \vec{V}

c) In the more general case, equations (2.1) – (2.9) represent the problem of rigid body motion in a viscous incompressible fluid due to the distribution velocity \vec{v}_* on the boundary that furnishes the “thrust”.

When a body moves in a fluid it experiences forces from the relative fluid flow which is taking place around it. If the body has arbitrary shape and orientation, the flow will exert forces and moments about all three coordinate axes. The force on the body along the flow direction is called *drag*. The drag is essentially a force opposing the motion of the body. Viscosity is responsible for the drag force, and the shape of the body generally determines the overall drag. In the design of transport vehicles, shapes experiencing minimum drag are considered, to keep the power consumption at a minimum. Low drag shapes are called *streamlined bodies* and high drag shapes are termed as *bluff bodies*.

Drag arises due to the difference in pressure between the front and back regions, these force is called *pressure or form drag* and the friction between the surface of body and the fluid causes viscous shear stress known as *skin friction* or *shear drag*.

The net force and torque exerted by fluid on an immersed body with surface Σ are

$$\vec{F} = \int_{\Sigma} \vec{\tau} dS, \quad \vec{M} = \int_{\Sigma} [\vec{r} \times \vec{\tau}] dS, \quad (2.10)$$

where $\vec{\tau} = T \cdot \vec{n}$ is the stress vector, \vec{n} is the unit vector normal to the Σ that points outside the region occupied by the fluid. The force per unit area exerted across a rigid boundary element with normal \vec{n} in an incompressible fluid

is defined by

$$\vec{\tau} = -p\vec{n} - \mu(\vec{n} \times \vec{\omega}) \quad (2.11)$$

where p is pressure and $\vec{\omega}$ is vorticity defined as $\vec{\omega} = \text{curl}\vec{v}$ (see Batchelor (2000)).

The problem of self-motion is to find solution of the Navier-Stokes equations (2.1) – (2.2) with boundary conditions (2.3) – (2.4) and additional constraints

$$\vec{F} = \vec{M} = 0. \quad (2.12)$$

2.2 Viscous Incompressible Fluid Flow Past Two Circular Cylinders.

It is natural to study the fluid flow in a boundary fitted curvilinear coordinate system. In order to study fluid flow past two circular cylinders, the reasonable coordinate system is the cylindrical bipolar coordinate system. The cylindrical bipolar coordinate system can be defined by the following equations

$$x = \frac{a \sinh \eta}{\cosh \eta - \cos \xi}, \quad y = \frac{a \sin \xi}{\cosh \eta - \cos \xi}, \quad z = z, \quad (2.13)$$

where $\xi \in [0, 2\pi)$, $\eta \in (-\infty, \infty)$, $z \in (-\infty, \infty)$, a is a characteristic length in the cylindrical bipolar coordinate system which is positive. The following identities show that curves of constant ξ and η are circles in xy -space

$$\begin{aligned} x^2 + (y - a \cot \xi)^2 &= a^2 \csc^2 \xi, \\ (x - a \coth \eta)^2 + y^2 &= a^2 \text{csch}^2 \eta. \end{aligned} \quad (2.14)$$

The coordinate surface $\eta = \text{const}$ corresponds to a family of nonintersecting cylinders whose centers lie along the x -axis. The value $\eta = 0$ is a cylinder of infinite radius and is equivalent to the entire plane $x = 0$. Figure 2.1 shows two cylinders that are chosen to be $\eta = \eta_1$ (with $\eta_1 > 0$) and $\eta = \eta_2$ (with $\eta_2 < 0$). The cylinders' radii r_1 and r_2 and the distances of their centers from the origin

d_1 and d_2 are given by

$$r_i = a \operatorname{csch} |\eta_i|, \quad d_i = a \operatorname{coth} |\eta_i|, \quad i = 1, 2. \quad (2.15)$$

The center to center distance between the cylinders equals $d = d_1 + d_2$. If r_1, r_2 and d are given, one can find a, η_1 and η_2 from relations (2.13) – (2.15) as follows

$$\eta_{1,2} = \ln \left[\left(\frac{d^2 + r_1^2 - r_2^2}{2dr_1} \right) \pm \sqrt{\left(\frac{d^2 + r_1^2 - r_2^2}{2dr_1} \right)^2 - 1} \right], \quad (2.16)$$

$$a = \sqrt{\frac{d^4 - 2d^2(r_1^2 + r_2^2) + (r_1^2 - r_2^2)^2}{4d^2}}.$$

The Navier-Stokes equations in the cylindrical bipolar coordinate system (ξ, η, z) are

$$\begin{aligned} & \frac{\partial v_\xi}{\partial t} + \frac{1}{h} \left(v_\xi \frac{\partial v_\xi}{\partial \xi} + v_\eta \frac{\partial v_\xi}{\partial \eta} \right) + v_z \frac{\partial v_\xi}{\partial z} \\ & - \frac{1}{a} (\sinh \eta (v_\xi v_\eta) - \sin \xi (v_\eta)^2) = -\frac{1}{h} \frac{1}{\rho} \frac{\partial p}{\partial \xi} + \nu \frac{\partial^2 v_\xi}{\partial z^2} \\ & + \frac{\nu}{h} \left\{ \frac{1}{h} \left(\frac{\partial^2 v_\xi}{\partial \xi^2} + \frac{\partial^2 v_\xi}{\partial \eta^2} \right) - \frac{2}{a} \left(\sinh \eta \frac{\partial v_\eta}{\partial \xi} - \sin \xi \frac{\partial v_\eta}{\partial \eta} \right) - \left(\frac{\cosh \eta + \cos \xi}{a} \right) v_\xi \right\}, \end{aligned} \quad (2.17)$$

$$\begin{aligned} & \frac{\partial v_\eta}{\partial t} + \frac{1}{h} \left(v_\xi \frac{\partial v_\eta}{\partial \xi} + v_\eta \frac{\partial v_\eta}{\partial \eta} \right) + v_z \frac{\partial v_\eta}{\partial z} \\ & + \frac{1}{a} (\sinh \eta (v_\xi)^2 - \sin \xi (v_\xi v_\eta)) = -\frac{1}{h} \frac{1}{\rho} \frac{\partial p}{\partial \eta} + \nu \frac{\partial^2 v_\eta}{\partial z^2} \\ & + \frac{\nu}{h} \left\{ \frac{1}{h} \left(\frac{\partial^2 v_\eta}{\partial \xi^2} + \frac{\partial^2 v_\eta}{\partial \eta^2} \right) + \frac{2}{a} \left(\sinh \eta \frac{\partial v_\xi}{\partial \xi} - \sin \xi \frac{\partial v_\xi}{\partial \eta} \right) - \left(\frac{\cosh \eta + \cos \xi}{a} \right) v_\eta \right\}, \end{aligned} \quad (2.18)$$

$$\begin{aligned} & \frac{\partial v_z}{\partial t} + \frac{1}{h} \left(v_\xi \frac{\partial v_z}{\partial \xi} + v_\eta \frac{\partial v_z}{\partial \eta} \right) + v_z \frac{\partial v_z}{\partial z} = \\ & -\frac{1}{\rho} \frac{\partial p}{\partial z} + \nu \left\{ \frac{1}{h^2} \left(\frac{\partial^2 v_z}{\partial \xi^2} + \frac{\partial^2 v_z}{\partial \eta^2} \right) + \frac{\partial^2 v_\xi}{\partial z^2} \right\}, \end{aligned} \quad (2.19)$$

$$\frac{1}{h^2} \left[\frac{\partial(hv_\xi)}{\partial \xi} + \frac{\partial(hv_\eta)}{\partial \eta} \right] + \frac{\partial v_z}{\partial z} = 0, \quad (2.20)$$

where $v_\xi, v_\eta,$ and v_z are the physical components of velocity vector $v = (v_\xi, v_\eta, v_z)$,

p is the pressure, $\nu = \frac{\mu}{\rho}$ is the coefficient of kinematic viscosity and

$$h = \frac{a}{(\cosh \eta - \cos \xi)}.$$

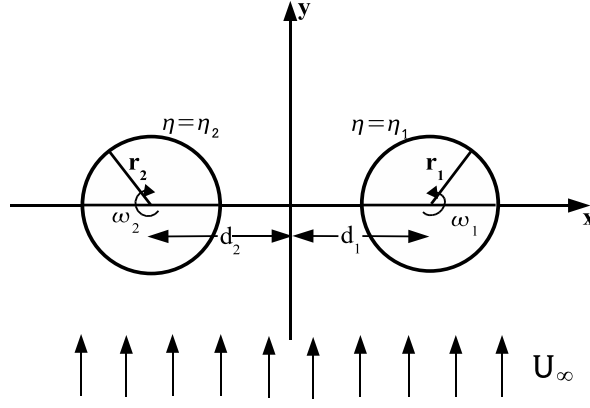


Figure 2.1 Physical coordinates.

In the present situation the boundary conditions are no-slip requirement on cylinders

$$v_\xi = \omega_i r_i, \quad v_\eta = 0, \quad \text{on } \eta = \eta_i, \quad \xi \in [0, 2\pi), \quad i = 1, 2, \quad (2.21)$$

where ω_i , $i = 1, 2$ are rotational velocities of the cylinder walls. Positive values of ω_i , $i = 1, 2$ correspond to counterclockwise rotation. Upstream and downstream boundary conditions at infinity are

$$v_x = 0, \quad v_y = U_\infty, \quad \text{as } r^2 = x^2 + y^2 \rightarrow \infty, \quad (2.22)$$

where v_x and v_y are components of the velocity vector in x and y directions respectively. Self motion requires that the resultant fluid force and torque on the combined system of the two cylinders are zero.

The main definitions of tensor-vector calculus and transformation of the Navier-Stokes equations into the cylindrical bipolar coordinate system are represented in Appendix A.

Equations (2.17)–(2.22) are dimensional. They can be made dimensionless if we redefine the dependent and independent variables to be dimensionless, by dividing them by *constant* reference properties appropriate to the flow. In this case, we set diameter of cylinder, D , is reference length and velocity at infinite,

U_∞ , is reference velocity. For such flows, the results depend not only on the Reynolds number Re but also on the non-dimensional gap spacing between the two cylinders, g , and on parameters, α_i representing the ratios of the rotational velocities of the cylinder walls to the oncoming flow velocity

$$Re = U_\infty D/\nu, \quad \alpha_i = D\omega_i/2U_\infty, \quad i = 1, 2, \quad \text{and} \quad g = \frac{d - r_1 - r_2}{D}, \quad (2.23)$$

where ω_i are constant angular velocities of the cylinders rotation and ν is the kinematic viscosity of the fluid.

For a two-dimensional flow (see Figure 2.1) of an incompressible fluid with constant properties, the nondimensional governing equations, in cylindrical bipolar coordinates are equations (2.17), (2.18) and (2.20) in which $\rho = 1$ and instead of ν , the term $\frac{1}{Re}$ will appear. The nondimensional no-slip boundary conditions on cylinders wall are

$$v_\xi = \alpha_i, \quad v_\eta = 0, \quad \text{at} \quad \eta = \eta_i, \quad \xi \in [0, 2\pi), \quad i = 1, 2, \quad (2.24)$$

Nondimensional upstream and downstream boundary conditions at infinity are

$$v_x = 0, \quad v_y = 1, \quad \text{as} \quad r^2 = x^2 + y^2 \rightarrow \infty, \quad (2.25)$$

CHAPTER III

NUMERICAL METHODS

3.1 Discretization of the Solution Domain

The first step in computing a numerical solution to the Navier-Stokes equations is the construction of a grid. A well-constructed grid generate improving the accuracy and quality of the solution. In this chapter, techniques for generating grid will be discussed. For the construction of a finite difference scheme the new independent variables are introduced

$$\xi = \chi_1(\hat{\xi}), \quad \eta = \chi_2(\hat{\eta}), \quad (3.1)$$

or by implication

$$\begin{aligned} \hat{\xi} &= \varphi_1(\xi), \quad \hat{\eta} = \varphi_2(\eta), \\ \mathbf{J} &= \frac{\partial(\xi, \eta)}{\partial(\hat{\xi}, \hat{\eta})} \neq 0. \end{aligned} \quad (3.2)$$

This mapping is used to transform the nonuniform mesh in physical space (ξ, η) into uniform rectangular mesh in computational domain $(\hat{\xi}, \hat{\eta})$. The sketch of meshes in physical and computational domain can be seen in Figure 3.1. The functions φ_1 and φ_2 establish the one-to-one correspondence between nodes of uniform mesh in the computational domain and nodes of nonuniform mesh in the physical domain. The functions φ_1 and φ_2 are constructed by tabular assigning points in the physical domain to the corresponding points in computational domain. The choice of mapping (3.1) and (3.2) enables as to condense the mesh node near solid boundaries and in the neighborhood of lines $\eta = 0$ and $\xi = 0$ ($\xi = 2\pi$). In the computational domain $(\hat{\xi}, \hat{\eta})$ the nodes of the mesh are distributed uniformly (see Figure 3.1).

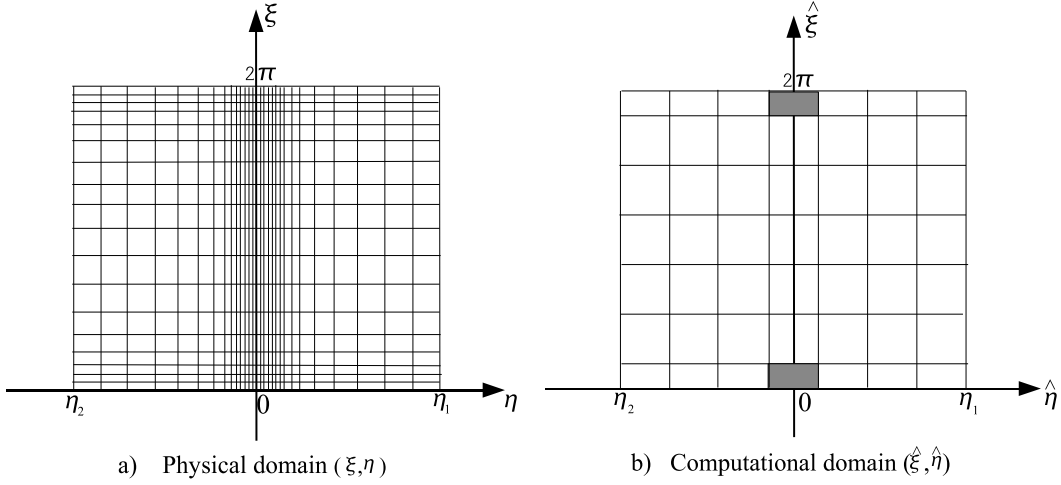


Figure 3.1 Sketch of the meshes in physical and computational domains.

It is not convenient to solve the governing equations over a nonuniform grid. The governing equations (2.17) – (2.20) recast according mesh transformations (3.1) and (3.2)

$$\begin{aligned}
& \frac{\partial v_\xi}{\partial t} + \frac{1}{h} \frac{1}{J} \left(v_\xi \eta_{\hat{\eta}} \frac{\partial v_\xi}{\partial \hat{\xi}} + v_\eta \xi_{\hat{\xi}} \frac{\partial v_\xi}{\partial \hat{\eta}} \right) - \frac{1}{a} (\sinh \eta (v_\xi v_\eta) - \sin \xi (v_\eta)^2) = \\
& = -\frac{1}{h} \frac{1}{J} \eta_{\hat{\eta}} \frac{\partial p}{\partial \hat{\xi}} + \frac{1}{Re} \frac{1}{h^2} \frac{1}{J} \left[\frac{\partial}{\partial \hat{\xi}} \left(\frac{\eta_{\hat{\eta}}}{\xi_{\hat{\xi}}} \frac{\partial v_\xi}{\partial \hat{\xi}} \right) + \frac{\partial}{\partial \hat{\eta}} \left(\frac{\xi_{\hat{\xi}}}{\eta_{\hat{\eta}}} \frac{\partial v_\xi}{\partial \hat{\eta}} \right) \right] - \\
& - \frac{1}{Re} \frac{1}{h} \left[\frac{1}{J} \frac{2}{a} \left(\sinh \eta \eta_{\hat{\eta}} \frac{\partial v_\eta}{\partial \hat{\xi}} - \sin \xi \xi_{\hat{\xi}} \frac{\partial v_\eta}{\partial \hat{\eta}} \right) + \left(\frac{\cosh \eta + \cos \xi}{a} \right) v_\xi \right], \quad (3.3)
\end{aligned}$$

$$\begin{aligned}
& \frac{\partial v_\eta}{\partial t} + \frac{1}{h} \frac{1}{J} \left(v_\xi \eta_{\hat{\eta}} \frac{\partial v_\eta}{\partial \hat{\xi}} + v_\eta \xi_{\hat{\xi}} \frac{\partial v_\eta}{\partial \hat{\eta}} \right) + \frac{1}{a} (\sinh \eta (v_\xi)^2 - \sin \xi (v_\xi v_\eta)) = \\
& = -\frac{1}{h} \frac{1}{J} \xi_{\hat{\xi}} \frac{\partial p}{\partial \hat{\eta}} + \frac{1}{Re} \frac{1}{h^2} \frac{1}{J} \left[\frac{\partial}{\partial \hat{\xi}} \left(\frac{\eta_{\hat{\eta}}}{\xi_{\hat{\xi}}} \frac{\partial v_\eta}{\partial \hat{\xi}} \right) + \frac{\partial}{\partial \hat{\eta}} \left(\frac{\xi_{\hat{\xi}}}{\eta_{\hat{\eta}}} \frac{\partial v_\eta}{\partial \hat{\eta}} \right) \right] + \\
& + \frac{1}{Re} \frac{1}{h} \left[\frac{1}{J} \frac{2}{a} \left(\sinh \eta \eta_{\hat{\eta}} \frac{\partial v_\xi}{\partial \hat{\xi}} - \sin \xi \xi_{\hat{\xi}} \frac{\partial v_\xi}{\partial \hat{\eta}} \right) - \left(\frac{\cosh \eta + \cos \xi}{a} \right) v_\eta \right], \quad (3.4)
\end{aligned}$$

$$\frac{1}{h^2} \frac{1}{J} \left[\eta_{\hat{\eta}} \frac{\partial (h v_\xi)}{\partial \hat{\xi}} + \xi_{\hat{\xi}} \frac{\partial (h v_\eta)}{\partial \hat{\eta}} \right] = 0. \quad (3.5)$$

3.2 Discretization of the Governing Equation

In this section, we give the time and space discretizations used in order to solve the Navier-Stokes equations (3.3) – (3.5). In order to describe the numerical

method it is convenient to represent the momentum and continuity equations in vector form

$$\frac{\partial \vec{v}}{\partial t} + L\vec{v} = -\nabla p + \vec{f}, \quad (3.6)$$

$$\operatorname{div} \vec{v} = 0. \quad (3.7)$$

Here the operator L includes convective and diffusive terms

$$L\vec{v} = (\vec{v} \cdot \nabla)\vec{v} - \frac{1}{Re}\Delta\vec{v}.$$

3.2.1 The Projection Method in Time

Most numerical methods for solving equations (3.6) and (3.7) in terms of primitive variables use a projection method. We will describe here the projection method in the form is suggested by Tolstykh (1991). Introducing the finite-difference analogues L_h , div_h and ∇_h of the operators L , div and ∇ on the grid Ω_h , the following approximations of equations (3.6) and (3.7) are considered

$$\alpha \frac{\tilde{\vec{v}} - \vec{v}^n}{\tau} + \theta L_h \tilde{\vec{v}} + (1 - \theta) L_h \vec{v}^n = -\nabla_h \kappa p^n + \beta_1 \vec{f}, \quad (3.8)$$

$$\frac{\vec{v}^{n+1} - \vec{v}^n}{\tau} + \theta L_h \tilde{\vec{v}} + (1 - \theta) L_h \vec{v}^n = -\frac{1}{\alpha} \nabla_h (p^{n+1} + (\alpha - 1)\kappa p^n) \beta_2 \vec{f}, \quad (3.9)$$

$$\operatorname{div}_h \vec{v}^{n+1} = 0. \quad (3.10)$$

The scalar parameters $\alpha, \theta, \beta_1, \beta_2$ and κ allowed us to vary the property of approximation and convergence. In particular case here $\alpha = 1$, $\theta = 0$, $\kappa = 0$. We have original projection method of Chorin (1968) and Temam (1991). Equations (3.8) – (3.10) are not convenient for computation. These equations can be reorganize by the following steps :

First, subtract equation (3.8) from equation (3.9) to eliminate convective and diffusive terms

$$\frac{\vec{v}^{n+1} - \vec{v}^n}{\tau} - \alpha \frac{\tilde{\vec{v}} - \vec{v}^n}{\tau} = - \left[\frac{1}{\alpha} \nabla_h (p^{n+1} + (\alpha - 1)\kappa p^n) - \nabla_h \kappa p^n \right] + (\beta_2 - \beta_1) \vec{f},$$

or we can rewrite in this form

$$\bar{v}^{n+1} = \alpha \tilde{v} + (1 - \alpha) \bar{v}^n - \frac{\tau}{\alpha} \nabla_h \delta p^{n+1} + \tau(\beta_2 - \beta_1) \vec{f}, \quad (3.11)$$

where $\delta p^{n+1} = p^{n+1} - \kappa p^n$ is called pressure-correction. Apply the divergence operator to both side of the last equation we get

$$\operatorname{div}_h \bar{v}^{n+1} = \alpha \operatorname{div}_h \tilde{v} + (1 - \alpha) \operatorname{div}_h \bar{v}^n - \frac{\tau}{\alpha} \operatorname{div}_h \nabla_h \delta p^{n+1} + \tau(\beta_2 - \beta_1) \operatorname{div}_h \vec{f}$$

Take into account (3.10), we have the following "elliptic equation" for pressure-correction

$$\operatorname{div}_h \nabla_h \delta p^{n+1} = \frac{\alpha^2}{\tau} \operatorname{div}_h \tilde{v} + \alpha(\beta_2 - \beta_1) \operatorname{div}_h \vec{f}. \quad (3.12)$$

Approximate solution of the Navier-Stokes equations (3.6) and (3.7) can be founded on three steps :

The first step consists on solving momentum equation (3.8) which yields an intermediate velocity field \tilde{v} , that do not satisfy the divergence constraint

$$\alpha \frac{\tilde{v} - \bar{v}^n}{\tau} + \theta L_h \tilde{v} + (1 - \theta) L_h \bar{v}^n = -\nabla_h \kappa p^n + \beta_1 \vec{f}.$$

This step is followed by the pressure correction step. Poisson equation for pressure-correction (3.12) is solved during second step

$$\operatorname{div}_h \nabla_h \delta p^{n+1} = \frac{\alpha^2}{\tau} \operatorname{div}_h \tilde{v} + \alpha(\beta_2 - \beta_1) \operatorname{div}_h \vec{f}.$$

On the solid wall the Neumann boundary conditions derived from the normal component of momentum equation or homogeneous Neumann boundary conditions, $\frac{\partial \delta p^{n+1}}{\partial \vec{n}} = 0$, is used. Note that the necessary compatibility condition is satisfied. Once δp^{n+1} is known, the last, third step of the method is to update the velocity field at the level $(n + 1)\Delta t$ by using equation (3.11).

$$\bar{v}^{n+1} = \alpha \tilde{v} + (1 - \alpha) \bar{v}^n - \frac{\tau}{\alpha} \nabla_h \delta p^{n+1} + \tau(\beta_2 - \beta_1) \vec{f},$$

As example, for parameters $\alpha = 1, \beta_1 = \beta_2 = 0, \theta = 0$ and $\kappa = 0$ above algorithm are the following : the intermediate velocity is computed in the first step

$$\tilde{\vec{v}} = \vec{v}^n - \tau L_h \vec{v}^n, \quad (3.13)$$

where $L_h \vec{v}^n = (\vec{v}^n \cdot \nabla) \vec{v}^n - \frac{1}{Re} \Delta \vec{v}^n$.

Next, pressure is computed from difference analog of the Poisson equation in second step

$$\operatorname{div}_h \nabla_h (p^{n+1}) = \frac{1}{\tau} \operatorname{div}_h \tilde{\vec{v}}, \quad (3.14)$$

Finally, the velocity at $(n + 1)$ level is computed

$$\vec{v}^{n+1} = \tilde{\vec{v}} - \tau \nabla_h (p^{n+1}) \quad (3.15)$$

Figure 3.2 shows the flow chart of numerical algorithm.

3.2.2 Discretization in Space

In this section, we give the space discretization used in order to solve the Navier-Steady equations. The staggered arrangement of unknown functions is used:

- velocity components v_ξ and v_η of velocity vector $\vec{v} = (v_\xi, v_\eta)$ are located at the centers of cell sides normal to them.
- pressure, p , is located at the cell center.

In Figure 3.3 the location of different functions is also shown.

Let us use the following notations: the upper index n denotes values of variables at the time $t_n = n * \Delta t$, lower indices i, j denote the quantity at the center of computational cell, $\xi_j = (j - 1) * \Delta \xi$, $\eta_i = \eta_2 + (i - 0.5) * \Delta \eta$, and lover indices $i + 1/2, j + 1/2$ correspond to the node $\xi_{j+1/2} = \xi_j + \frac{\Delta \xi}{2}$, $\eta_{i+1/2} = \eta_2 + i * \frac{\Delta \eta}{2}$.

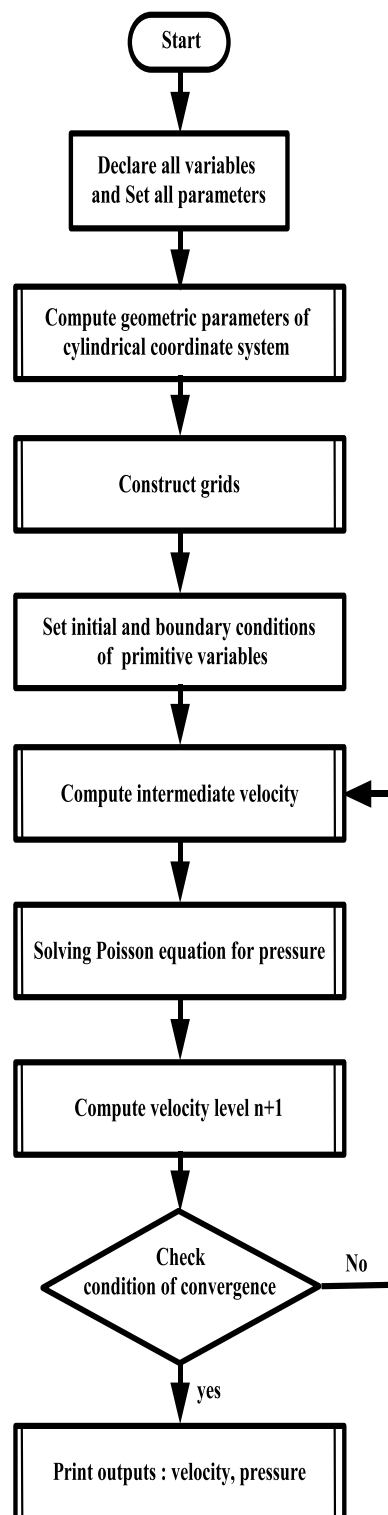


Figure 3.2 The flow chart of the numerical algorithm.

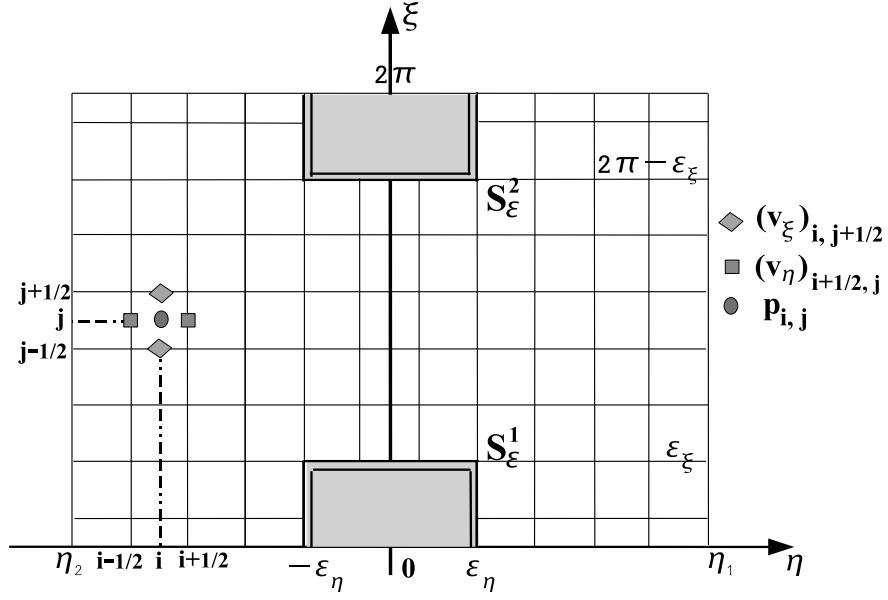


Figure 3.3 Staggered arrangement of v_ξ , v_η and p

Boundary Condition at Infinity

The behavior of pressure and velocity field at large distances from a rigid body placed in a uniform stream of velocity \vec{U}_∞ is analyze. From the analytical point of view, it is known that (see Boundary condition (2.22))

$$\lim_{|\vec{x}| \rightarrow \infty} \vec{v}(\vec{x}, t) = \vec{U}_\infty \quad (3.16)$$

In a numerical simulation it is impractical to use equation (3.16) for high Reynolds number flow as it involves the placement of the outer boundary at vary large distance from the body. In our research, we study only steady fluid flow past rigid circular cylinders. The highest Reynolds number Re_{crit} for which the flow remain steady is about $Re_{crit} = 45$. Therefore, in our research, a slightly lower values of Reynolds number is used $Re \leq 40$, guaranteeing steady-state flow. For steady-state flow the boundary conditions at infinity shift on the boundary of sufficiently large domain. In this thesis, it is assumed that at sufficiently far from two-cylinders boundary, the uniform stream boundary conditions are utilized.

$$\vec{U} = \vec{U}_\infty \text{ and } p = p_\infty.$$

To be more exact we choose far boundary as the following

$$S_\varepsilon^1 = \{(\xi, \eta) | (\eta = \pm\varepsilon_\eta \text{ and } 0 \leq \xi \leq \varepsilon_\xi) \cup (\xi = \varepsilon_\xi \text{ and } -\varepsilon_\eta \leq \eta \leq \varepsilon_\eta)\}$$

$$S_\varepsilon^2 = \{(\xi, \eta) | (\eta = \pm\varepsilon_\eta \text{ and } 2\pi - \varepsilon_\xi \leq \xi \leq 2\pi) \cup (\xi = 2\pi - \varepsilon_\xi \text{ and } -\varepsilon_\eta \leq \eta \leq \varepsilon_\eta)\}$$

where $\varepsilon_\xi, \varepsilon_\eta$ sufficiently small positive numbers.

In Figure 3.3 this far boundaries are shown by doubled lines. For sake of simplicity of computational code boundaries S_ε^1 and S_ε^2 coincide with coordinate lines $\xi = \text{const}$ and $\eta = \text{const}$. So, in the shadowed domain (see Figure 3.3) we do not compute velocity and pressure. At the nodes of mesh which located on S_ε^1 and S_ε^2 we assumed that

$$\begin{aligned} v_\xi = v &= \left(-\frac{h}{a} \sinh \eta \sin \xi\right)(v_x)_\infty + \left(\frac{h}{a}(\cosh \eta \cos \xi - 1)\right)(v_y)_\infty, \\ v_\eta = u &= \left(-\frac{h}{a}(\cosh \eta \cos \xi - 1)\right)(v_x)_\infty + \left(-\frac{h}{a} \sinh \eta \sin \xi\right)(v_y)_\infty. \\ p &= p_\infty \end{aligned} \quad (3.17)$$

Space Discretization

For the sake of simplicity we consider only explicit projection method without pressure correction ($\alpha = 1, \theta = k = 0, \beta_1 = \beta_2 = 0$). In the projection method, the first step consists on solving an analog to equation (3.8) which yields an intermediate velocity field $\tilde{\vec{v}} = (\tilde{v}_\xi, \tilde{v}_\eta) = (\tilde{v}, \tilde{u})$ that do not satisfy the divergence constraint. We used the following finite difference approximation of equation (3.8) in the component form

$$\begin{aligned}
& \frac{\tilde{v}_{i,j+1/2} - v_{i,j+1/2}^n}{\Delta t} + \\
& + \frac{1}{h_{i,j+1/2}} \left(v_{i,j+1/2}^n \left(\frac{\partial v}{\partial \xi} \right)_{i,j+1/2}^n + u_{i,j+1/2}^n \left(\frac{\partial v}{\partial \eta} \right)_{i,j+1/2}^n \right) - \\
& - \frac{1}{a} \left(\sinh \eta (v_{i,j+1/2}^n u_{i,j+1/2}^n) - \sin \xi (u_{i,j+1/2}^n)^2 \right) = \\
& = - \frac{1}{h_{i,j+1/2}} \left(\frac{\partial p}{\partial \xi} \right)_{i,j+1/2}^n + \\
& + \frac{1}{Re} \frac{1}{h_{i,j+1/2}^2} \left[\left(\frac{\partial^2 v}{\partial \xi^2} \right)_{i,j+1/2}^n + \left(\frac{\partial^2 v}{\partial \eta^2} \right)_{i,j+1/2}^n \right] - \\
& - \frac{1}{Re} \frac{1}{h_{i,j+1/2}} \left[\frac{2}{a} \left(\sinh \eta \left(\frac{\partial u}{\partial \xi} \right)_{i,j+1/2}^n - \sin \xi \left(\frac{\partial u}{\partial \eta} \right)_{i,j+1/2}^n \right) \right] - \\
& - \frac{1}{Re} \frac{1}{h_{i,j+1/2}} \left[\left(\frac{\cosh \eta + \cos \xi}{a} \right) v_{i,j+1/2}^n \right],
\end{aligned} \tag{3.18}$$

$$\begin{aligned}
& \frac{\tilde{u}_{i+1/2,j} - u_{i+1/2,j}^n}{\Delta t} + \\
& + \frac{1}{h_{i+1/2,j}} \left(v_{i+1/2,j}^n \left(\frac{\partial u}{\partial \xi} \right)_{i+1/2,j}^n + u_{i+1/2,j}^n \left(\frac{\partial u}{\partial \eta} \right)_{i+1/2,j}^n \right) + \\
& + \frac{1}{a} \left(\sinh \eta (v_{i+1/2,j}^n)^2 - \sin \xi (v_{i+1/2,j}^n u_{i+1/2,j}^n) \right) = \\
& = - \frac{1}{h_{i+1/2,j}} \left(\frac{\partial p}{\partial \eta} \right)_{i+1/2,j}^n + \\
& + \frac{1}{Re} \frac{1}{h_{i+1/2,j}^2} \left[\left(\frac{\partial^2 u}{\partial \xi^2} \right)_{i+1/2,j}^n + \left(\frac{\partial^2 u}{\partial \eta^2} \right)_{i+1/2,j}^n \right] + \\
& + \frac{1}{Re} \frac{1}{h_{i+1/2,j}} \left[\frac{2}{a} \left(\sinh \eta \left(\frac{\partial v}{\partial \xi} \right)_{i+1/2,j}^n - \sin \xi \left(\frac{\partial v}{\partial \eta} \right)_{i+1/2,j}^n \right) \right] + \\
& + \frac{1}{Re} \frac{1}{h_{i+1/2,j}} \left[\left(\frac{\cosh \eta + \cos \xi}{a} \right) u_{i+1/2,j}^n \right],
\end{aligned}$$

where for the sake of simplicity we introduced the following notations

$$\begin{aligned}
u_{i,j+1/2}^n &= \frac{1}{4} [u_{i-1/2,j} + u_{i+1/2,j} + u_{i+1/2,j+1} + u_{i-1/2,j+1}] \\
\left(\frac{\partial v}{\partial \xi} \right)_{i,j+1/2}^n &= \frac{1}{J_{i,j+1/2}} \left(\frac{\eta_{i+1/2} - \eta_{i-1/2}}{\Delta \eta} \right) \left[\frac{v_{i,j+3/2} - v_{i,j-1/2}}{2\Delta \xi} \right]
\end{aligned}$$

$$\begin{aligned}
\left(\frac{\partial v}{\partial \eta}\right)_{i,j+1/2}^n &= \frac{1}{J_{i,j+1/2}} \left(\frac{\xi_{j+1} - \xi_j}{\Delta \xi}\right) \left[\frac{v_{i+1,j+1/2} - v_{i-1,j+1/2}}{2\Delta \eta}\right] \\
\left(\frac{\partial p}{\partial \xi}\right)_{i,j+1/2}^n &= \frac{1}{J_{i,j+1/2}} \left(\frac{\eta_{i+1/2} - \eta_{i-1/2}}{\Delta \eta}\right) \left[\frac{p_{i,j+1} - p_{ij}}{\Delta \xi}\right] \\
\left(\frac{\partial^2 v}{\partial \xi^2}\right)_{i,j+1/2}^n &= \frac{1}{J_{i,j+1/2}} \left[\left(\frac{\eta_{i+1/2} - \eta_{i-1/2}}{\Delta \eta} \frac{\Delta \xi}{\xi_{j+3/2} - \xi_{j+1/2}}\right) (v_{i,j+3/2} - v_{i,j+1/2}) - \right. \\
&\quad \left. - \left(\frac{\eta_{i+1/2} - \eta_{i-1/2}}{\Delta \eta} \frac{\Delta \xi}{\xi_{j+1/2} - \xi_{j-1/2}}\right) (v_{i,j+1/2} - v_{i,j-1/2})\right] / (\Delta \xi)^2 \\
\left(\frac{\partial^2 v}{\partial \eta^2}\right)_{i,j+1/2}^n &= \frac{1}{J_{i,j+1/2}} \left[\left(\frac{\xi_{j+1} - \xi_j}{\Delta \xi} \frac{\Delta \eta}{\eta_{i+1} - \eta_i}\right) (v_{i+1,j+1/2} - v_{i,j+1/2}) - \right. \\
&\quad \left. - \left(\frac{\xi_i - \xi_{i-1}}{\Delta \xi} \frac{\Delta \eta}{\eta_i - \eta_{i-1}}\right) (v_{i,j+1/2} - v_{i-1,j+1/2})\right] / (\Delta \eta)^2 \\
\left(\frac{\partial u}{\partial \xi}\right)_{i,j+1/2}^n &= \frac{1}{J_{i,j+1/2}} \left(\frac{\eta_{i+1/2} - \eta_{i-1/2}}{\Delta \eta}\right) [(u_{i+1/2,j+1} + u_{i-1/2,j+1}) - \\
&\quad - (u_{i+1/2,j} + u_{i-1/2,j})] / 2\Delta \xi \\
\left(\frac{\partial u}{\partial \eta}\right)_{i,j+1/2}^n &= \frac{1}{J_{i,j+1/2}} \left(\frac{\xi_{j+1} - \xi_j}{\Delta \xi}\right) [(u_{i+1/2,j+1} + u_{i+1/2,j}) - \\
&\quad - (u_{i-1/2,j+1} + u_{i-1/2,j})] / 2\Delta \eta \\
v_{i+1/2,j}^n &= \frac{1}{4} [v_{i,j-1/2} + v_{i+1,j-1/2} + v_{i+1,j+1/2} + v_{i,j+1/2}] \\
\left(\frac{\partial u}{\partial \xi}\right)_{i+1/2,j}^n &= \frac{1}{J_{i+1/2,j}} \left(\frac{\eta_{i+1} - \eta_{i-1}}{2\Delta \eta}\right) \left[\frac{u_{i+1/2,j+1} - u_{i+1/2,j-1}}{2\Delta \xi}\right] \\
\left(\frac{\partial u}{\partial \eta}\right)_{i+1/2,j}^n &= \frac{1}{J_{i+1/2,j}} \left(\frac{\xi_{j+1} - \xi_{j-1}}{2\Delta \xi}\right) \left[\frac{u_{i+3/2,j} - u_{i-1/2,j}}{2\Delta \eta}\right] \\
\left(\frac{\partial p}{\partial \eta}\right)_{i+1/2,j}^n &= \frac{1}{J_{i+1/2,j}} \left(\frac{\xi_{j+1} - \xi_{j-1}}{2\Delta \eta}\right) \left[\frac{p_{i+1,j} - p_{ij}}{\Delta \eta}\right] \\
\left(\frac{\partial^2 u}{\partial \xi^2}\right)_{i+1/2,j}^n &= \frac{1}{J_{i+1/2,j}} \left[\left(\frac{\eta_{i+1} - \eta_i}{\Delta \eta} \frac{\Delta \xi}{\xi_{j+1} - \xi_j}\right) (u_{i+1/2,j+1} - u_{i+1/2,j}) - \right. \\
&\quad \left. - \left(\frac{\eta_{i+1} - \eta_i}{\Delta \eta} \frac{\Delta \xi}{\xi_j - \xi_{j-1}}\right) (u_{i+1/2,j} - u_{i+1/2,j-1})\right] / (\Delta \xi)^2 \\
\left(\frac{\partial^2 u}{\partial \eta^2}\right)_{i+1/2,j}^n &= \frac{1}{J_{i+1/2,j}} \left[\left(\frac{\xi_{j+1/2} - \xi_{j-1/2}}{\Delta \xi} \frac{\Delta \eta}{\eta_{i+3/2} - \eta_{i+1/2}}\right) (u_{i+3/2,j} - u_{i+1/2,j}) - \right. \\
&\quad \left. - \left(\frac{\xi_{j+1/2} - \xi_{j-1/2}}{\Delta \xi} \frac{\Delta \eta}{\eta_{i+1/2} - \xi_{i-1/2}}\right) (u_{i+1/2,j} - u_{i-1/2,j})\right] / (\Delta \eta)^2 \\
\left(\frac{\partial v}{\partial \xi}\right)_{i+1/2,j}^n &= \frac{1}{J_{i+1/2,j}} \left(\frac{\eta_{i+1} - \eta_i}{\Delta \eta}\right) [(v_{i+1,j+1/2} + v_{i,j+1/2}) - \\
&\quad - (v_{i+1,j-1/2} + v_{i,j-1/2})] / 2\Delta \xi \\
\left(\frac{\partial v}{\partial \eta}\right)_{i+1/2,j}^n &= \frac{1}{J_{i+1/2,j}} \left(\frac{\xi_{j+1/2} - \xi_{j-1/2}}{\Delta \xi}\right) [(v_{i+1,j+1/2} + v_{i+1,j-1/2}) - \\
&\quad - (v_{i,j+1/2} + v_{i,j-1/2})] / 2\Delta \eta
\end{aligned}$$

Since, u^n, v^n are known in all nodes of the computational domain, including the boundaries, the above explicit method allows to determine \tilde{u}, \tilde{v} in all nodes of computational domain, including the boundaries. (To approximate the derivative near the boundary we use onside second order finite differences on nonuniform stencil). That is to say, in the present explicit scheme, no specific boundary conditions are needed for the intermediate velocity field $\tilde{\vec{v}} = (\tilde{v}_\xi, \tilde{v}_\eta) = (\tilde{v}, \tilde{u})$ at each time step.

Finite difference approximation of the incompressibility condition (3.5) becomes, for each cells of computational domain,

$$\begin{aligned} & \left(\frac{1}{h_{ij}} \right)^2 \frac{1}{J_{ij}} \left\{ (\eta_{\hat{\eta}})_{ij} \left[\frac{(hv^{n+1})_{i,j+1/2} - (hv^{n+1})_{i,j-1/2}}{\Delta\xi} \right] + \right. \\ & \left. + (\xi_{\hat{\xi}})_{ij} \left[\frac{(hu^{n+1})_{i+1/2,j} - (hu^{n+1})_{i-1/2,j}}{\Delta\eta} \right] \right\} = 0 \end{aligned} \quad (3.19)$$

where

$$(\eta_{\hat{\eta}})_{ij} = \left(\frac{\partial\eta}{\partial\hat{\eta}} \right)_{ij} = \frac{\eta_{i+1} - \eta_{i-1}}{2\Delta\eta}, \quad (\xi_{\hat{\xi}})_{ij} = \left(\frac{\partial\xi}{\partial\hat{\xi}} \right)_{ij} = \frac{\xi_{j+1} - \xi_{j-1}}{2\Delta\xi}$$

Now to obtain the finite difference equation for pressure, we take the discrete divergence (defined as for equation (3.19)), of equation (3.15). First, inside the domain (see Figure 3.4), we have

$$\begin{aligned} \frac{(v^{n+1})_{i,j+1/2} - (\tilde{v})_{i,j+1/2}}{\Delta t} &= - \left(\frac{1}{h_{ij}} \right)^2 \left(\frac{p_{i,j+1}^{n+1} - p_{i,j}^{n+1}}{\Delta\xi} \right) \\ \frac{(u^{n+1})_{i+1/2,j} - (\tilde{u})_{i+1/2,j}}{\Delta t} &= - \left(\frac{1}{h_{ij}} \right)^2 \left(\frac{p_{i+1,j}^{n+1} - p_{i,j}^{n+1}}{\Delta\eta} \right) \end{aligned} \quad (3.20)$$

Hence, using the incompressibility condition (3.19) :

$$\begin{aligned} & \frac{1}{J_{ij}} \left\{ \frac{1}{(\Delta\xi)^2} \left[\left(\frac{\eta_{\hat{\eta}}}{\xi_{\hat{\xi}}} \right)_{i,j+1/2} (p_{i,j+1}^{n+1} - p_{ij}^{n+1}) - \left(\frac{\eta_{\hat{\eta}}}{\xi_{\hat{\xi}}} \right)_{i,j-1/2} (p_{i,j}^{n+1} - p_{i,j-1}^{n+1}) \right] \right. \\ & \left. + \frac{1}{(\Delta\eta)^2} \left[\left(\frac{\xi_{\hat{\xi}}}{\eta_{\hat{\eta}}} \right)_{i+1/2,j} (p_{i+1,j}^{n+1} - p_{ij}^{n+1}) - \left(\frac{\xi_{\hat{\xi}}}{\eta_{\hat{\eta}}} \right)_{i-1/2,j} (p_{i,j}^{n+1} - p_{i-1,j}^{n+1}) \right] \right\} \\ &= \frac{1}{J_{ij}} \frac{1}{\Delta t} \left\{ (\eta_{\hat{\eta}})_{ij} \left[\frac{(h\tilde{v})_{i,j+1/2} - (h\tilde{v})_{i,j-1/2}}{\Delta\xi} \right] \right. \\ & \left. + (\xi_{\hat{\xi}})_{ij} \left[\frac{(h\tilde{u})_{i+1/2,j} - (h\tilde{u})_{i-1/2,j}}{\Delta\eta} \right] \right\} \end{aligned} \quad (3.21)$$

Then, near the boundary, for example when $i = 2$ (see Figure 3.4), equation (3.19) becomes

$$(\eta_{\hat{\eta}})_{2j} \left[\frac{(hv^{n+1})_{2,j+1/2} - (hv^{n+1})_{2,j-1/2}}{\Delta\xi} \right] + (\xi_{\hat{\xi}})_{ij} \left[\frac{(hu^{n+1})_{5/2,j} - (hu^{n+1})_{3/2,j}}{\Delta\eta} \right] = 0$$

So, when we apply this discrete divergency to equation (3.15), we find pressure at $(n+1)\Delta t$ for $i = 2$ and $j = 2, \dots, N+1$

$$\begin{aligned} & \frac{1}{(\Delta\xi)^2} \left[\left(\frac{\eta_{\hat{\eta}}}{\xi_{\hat{\xi}}} \right)_{2,j+1/2} (p_{2,j+1}^{n+1} - p_{2j}^{n+1}) - \left(\frac{\eta_{\hat{\eta}}}{\xi_{\hat{\xi}}} \right)_{2,j-1/2} (p_{2,j}^{n+1} - p_{2,j-1}^{n+1}) \right] \\ & + \frac{1}{(\Delta\eta)^2} \left[\left(\frac{\xi_{\hat{\xi}}}{\eta_{\hat{\eta}}} \right)_{5/2,j} (p_{3,j}^{n+1} - p_{2,j}^{n+1}) - \left(\frac{\xi_{\hat{\xi}}}{\eta_{\hat{\eta}}} \right)_{3/2,j} (p_{2,j}^{n+1} - p_{1,j}^{n+1}) \right] \\ & = (\eta_{\hat{\eta}})_{2j} \left[\frac{(h\tilde{v})_{2,j+1/2} - (h\tilde{v})_{2,j-1/2}}{\Delta\xi} \right] + (\xi_{\hat{\xi}})_{2j} \left[\frac{(h\tilde{u})_{5/2,j} - (h\tilde{u})_{3/2,j}}{\Delta\eta} \right] \end{aligned}$$

with the following definition for the pressure on the fiction mesh points

$$p_{1,j}^{n+1} = p_{2,j}^{n+1}.$$

The same technique is used near the boundary $\eta = \eta_1$.

The discrete divergency is used to construct difference equation for pressure near boundaries S_ε^1 and S_ε^2 . The pressure at the fictitious mesh points is assumed to be equal p_∞ . As a result, owing to discrete incompressibility condition for each computational cells we have finite difference equation for pressure with the Neuman type boundary conditions on rigid boundaries $\eta = \eta_1, \eta = \eta_2$, periodic boundary condition on boundaries $\xi = 0, \xi = 2\pi$ ($p(0, \eta) = p(2\pi, \eta)$) and the Dirichlet type boundary condition on boundaries S_ε^1 and S_ε^2 . This system of algebraic equations is solved by iterative method of stabilizing corrections (Yanenko (1970)). Detailed description of the method of stabilizing corrections can be found in the Appendix.

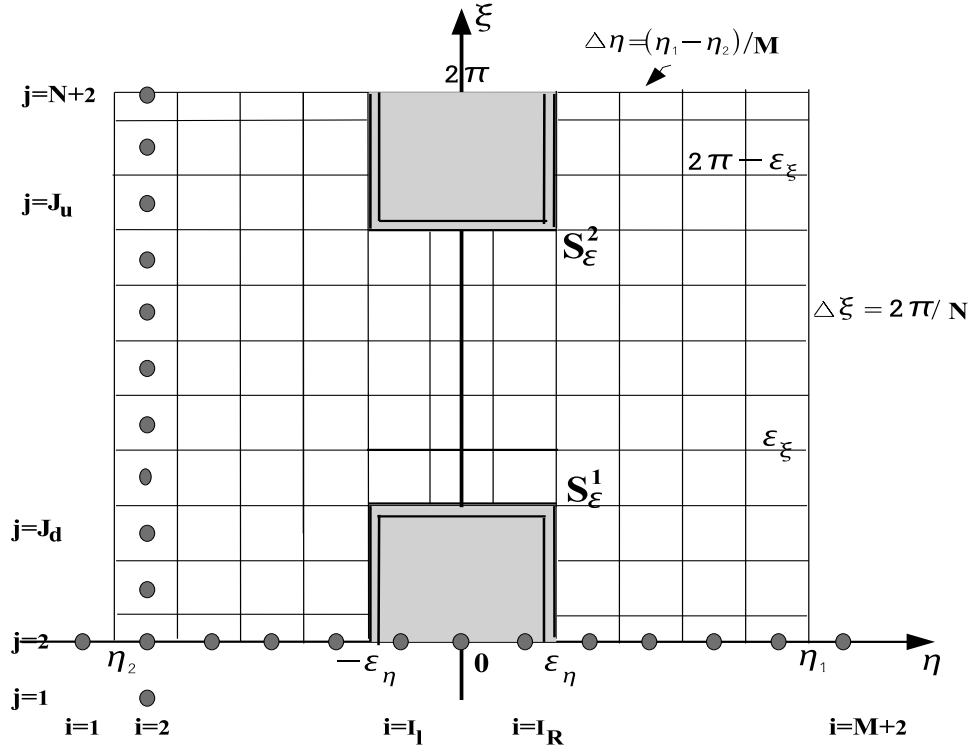


Figure 3.4 Grid construction

Once p is known, the last step of the method is to update the velocity field at the instant $(n+1)\Delta t$ by using equation (3.15)

$$\begin{aligned}
 v_{i,j+1/2}^{n+1} &= \tilde{v}_{i,j+1/2} - \Delta t \left(\frac{1}{h_{ij}} \right)^2 \left(\frac{p_{i,j+1}^{n+1} - p_{i,j}^{n+1}}{\Delta \xi} \right) \\
 u_{i+1/2,j}^{n+1} &= \tilde{u}_{i+1/2,j} - \Delta t \left(\frac{1}{h_{ij}} \right)^2 \left(\frac{p_{i+1,j}^{n+1} - p_{i,j}^{n+1}}{\Delta \eta} \right)
 \end{aligned} \tag{3.22}$$

$$i = 2, \dots, M+1; j = 2, \dots, N+1.$$

The steady state compute solution is defined by

$$\frac{\|\theta^{n+1} - \theta^n\|}{\Delta t \|\theta^{n+1}\|} < \varepsilon \tag{3.23}$$

where $\theta = (v_\xi, v_\eta, C_D, C_L)$; Δt is the time step and θ^n refers to numerical approximation at time $n\Delta t$, ε is sufficiently small positive number (ε has been chosen such that variation of C_D and C_L on the large time interval less than 0.1%).

3.3 Force Computation

When a solid body is placed in a fluid flow the direction of the force on the body does not coincide with the direction of the (undisturbed) flow. It is very convenient to decompose the force into components F_L and F_D , perpendicular and parallel to the flow direction, respectively. F_L is the lift force. F_D is the drag force, the resistance. In self-propelled steady motion F_D has to be balanced by the thrust force generated by the engines. The lift and drag forces are usually expressed as

$$F_L = 0.5C_L\rho AU_\infty^2,$$

$$F_D = 0.5C_D\rho AU_\infty^2,$$

where F_L, F_D are lift and drag force, respectively, C_L and C_D are called lift and drag coefficient, ρ is fluid density, A is reference area (choice of reference area A affects the value of C_D and C_L).

Let us turn back to the fluid flow past two cylinders. If F_{x_i} and F_{y_i} , $i = 1, 2$ are the lift and drag on the cylinders, the lift and drag coefficients are defined by

$$C_{L_i} = \frac{F_{x_i}}{\rho U_\infty D}, \quad C_{D_i} = \frac{F_{y_i}}{\rho U_\infty D}, \quad i = 1, 2, \quad (3.24)$$

and each consists of components due to the friction forces and the pressure. Hence

$$C_L = C_{L_f} + C_{L_p}, \quad C_D = C_{D_f} + C_{D_p}, \quad (3.25)$$

where

$$C_{L_p} = -\frac{1}{\rho U_\infty D} \int_{\Sigma} p\vec{n} \cdot \vec{i}_x \, dS,$$

$$C_{L_f} = -\frac{1}{\rho U_\infty D} \int_{\Sigma} \mu(\vec{n} \times \vec{\omega}) \cdot \vec{i}_x \, dS,$$

$$C_{D_p} = -\frac{1}{\rho U_\infty D} \int_{\Sigma} p\vec{n} \cdot \vec{i}_y \, dS,$$

$$C_{D_f} = -\frac{1}{\rho U_\infty D} \int_{\Sigma} \mu(\vec{n} \times \vec{\omega}) \cdot \vec{i}_y \, dS,$$

Here \vec{i}_x, \vec{i}_y are unit vectors in x and y axes directions.

This non-dimensional coefficients C_L and C_D are evaluated by an integration around cylinders walls. The formulas for coefficients in cylindrical bipolar coordinates are the following

$$\begin{aligned}
C_{L_p} &= - \int_0^{2\pi} hp \left[\left(-\frac{h}{a} \sinh \eta \sin \xi \right) n_\xi + \left(-\frac{h}{a} (\cosh \eta \cos \xi - 1) \right) n_\eta \right] d\xi \\
C_{L_f} &= - \int_0^{2\pi} h\mu\omega \left[\left(-\frac{h}{a} \sinh \eta \sin \xi \right) n_\eta + \left(-\frac{h}{a} (\cosh \eta \cos \xi - 1) \right) n_\xi \right] d\xi \\
C_{D_p} &= - \int_0^{2\pi} hp \left[\left(\frac{h}{a} (\cosh \eta \cos \xi - 1) \right) n_\xi + \left(-\frac{h}{a} \sinh \eta \sin \xi \right) n_\eta \right] d\xi \\
C_{D_f} &= - \int_0^{2\pi} h\mu\omega \left[\left(\frac{h}{a} (\cosh \eta \cos \xi - 1) \right) n_\eta + \left(-\frac{h}{a} \sinh \eta \sin \xi \right) n_\xi \right] d\xi
\end{aligned} \tag{3.26}$$

where n_ξ and n_η are component of outward unit normal vector in ξ and η direction, respectively and ω is component of vorticity in direction z

$$\omega = -\frac{1}{h} \left[\frac{\partial v_\xi}{\partial \eta} - \frac{\partial v_\eta}{\partial \xi} - \frac{h}{a} (\sinh \eta v_\xi - \sin \xi v_\eta) \right]$$

To evaluate integrals in equation (3.26), we used trapezoidal rule.

CHAPTER IV

VALIDATION OF NUMERICAL ALGORITHM

It is well known that for large gap spacing between the two surfaces of the cylinders the mutual influence between cylinders disappear, leading to separate flow over single cylinders. To validate the present numerical algorithm, the uniform flow past fixed and rotating circular cylinders with $0 \leq Re \leq 40$, $0 \leq \alpha_1 (= \alpha_2) \leq 2.5$ and with a large gap between cylinder surfaces, $g = 14$, have been calculated and the results are compared with experimental and simulation data for flow past a single cylinder. All the simulations have been performed in a large domain so as to reduce the influence of the outer boundary. A sequence of uniform grids is used. Because the cylinder wake is stable to perturbations in the flow regime below $Re \leq 46 \pm 1$ the flow will reach a steady state for $Re \leq 40$.

4.1 Flow Past Two Nonrotating Circular Cylinders (Large Gap Spacing)

We begin code validation with flow that tests the spatial fidelity of algorithm without the complication associated with nontrivial boundary condition on cylinders surface. In this paragraph, we consider the two-dimensional flow over two identical circular cylinders in a side by side arrangement at the low Reynolds numbers ($5 \leq Re \leq 40$) and large gap spacing between cylinder centers, $g = 14$. Figure 4.1 shows variations of the drag and lift coefficients (C_D and C_L) with

the gap spacing at fixed Reynolds number $Re = 20$. Obviously the quantities depend on gap spacing and for large gap spacing approach the value of drag coefficient of single-cylinder. It is shown that the drag coefficient stay nearly constant, with values slightly larger than the single-cylinder one, in the range of $g \geq 8 \div 9D$. In the same range of g the lift coefficient almost zero. In the range of $4 \div 5D \leq g \leq 8 \div 9D$, C_D is up to 10% larger than the C_D of the single-cylinder. Drag coefficient steeply increases with decreasing g in the range $g \leq 4 \div 5D$. The lift coefficient steeply increases with decreasing g in the range $g \leq 3D$.

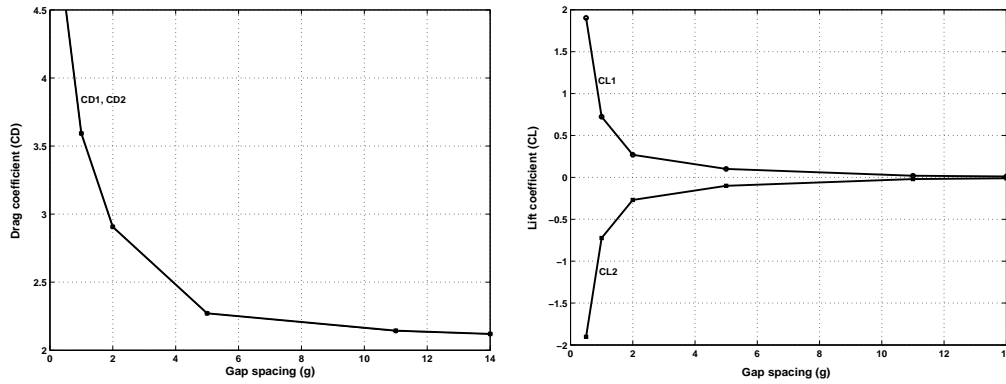


Figure 4.1 Variations of the drag and lift coefficients with g at $Re = 20$

Figure 4.2 shows comparison of pressure distribution around the cylinder surface for the Reynolds number $Re = 40$ with experimental results from Thom for $Re = 36, 45$ and numerical results from Apelt and Kawaguti for $Re = 40$ (see in Batchelor (2000)). Our results are shown by solid line. The wake of an isolated cylinder consist of a recirculation zone with steady closed streamline for Reynolds number above $Re \approx 1$ but less than $Re \approx 40$. The length of the region of closed streamlines behind circular cylinders are shown in Figure 4.3 which our results are shown by solid square sign and circle sign represent length which are measured by Taneda (1956). The calculated nondimensional steady-state wake length L_w (the distance from the cylinder trailing edge to the reattachment point) and the drag coefficient $C_D = C_{D_p} + C_{D_f}$ are compared with

previously established results. The current results of wake length and drag coefficient are compared to the numerical simulations and experimental data in Tables 4.1 and 4.2. In Table 4.2, C_{D_p} and C_{D_f} denote the pressure and friction drag coefficients, respectively. The spatial resolution of the mesh is shown in brackets

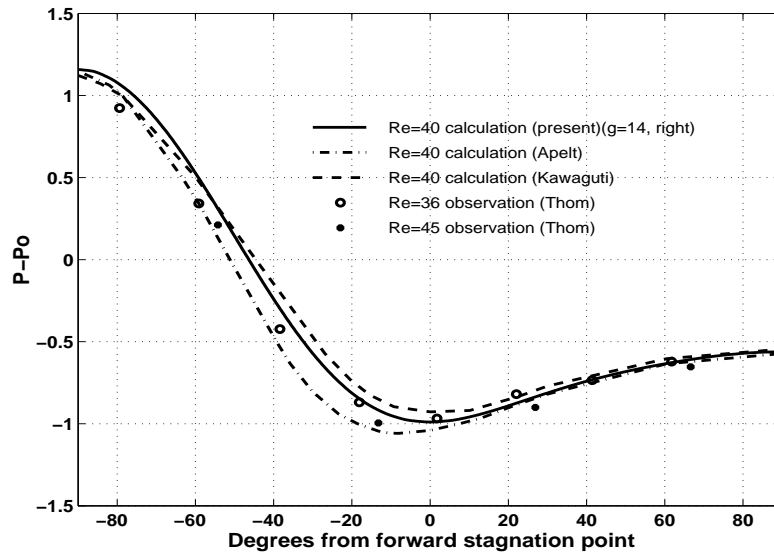


Figure 4.2 Pressure distribution at the surface of a circular cylinder (right), $Re = 40$, $g = 14$

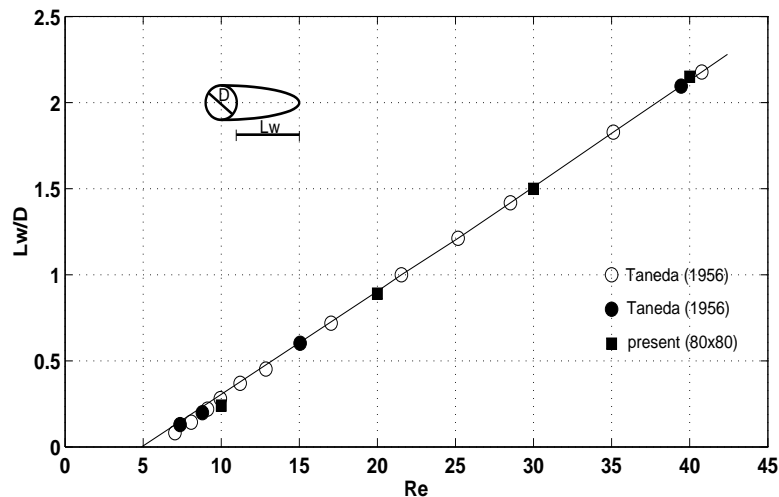


Figure 4.3 Observed lengths of the region of close streamlines behind a circular cylinder

Figures 4.4, 4.5 and 4.6 show the steady-state streamlines, pressure and

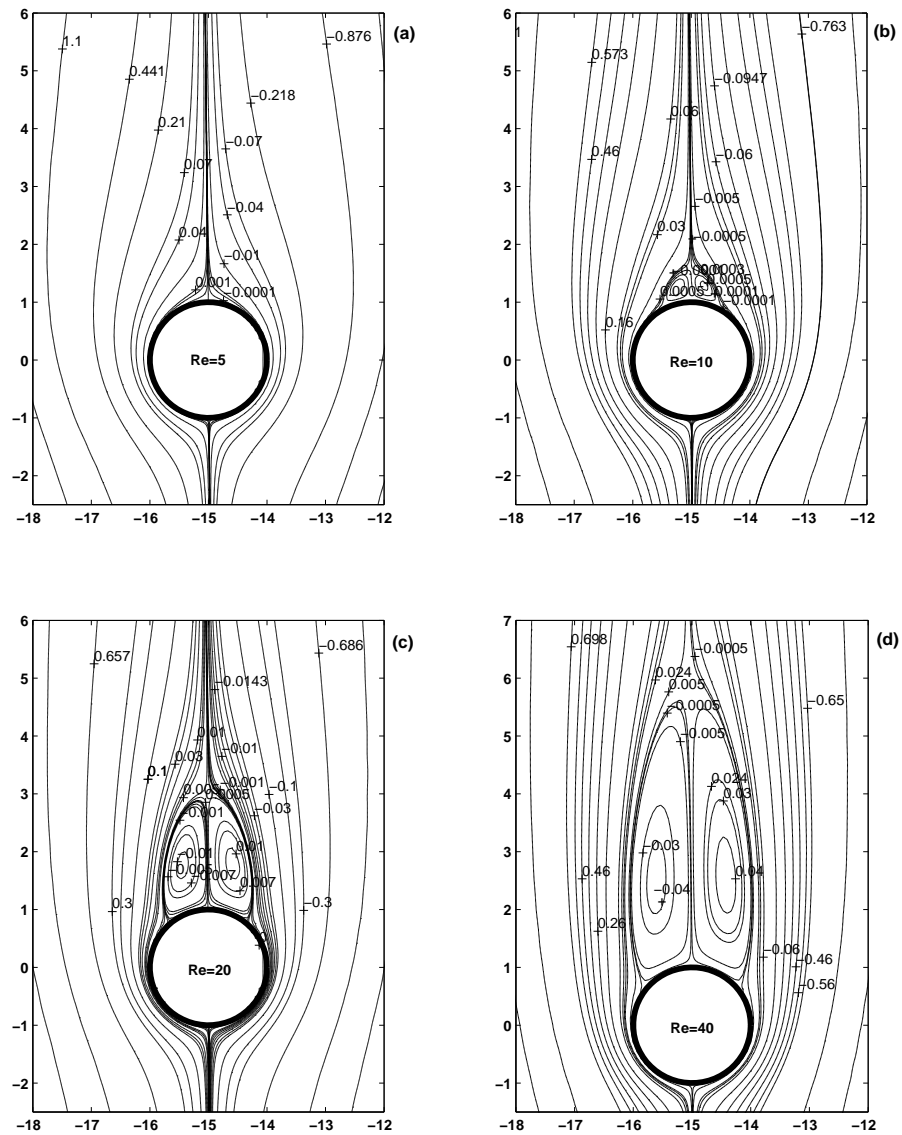


Figure 4.4 Streamline patterns of flow over two circular cylinders (near left cylinder) at $Re = 5, 10, 20$ and 40 with $g = 14D$

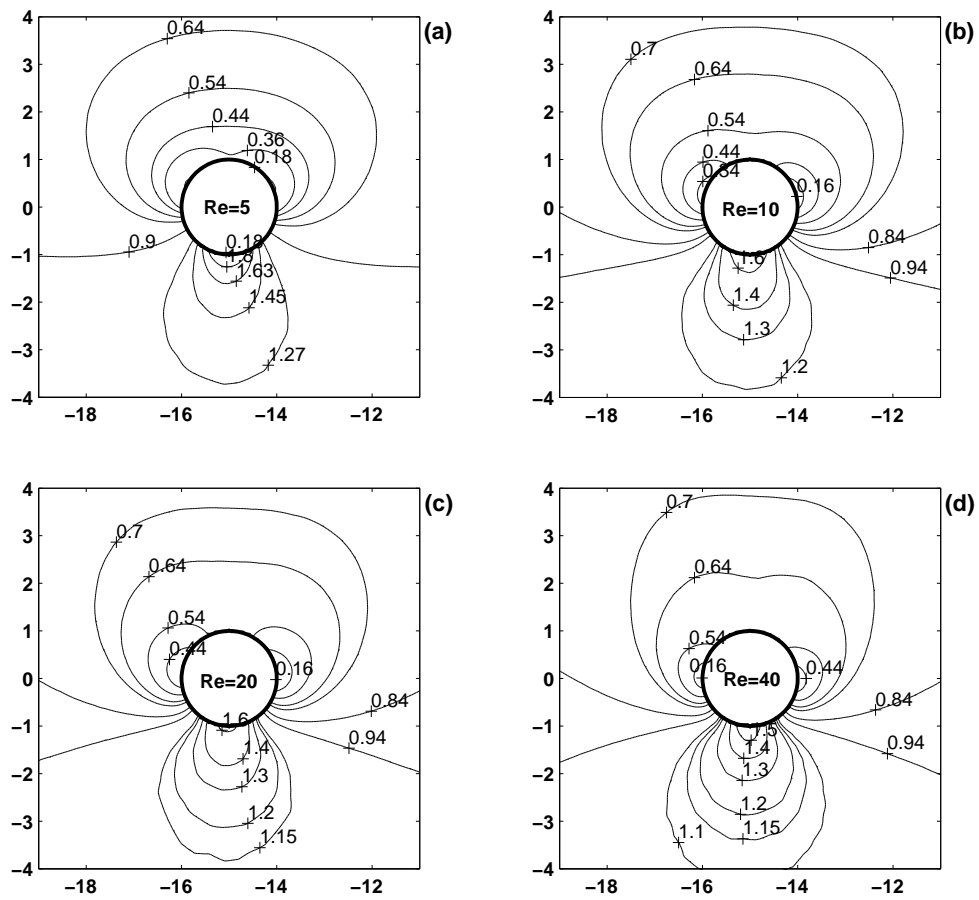


Figure 4.5 Pressure patterns of flow over two circular cylinders (near left cylinder) at $Re = 5, 10, 20$ and 40 with $g = 14D$

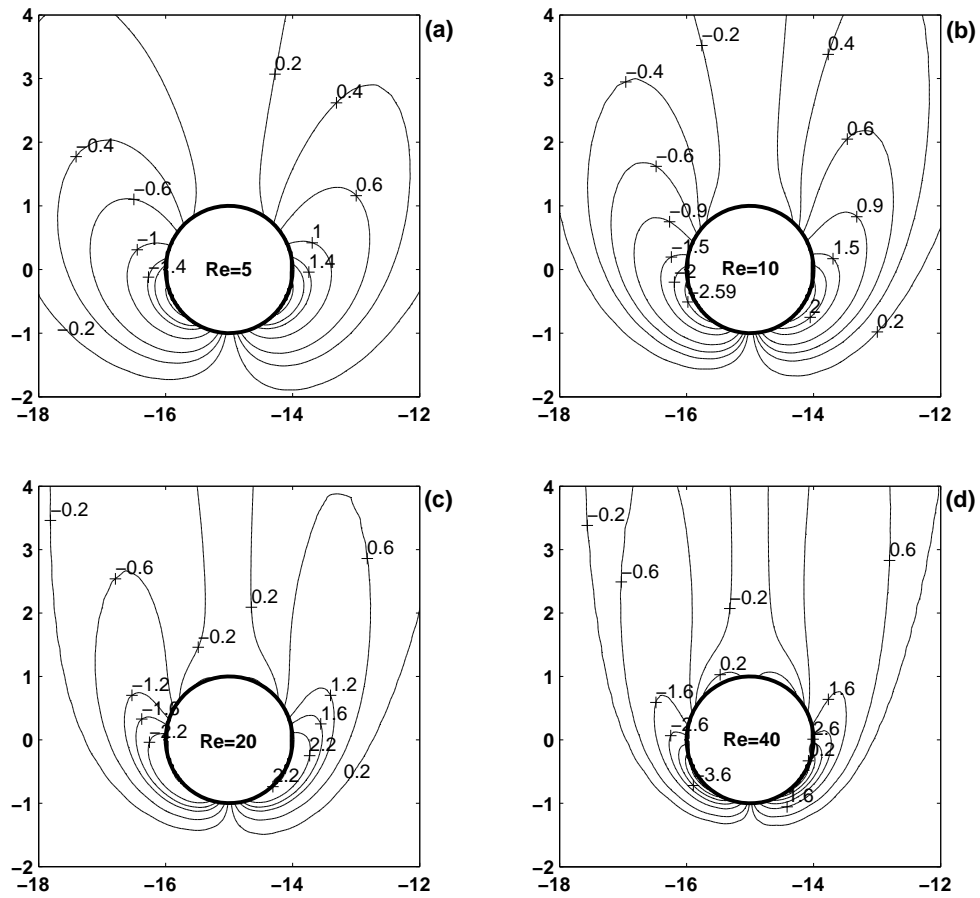


Figure 4.6 Vorticity patterns of flow over two circular cylinders (near left cylinder) at $Re = 5, 10, 20$ and 40 with $g = 14D$

Renolds number	10	20	30	40
Takanmi & Keller (1969)	—	1.870	3.223	4.650
Dennis & Chang (1970)	—	1.880	—	4.690
Nieuwstadt & Kalln (1973)	—	1.786	3.086	4.357
Ta (1975)	—	1.870	—	4.270
Present(80 × 80)	0.525	1.868	3.070	4.408

Table 4.1 Length of wake bubble

vorticity patterns corresponding to the case $Re = 5; 10; 20$ and 40 , $g = 14$, respectively. Due to the symmetry about y -axis we represent the all patterns only around left cylinder. The present all patterns near left cylinder are very similar to those in case of flow past single cylinder at the same Reynolds number. The accuracy of the numerical results is checked by computations on various grids. We performed calculations on sequences of grids with number of nodes 40×40 ($\Delta\xi = 0.16535$, $\Delta\eta = 0.17436$), 80×80 ($\Delta\xi = 0.080554$, $\Delta\eta = 0.086078$) and 160×160 ($\Delta\xi = 0.039767$, $\Delta\eta = 0.042759$). Some data on comparison of the calculation results are represented in Tables 4.2 and 4.3. The comparisons made above show that the present results are in a good agreement with previous results.

4.2 Flow Past Two Rotating Circular Cylinders (Large Gap Spacing)

In this paragraph we study the two-dimensional flow past two rotating circular cylinders of equal radii in side-by-side arrangement at low Reynolds number, $Re \leq 40$, large gap spacing, $g = 14$, and variable rate of rotation ($0.1 \leq \alpha \leq 2$). Both cylinders are placed in a stream (from down to up-positive direction at y -axis) of uniform speed U_∞ at infinite. Left cylinder rotating with constant

Re	Contribution	C_D	C_{D_p}	C_{D_f}	L_W/D
5	Present (20×20)	3.748	1.883	1.865	—
	Present (40×40)	4.050	2.099	1.960	—
	Ingham <i>et al.</i> (1990)(one cylinder)	3.997	2.104	1.843	—
	Batchelor (2000)(one cylinder)	3.995	—	—	—
20	Present (20×20)	2.022	1.193	0.829	0.720
	Present (40×40)	2.069	1.229	0.840	0.840
	Present (80×80)	2.120	1.270	0.850	0.934
	Relf (1913) (one cylinder)	2.160	—	—	—
	Tritton (1959) (one cylinder)	2.080	—	—	—
	Chung (2006) (one cylinder)	2.050	—	—	0.960
	Ingham <i>et al.</i> (1990) (one cylinder)	1.995	1.201	0.794	—
Batchelor (2000) (one cylinder)	2.001	—	—	0.900	
40	Present (40×40)	1.539	1.002	0.537	2.160
	Relf (1913) (one cylinder)	1.620	—	—	—
	Tritton (1959) (one cylinder)	1.590	—	—	—
	Chung (2006) (one cylinder)	1.540	—	—	2.300
	Batchelor (2000) (one cylinder)	1.538	—	—	2.150

Table 4.2 Validation of the numerical algorithm; comparison study for flow over two side-by-side circular cylinders at $g = 14$ with flow over a single cylinder

grid	C_D	C_{D_p}	C_{D_f}	C_L	C_{L_p}	C_{L_f}
40×40	2.069	1.229	0.840	0.020	0.010	0.010
80×80	2.120	1.270	0.850	0.019	0.010	0.009
160×160	2.124	1.274	0.850	0.019	0.010	0.009

Table 4.3 Sequence of grid; Drag and lift coefficient at $Re = 20$ and $g = 14$

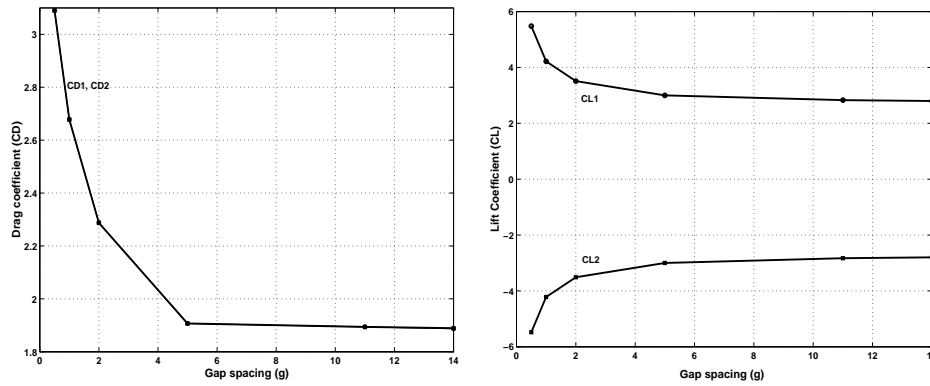


Figure 4.7 Variations of the drag and lift coefficients with g at $Re = 20$ and $\alpha = 1.0$

clockwise angular velocity. Right cylinder rotating with the same constant anti-clockwise angular velocity.

To the author's knowledge, there are very few published data of drag and lift coefficients at $Re \leq 40$ and angular speed even for flow past single cylinders. Figure 4.7 shows variations of the drag and lift coefficient (C_D and C_L) with the gap spacing at fixed Reynolds number $Re = 20$ and fixed angular velocity $\omega = |\omega_1| = |\omega_2| = 1$. For large gap spacing the values of drag coefficients approach the values of drag and lift coefficients of single cylinder rotating in uniform stream.

Table 4.4 lists lift and drag coefficients from our calculation and makes a comparison with Ingham *et al.* (1990), Badr *et al.* (1989) and Chung (2006). It can be seen that the differences are acceptable for C_D and C_L . For $Re = 20$, the flow induced by several angular speeds in interval $0 \leq \alpha_i \leq 2.5$ have been computed. To check accuracy of our algorithm in case of rotation cylinder. We make computation on sequence of grid. Table 4.5 shows the result of our simulation on sequence of grid in case $Re = 20$ with $g = 14$ and $\alpha = 1.0$. Figure 4.8 shows the predicted steady-state streamline patterns for $\alpha = 0.1; 0.5; 1.0; 2.0$, respectively. Due to symmetry we only present the streamline patterns around the left cylinder in Figures 4.8 – 4.9. For the case of a large gap between cylinders

Re	Contribution	C_D			C_L		
		$\alpha = 0.1$	$\alpha = 1.0$	$\alpha = 2.0$	$\alpha = 0.1$	$\alpha = 1.0$	$\alpha = 2.0$
20	Present (80×80)	2.119	1.887	1.363	0.291	2.797	5.866
	Badr <i>et al.</i> (1989)	1.990	2.000	—	0.276	2.740	—
	Ingham <i>et al.</i> (1990)	1.995	1.925	1.627	0.254	2.617	5.719
	Chung (2006)	2.043	1.888	1.361	0.258	2.629	5.507

Table 4.4 Hydrodynamic parameters of flow over a rotating circular cylinder at $Re = 20$ with $g = 14$

grid	C_D	C_{D_p}	C_{D_f}	C_L	C_{L_p}	C_{L_f}
40×40	1.858	1.033	0.825	2.740	2.393	0.347
80×80	1.887	1.061	0.826	2.797	2.437	0.360
160×160	1.901	1.074	0.827	2.802	2.440	0.362

Table 4.5 Sequence of grid; Drag and lift coefficient at $Re = 20$ and $g = 14$, $\alpha = 1.0$

the streamline patterns are similar to those in the flow behind a single cylinder, M.H.Chung (2006) and Batchelor (2000).

4.3 Flow Past Two Nonrotating Circular Cylinders (Small Gap Spacing, $g = 1$)

For the case of small gap between fixed cylinder there is a very few data. In the case of $Re = 40$ and $g = 1$ wake streamline patterns are similar to those in Kang (2003). The computed drag coefficients for both cylinders are nearly the same. The lift coefficients are in the opposite directions. The lift force try to move out cylinders from each other along y -axis. There is about 10% difference

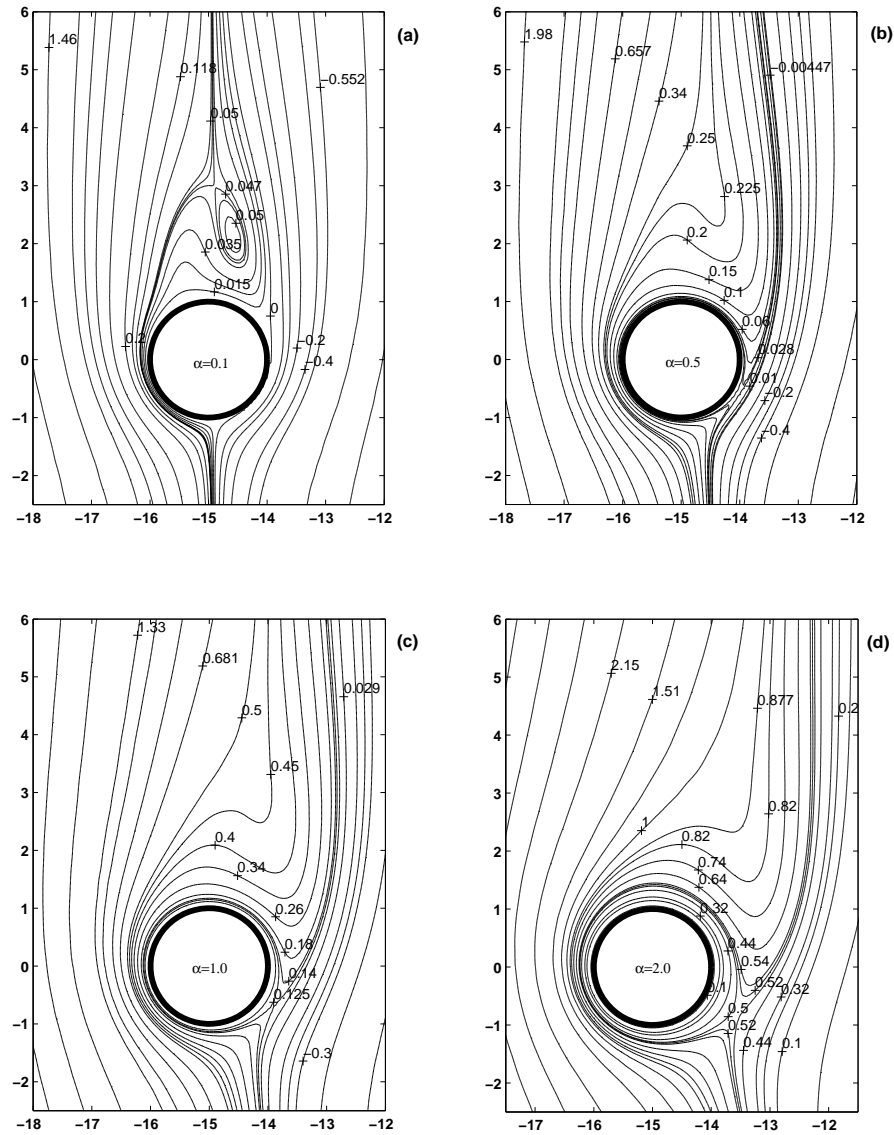


Figure 4.8 Streamline patterns of flow over two rotating circular cylinders at $Re = 20$, $g = 14$, and $\alpha = 0.1, 0.5, 1.0, 2.0$.

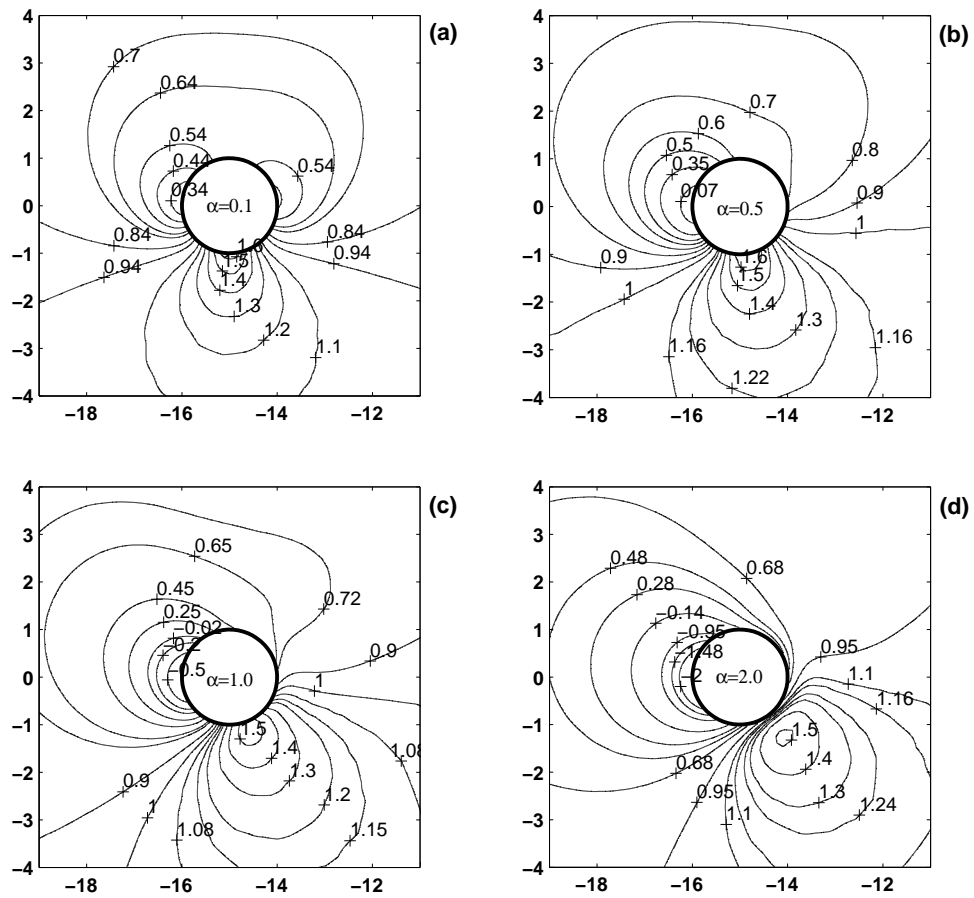


Figure 4.9 Pressure patterns of flow over two rotating circular cylinders at $Re = 20$, $g = 14$, and $\alpha = 0.1, 0.5, 1.0, 2.0$.

in C_D between the present calculation ($C_D = 1.514$) and C_D reported by Kang ($C_{D_{Kang}} = 1.70$). The same difference is occurred for lift coefficient $C_{L_{present}} = 0.358$ and $C_{L_{Kang}} = 0.4$, Relative difference is 10%.

4.4 Results of Validation

The comparison of the data between our computational results and the experimental and numerical data available in the literature shown in Figures 4.1 – 4.9 and Tables 4.1 – 4.4 indicates a satisfactory level of agreement within 10%.

CHAPTER V

SIMULATION RESULTS

After verifying the numerical method, we have conducted numerical simulations of flow past constantly rotating circular cylinders of equal radii in a side-by-side arrangement at Reynolds number $Re = 10, 20$ and 40 , rate of rotation $0.5 \leq \alpha \leq 2.5$ and nondimensional gap spacing $0.5 \leq g \leq 1.5$. Both cylinders are placed in a stream (from down to up) of uniform speed U_∞ at infinity. The left cylinder is rotating with constant clockwise angular velocity. The right cylinder is rotating with the same constant anti-clockwise angular velocity. The sketch of the present problem is shown in Figure 2.1. One of the target of present research is to find self-propelled regime of motion. In the case of two rotating cylinders, drag and lift forces depend on Reynolds number, gap spacing and rate of rotation are defined as follows:

$$C_D = C_D(Re, g, \alpha), \quad C_L = C_L(Re, g, \alpha).$$

Self-propelled motion corresponds to $C_D = C_D(Re, g, \alpha) = 0$, and $C_L = C_L(Re, g, \alpha) = 0$. Let us define α_{crit} as that produces zero drag on a combined body, i.e. at $\alpha = \alpha_{crit}$, $C_D(Re, g, \alpha_{crit}) = 0$, and $C_L = C_L(Re, g, \alpha_{crit}) = 0$. It is clear that α_{crit} depends on Re and g , i.e. $\alpha_{crit} = \alpha_{crit}(Re, g)$.

5.1 Wake Patterns Depending on the Reynolds Number and Rate of Rotation

The influence of the rotation rate $\alpha = \alpha_1 = \alpha_2 = |\omega_i|D/2U_\infty$ is demonstrated in Table 5.1 and Figure 5.1. Table 5.1 and Figure 5.1 give the values of

drag and lift coefficients in case $Re = 10, 20, 40$ and $g = 1$ for $0.5 \leq \alpha \leq 2.5$. Indexes 1 and 2 correspond to the right and left cylinder, respectively. The fluid forces are distributed over the two cylinders such that lift forces in x -direction on the combined system are in equilibrium, $C_{L_1} + C_{L_2} \equiv 0$. However, the fluid forces acting upon an individual cylinder demand that some additional external forces are applied to it in order for its position to remain fixed. There is a repulsive force acting on the cylinders, $C_{L_1} > 0, C_{L_2} < 0$. The absolute values of lift coefficients increase with increasing α , as shown in the sixth column of Table 5.1. The lift forces acting on cylinders are mostly resulted from the pressure force, as can be seen in two last columns of Table 5.1. The pressure contribution in C_L increases with increasing Re , which is the same behavior as observed in the study of Stojkovic *et al.* (2002) for the case of a single rotating cylinder. The drag coefficients decrease with increasing α , see third column of Table 5.1. For $\alpha_{crit} \approx 1.65$ ($Re = 10$), $\alpha_{crit} \approx 1.74$ ($Re = 20$) and $\alpha_{crit} \approx 1.755$ ($Re = 40$) the drag force becomes zero. This case corresponds to the self-propelled motion of cylinders as a coupled body. It is interesting that both C_{D_p} and C_{D_f} decrease with increasing α , see columns 4 and 5 in Table 5.1, resulting in negative values of C_{D_p} and C_{D_f} for higher rotational velocities. This is opposite to the case of flow past single rotating cylinder, where C_{D_f} increases and C_{D_p} decreases with increasing α (Stojkovic *et al.* (2002)). Additionally, for $\alpha \geq 2.0$ the total drag force is negative. In the case of flow around a single rotating cylinder the effect is quite different. It has to be pointed out that the self-propelled regime happened due to different reasons at $Re = 10$, at $Re = 20$ and at $Re = 40$. In case of $Re = 10$ the drag $C_D \simeq 0$ due to $C_{D_p} \approx -C_{D_f} \approx 0.33$. In the case of $Re = 20$ self-propelled regime corresponds to $C_D \simeq 0$ due to $C_{D_p} \approx -C_{D_f} \approx 0$. In case of $Re = 40$ self-propelled regime corresponds to $C_D \simeq 0$ due to $C_{D_p} \approx -C_{D_f} \approx -0.141$. In

α	Re	C_D	C_{D_p}	C_{D_f}	$C_{L_{1,2}}$	$C_{L_{p_{1,2}}}$	$C_{L_{f_{1,2}}}$
0.5	10	1.942	1.219	0.723	± 2.181	± 1.623	± 0.558
	20	1.485	0.919	0.566	± 1.721	± 1.382	± 0.339
	40	1.129	0.727	0.402	± 1.457	± 1.245	± 0.212
1.0	10	1.094	0.824	0.270	± 3.028	± 2.355	± 0.673
	20	0.862	0.530	0.332	± 2.774	± 2.300	± 0.474
	40	0.680	0.389	0.291	± 2.511	± 2.198	± 0.313
1.5	10	0.247	0.440	-0.193	± 3.544	± 2.811	± 0.733
	20	0.260	0.151	0.109	± 3.645	± 3.065	± 0.580
	40	0.222	0.035	0.187	± 3.482	± 3.078	± 0.404
1.65	10	0.004	0.335	-0.331	± 3.633	± 2.894	± 0.739
1.74	20	-0.001	-0.004	0.003	± 3.958	± 3.345	± 0.613
1.755	40	0.000	-0.141	0.141	± 3.971	± 3.520	± 0.451
2.0	10	-0.516	0.134	-0.650	± 3.713	± 2.983	± 0.730
	20	-0.265	-0.152	-0.113	± 4.196	± 3.563	± 0.633
	40	-0.205	-0.305	0.100	± 4.437	± 3.944	± 0.493
2.5	10	-1.199	-0.076	-1.123	± 3.415	± 2.767	± 0.648
	20	-0.685	-0.330	-0.355	± 4.214	± 3.608	± 0.606
	40	-0.502	-0.504	0.002	± 4.988	± 4.461	± 0.527

Table 5.1 Drag and lift coefficient of flow over two rotating circular cylinders at $Re = 10, 20$ and 40 with $g = 1$

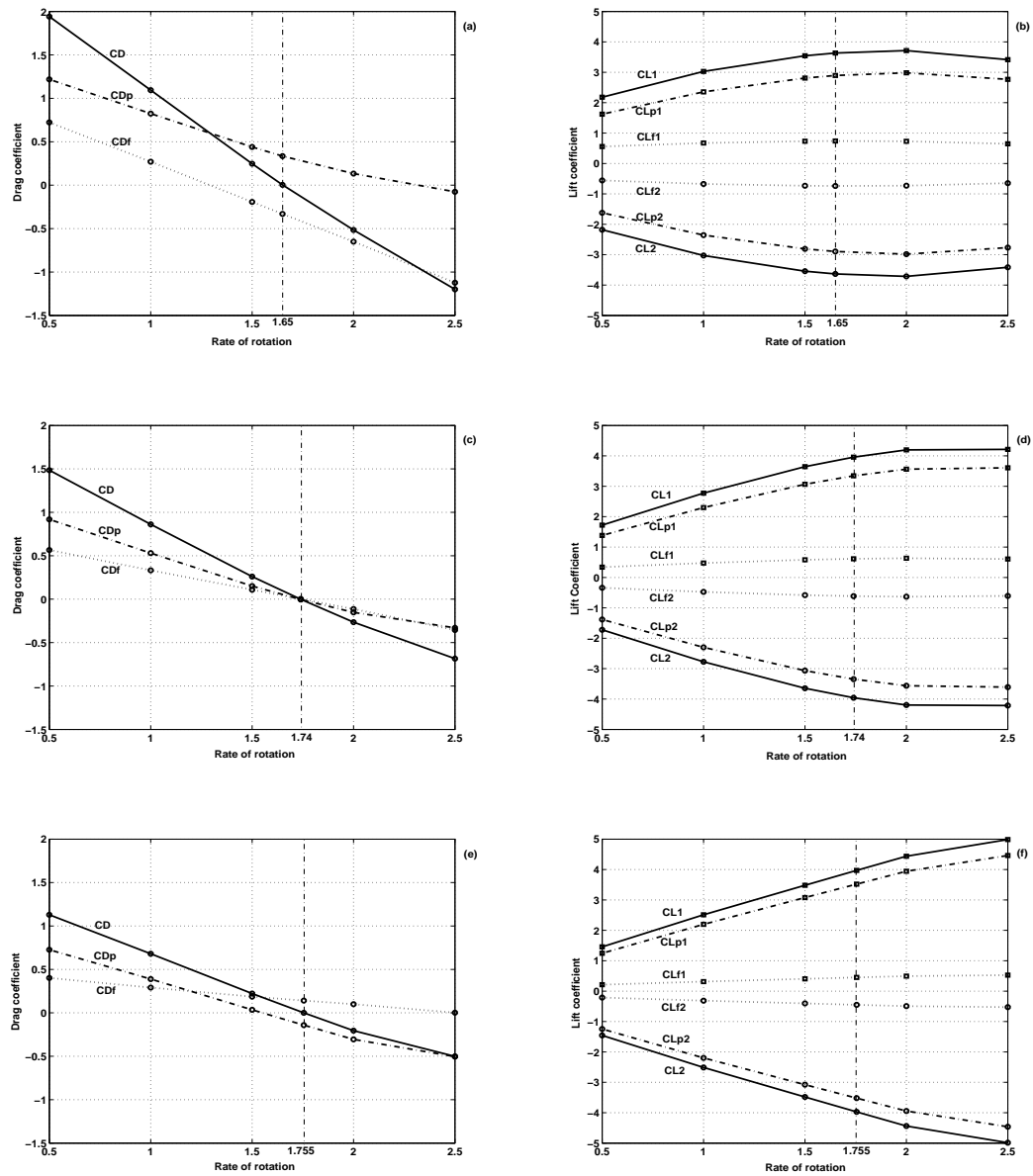


Figure 5.1 Drag and lift coefficients at $Re = 10(a) - (b)$, $20(c) - (d)$, $40(e) - (f)$ and $g = 1$, $\alpha \in [0.5, 2.5]$

Figures 5.2 – 5.4 streamlines patterns are displayed for $Re = 10, 20$ and 40 , $g = 1$ and different rate of rotation $0.5 \leq \alpha \leq 2.5$. All streamline patterns are symmetrical about the y -axis. There are regions of closed streamlines near cylinders for all values of α . These streamlines only exist very close to the cylinders for small values of α . However, as α increases they exist in larger and larger regions as illustrated in Figures 5.2 – 5.4. For small α the space between regions of closed streamlines is sufficiently large that fluid can go through gap between cylinders, see Figures 5.2(a), 5.3(a) and 5.4(a)-(b). As α increases the stagnation points rotate in the direction opposite to the direction of the cylinders rotation and depart from the surfaces of the cylinders and approach the y -axis at the smallest spacing between cylinders. Finally, the space between cylinders surfaces becomes narrow for further increasing of the closed streamlines regions. At α between ~ 1.0 and ~ 1.5 these regions touch each other along y -axis. The stagnation points are now located on the y -axis, both upstream and downstream, as illustrated in Figures 5.2(b)-(d) and 5.3(b)-(d). Further increases in angular velocity of cylinders is a reason of increasing of closed contour regions around the cylinders, see Figures 5.2(c)-(d) and 5.3(c)-(d). The stagnation points on y -axis move upstream and downstream of the cylinders. The stagnation point moves far away from the line between the center of the cylinders. The streamline patterns of the self-propelled regime are represented by Figures 5.2(c) and 5.3(c) for $Re = 10$ and $Re = 20$, respectively. For $Re = 40$, the self-propelled regime $C_D \simeq 0$ occurred before the stagnation point located on y -axis, small amount of fluid can go through gap between cylinders, at $\alpha = 1.755$ (see Figure 5.4(c)).

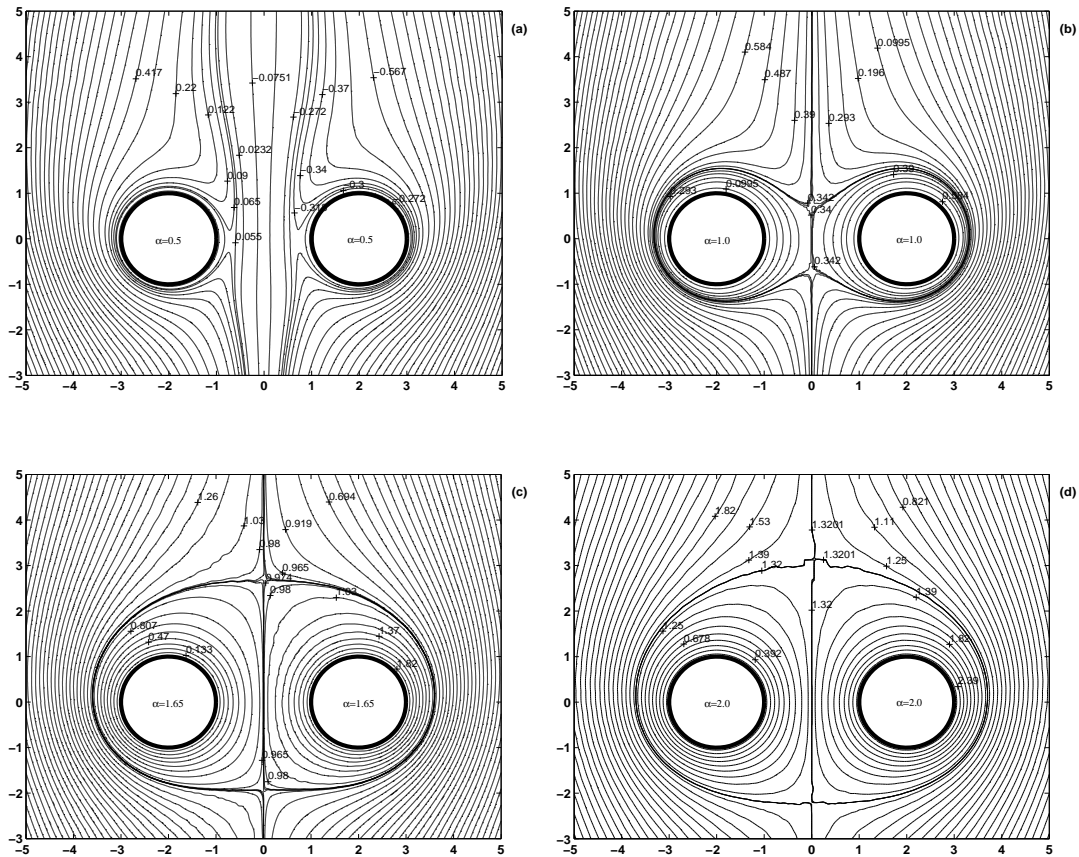


Figure 5.2 Streamline patterns of flow over two circular cylinders at $Re = 10$, $g = 1$, and $\alpha = 0.5, 1.0, 1.65, 2.0$.

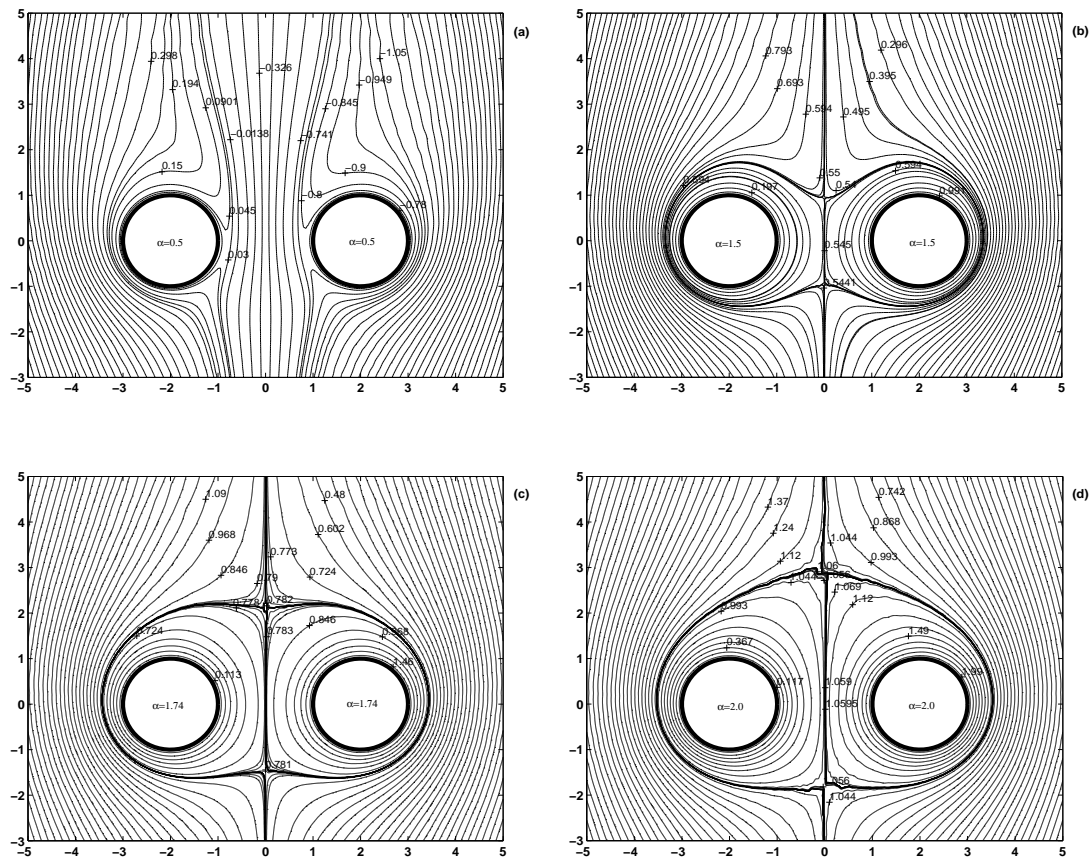


Figure 5.3 Streamline patterns of flow over two circular cylinders at $Re = 20$, $g = 1$, and $\alpha = 0.5, 1.5, 1.74, 2.0$.

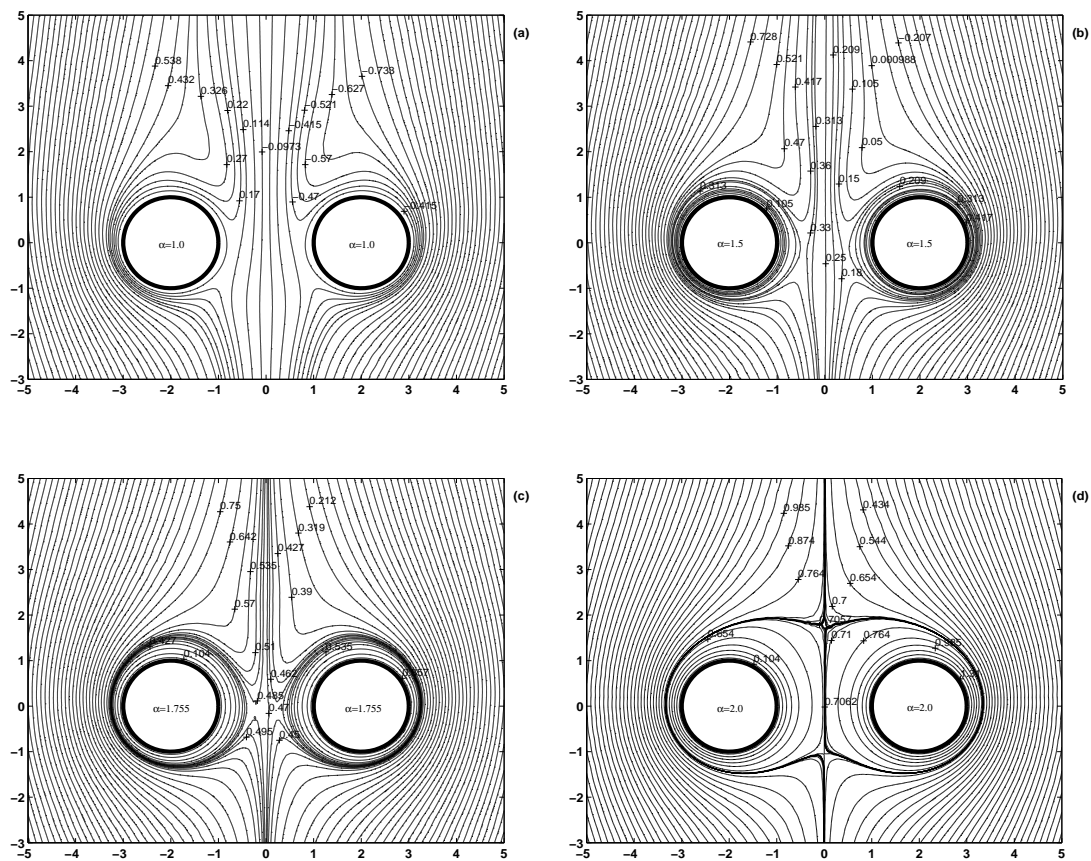


Figure 5.4 Streamline patterns of flow over two circular cylinders at $Re = 40$, $g = 1$, and $\alpha = 1.0, 1.5, 1.755, 2.0$.

5.2 Wake Pattern Depending on Gap Spacing and Rate of Rotation

In this section, we show the results of our numerical simulations in case of fixed Reynolds number, $Re = 20$, and gap spacing $g = 0.5, 1.0, 1.5$ for rate of rotation $0.5 \leq \alpha \leq 2.5$. Table 5.2 gives the values of drag and lift coefficient in case $Re = 20, g = 0.5, 1.0, 1.5$ for $0.5 \leq \alpha \leq 2.5$. We used the same notations as in Table 5.2. The absolute values of lift coefficients increase with increasing g at fixed α , as shown at the six column of Table 5.2. The lift force acting on cylinders mostly result from the pressure force, as can be seen in two last column of Table 5.2. The pressure contribution in C_L increases with increasing gap spacing, g , at fixed rotation rate in case $1.0 \leq \alpha \leq 2.5$. In case $\alpha = 0.5$, small rotation rate, behavior of C_L and C_{L_p} is different. Lift force decreases with increasing g , at the same time C_{L_p} first decreases in case g increases from 0.5 to 1.0 and when g increases from 1.0 to 1.5, C_{L_p} increases slightly. This behavior has to be analyze more carefully and it is a aim of future work.

The drag coefficient increases with increasing, g , at fixed α , see the third column of Table 5.2. Both C_{D_p} and C_{D_f} increase with increasing gap spacing at fixed rate of rotation. The self-propelled regime happen at different rate of rotation when g increase. Rate of rotation corresponding to zero drag force increases with g increase. In the last three rows of Table 5.2 the parameters of self-propelled cylinders are demonstrated. It is interesting that, If $g = 0.5, C_D \approx 0$ due to $-C_{D_f} \approx C_{D_p} = 0.146$, if $g = 1.0, C_D \approx 0$ due to $-C_{D_f} \approx C_{D_p} = 0$, if $g = 1.5, C_D \approx 0$ due to $-C_{D_f} \approx C_{D_p} = -0.196$. For all calculation with $Re = 20$, (represented in Table 5.2) the results for corresponding drag and lift coefficient are shown in Figure 5.5. In Figures 5.6 – 5.9 streamlines for three different gap spacing $g = 0.5, 1.0, 1.5$ at $Re = 20$ and $\alpha = 0.5, 1.5, 2.0, 2.5$ are

α	g	C_D	C_{D_p}	C_{D_f}	$C_{L_{1,2}}$	$C_{L_{p_{1,2}}}$	$C_{L_{f_{1,2}}}$
	0.5	1.039	0.707	0.332	± 1.984	± 1.541	± 0.443
0.5	1.0	1.485	0.919	0.566	± 1.721	± 1.382	± 0.339
	1.5	1.909	1.176	0.733	± 1.684	± 1.392	± 0.292
	0.5	0.311	0.305	0.006	± 2.511	± 2.030	± 0.481
1.0	1.0	0.862	0.530	0.332	± 2.774	± 2.300	± 0.474
	1.5	1.427	0.859	0.568	± 2.954	± 2.506	± 0.448
	0.5	-0.413	-0.053	-0.360	± 2.456	± 2.021	± 0.435
1.5	1.0	0.260	0.151	0.109	± 3.645	± 3.065	± 0.580
	1.5	0.897	0.485	0.412	± 4.169	± 3.571	± 0.598
	0.5	-0.974	-0.268	-0.706	± 2.056	± 1.706	± 0.350
2.0	1.0	-0.265	-0.152	-0.113	± 4.196	± 3.563	± 0.633
	1.5	0.338	0.068	0.270	± 5.378	± 4.630	± 0.748
	0.5	-1.424	-0.343	-1.081	± 0.971	± 0.792	± 0.179
2.5	1.0	-0.685	-0.330	-0.355	± 4.214	± 3.608	± 0.606
	1.5	-0.190	-0.339	0.149	± 6.606	± 5.714	± 0.892
1.245	0.5	-0.002	0.146	-0.148	± 2.664	± 2.180	± 0.484
1.74	1.0	-0.001	-0.004	0.003	± 3.958	± 3.345	± 0.613
2.32	1.5	-0.005	-0.196	0.191	± 6.171	± 5.329	± 0.842

Table 5.2 Drag and lift coefficient of flow over two rotating circular cylinder at $Re = 20$ with $g = 0.5, 1, 1.5$

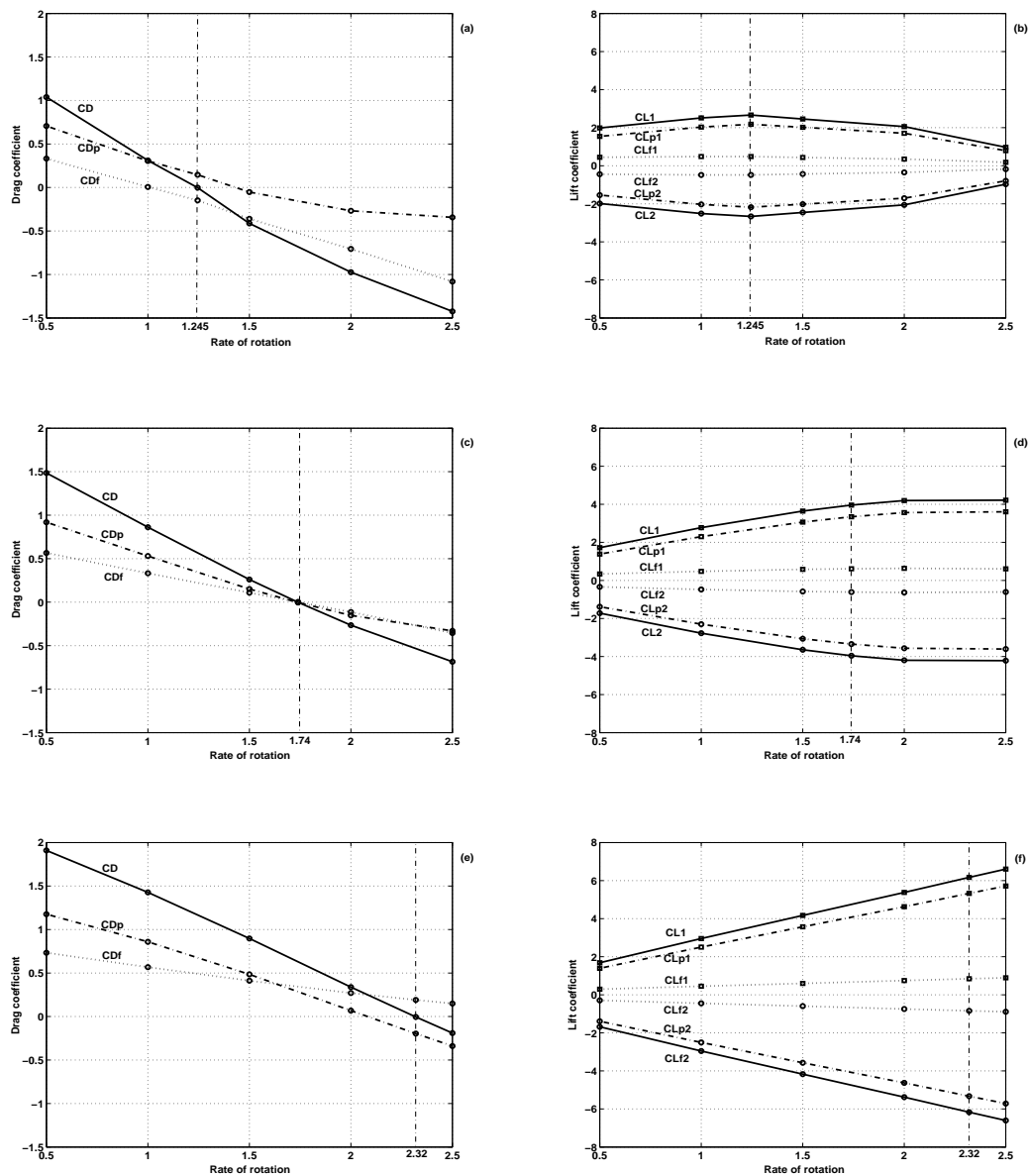


Figure 5.5 Comparison of drag and lift coefficients for different gap spacing $g = 0.5(a) - (b)$, $1.0(c) - (d)$, $1.5(e) - (f)$ and $\alpha \in [0.5, 2.5]$ at $Re = 20$

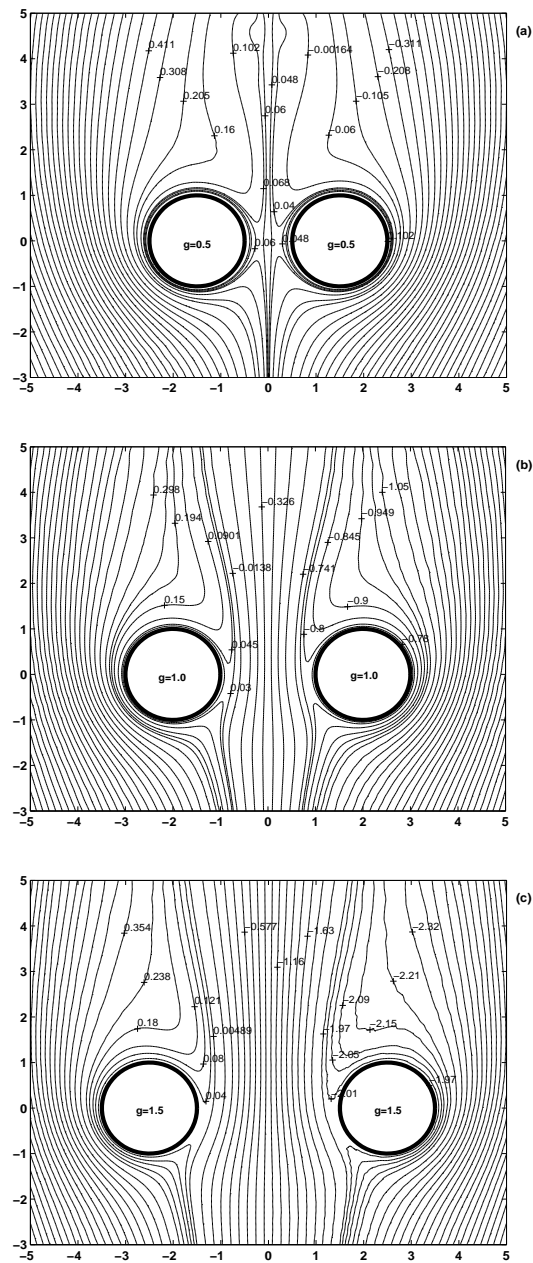


Figure 5.6 Streamline patterns of flow over two circular cylinders at $Re = 20$, $\alpha = 0.5$ and $g = 0.5; 1.0; 1.5$

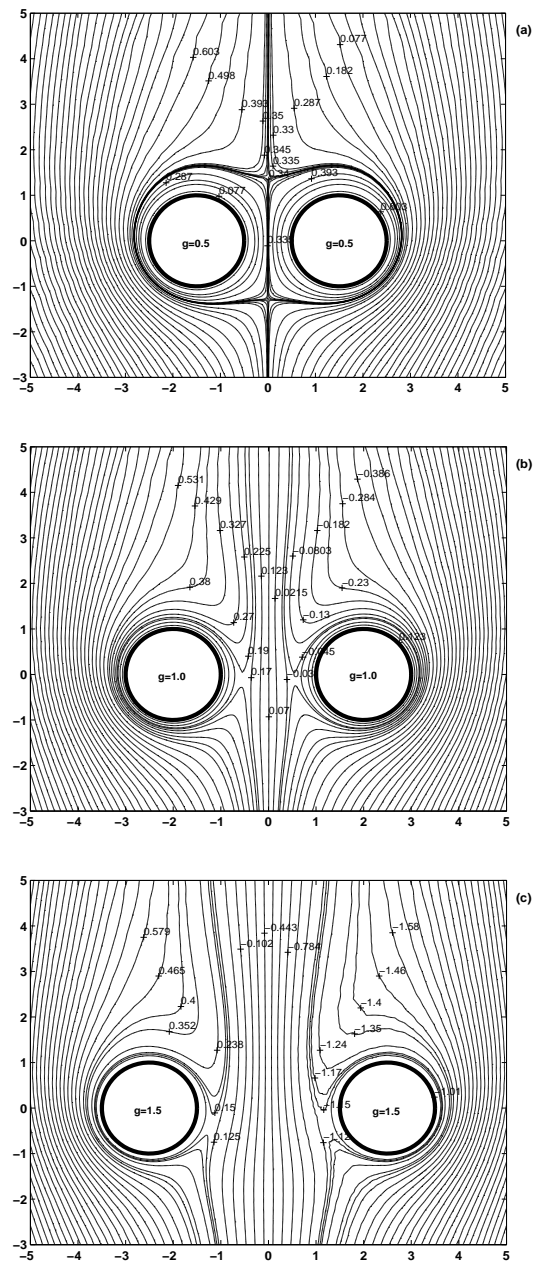


Figure 5.7 Streamline patterns of flow over two circular cylinders at $Re = 20$, $\alpha = 1.0$ and $g = 0.5; 1.0; 1.5$

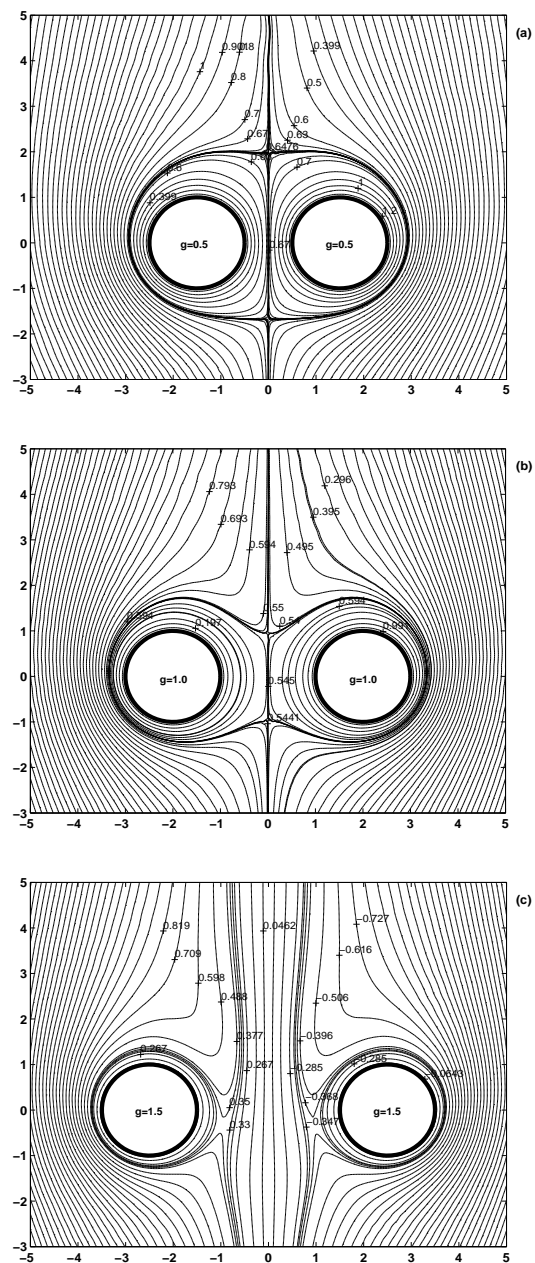


Figure 5.8 Streamline patterns of flow over two circular cylinders at $Re = 20$, $\alpha = 1.5$ and $g = 0.5; 1.0; 1.5$

displayed. Figures 5.10 – 5.13 depicts the pressure distribution around cylinders for the same cases. Figures 5.14 and 5.15 show the streamline patterns and pressure field for $Re = 20$, $\alpha = \alpha_{crit}$ (self-propelled regime) and $g = 0.5, 1.0$ and 1.5.

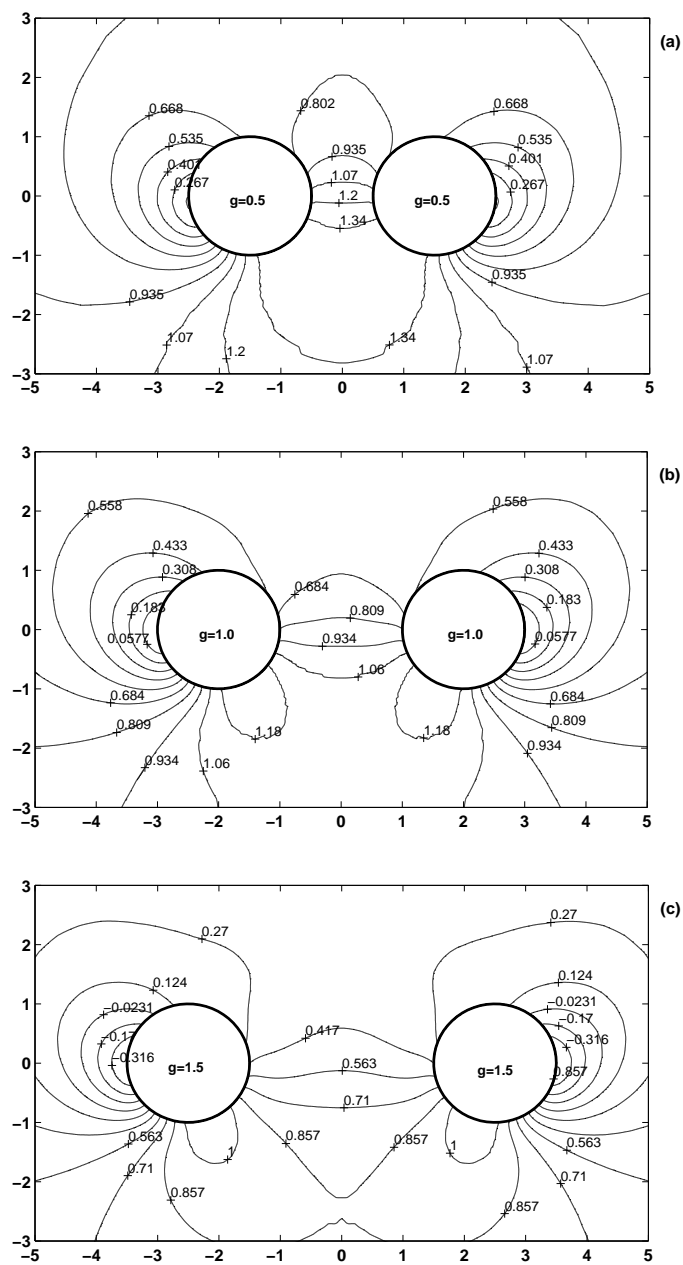


Figure 5.10 Pressure patterns of flow over two circular cylinders at $Re = 20$, $\alpha = 0.5$ and $g = 0.5; 1.0; 1.5$

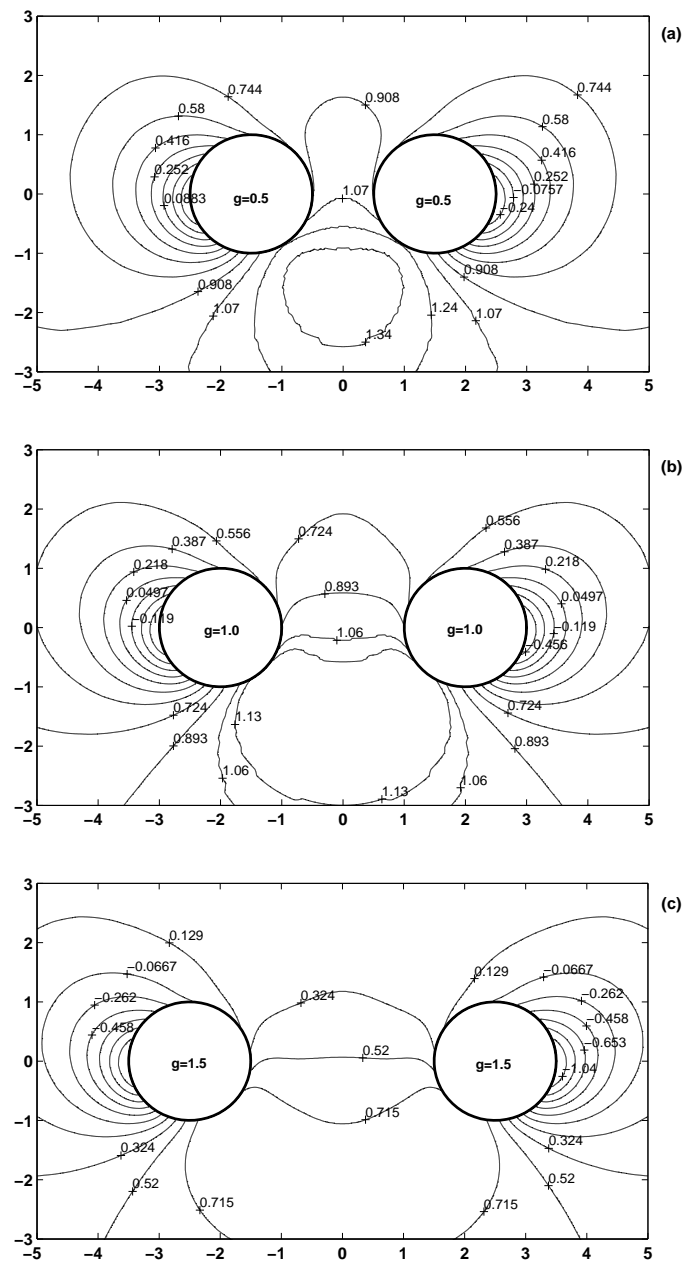


Figure 5.11 Pressure patterns of flow over two circular cylinders at $Re = 20$, $\alpha = 1.0$ and $g = 0.5; 1.0; 1.5$

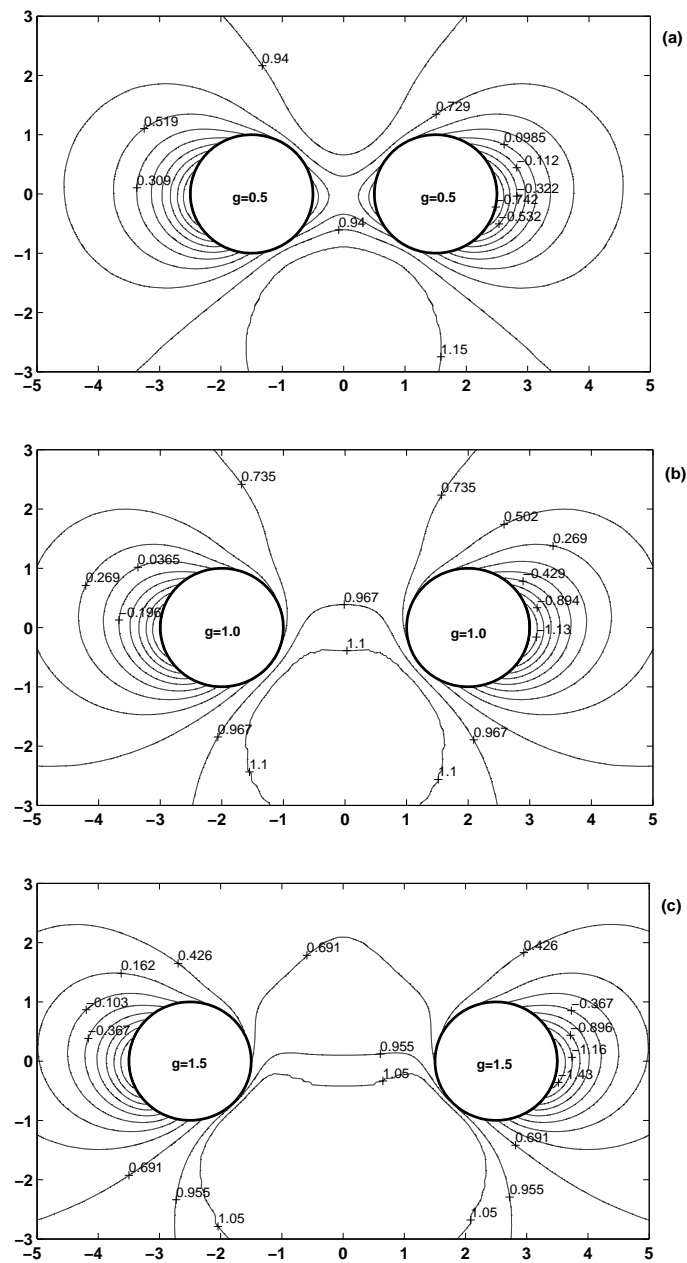


Figure 5.12 Pressure patterns of flow over two circular cylinders at $Re = 20$, $\alpha = 1.5$ and $g = 0.5; 1.0; 1.5$

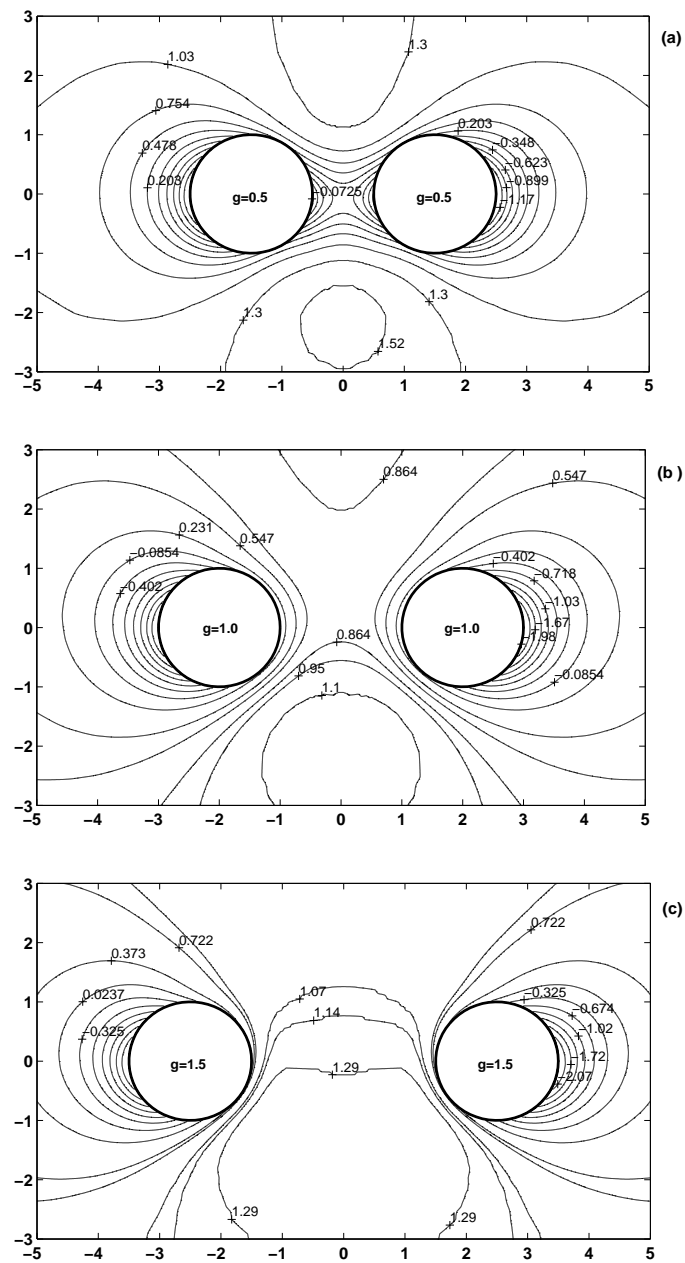


Figure 5.13 Pressure patterns of flow over two circular cylinders at $Re = 20$, $\alpha = 2.0$ and $g = 0.5; 1.0; 1.5$

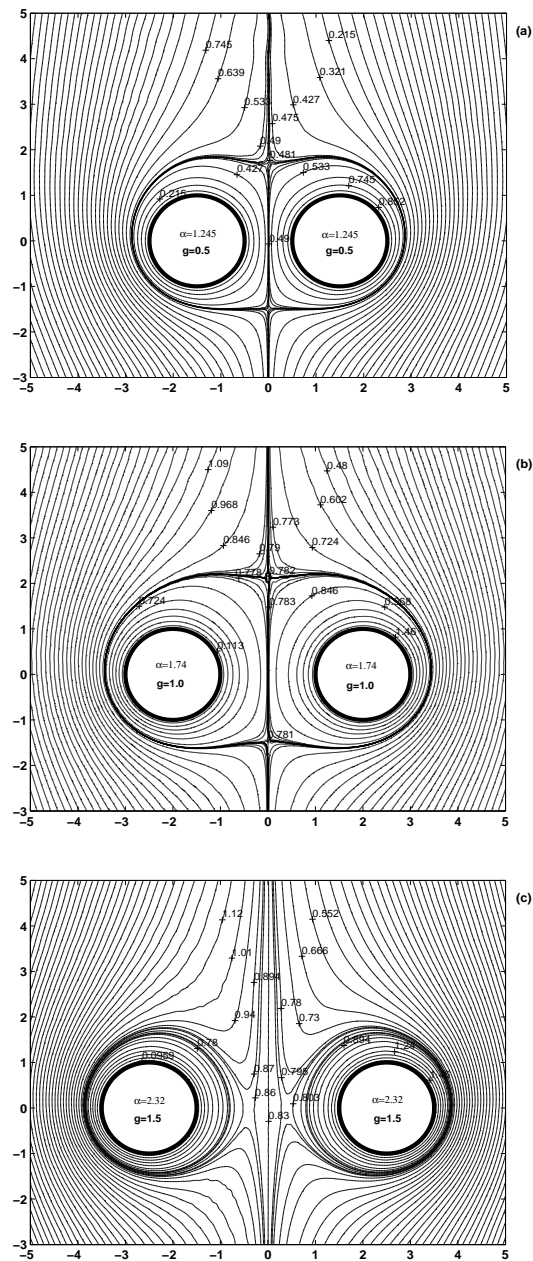


Figure 5.14 Streamline patterns of self-motion at $Re = 20$, $\alpha = \alpha_{crit}$ and $g = 0.5; 1.0; 1.5$

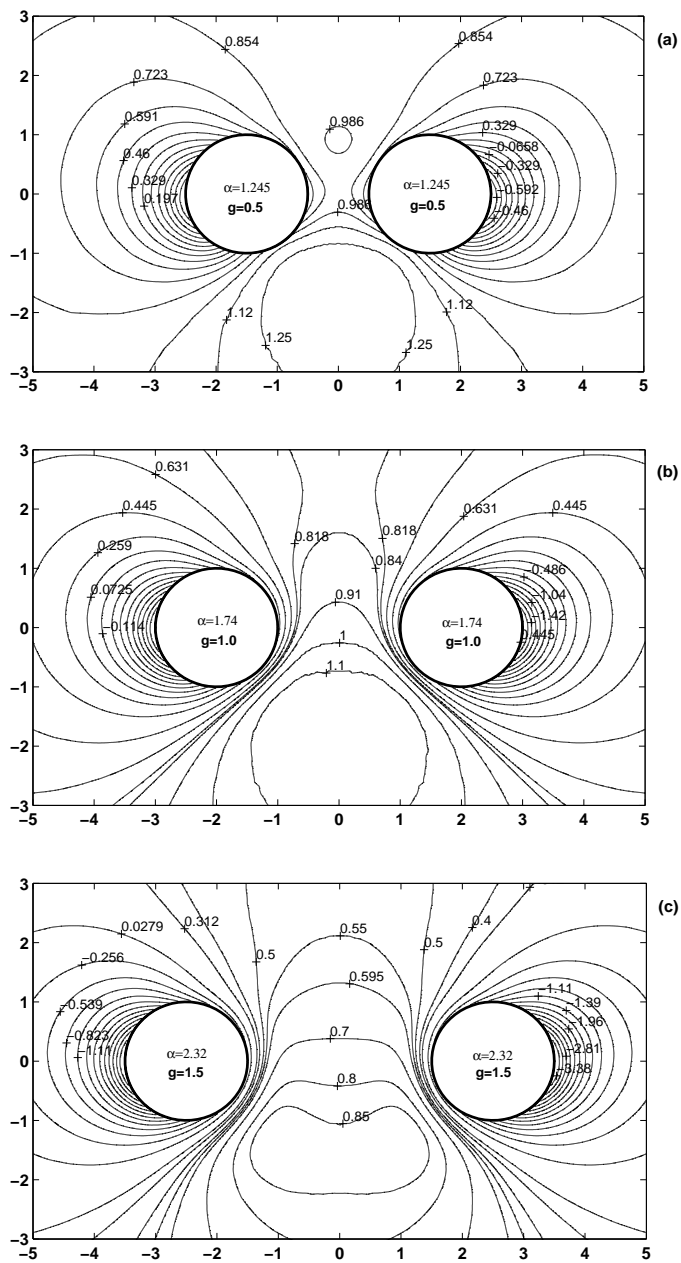


Figure 5.15 Pressure patterns of self-motion at $Re = 20$, $\alpha = \alpha_{crit}$ and $g = 0.5; 1.0; 1.5$

CHAPTER VI

CONCLUSIONS

In the present study, we have numerically investigated steady viscous incompressible fluid flow over two rotating circular cylinders in a side-by-side arrangement at moderate Reynolds numbers, $5 \leq Re \leq 40$, with gap spacing and the rate of rotation in the range of $0.5 \leq g \leq 14$ and $0 \leq \alpha \leq 2.5$, respectively. Special emphasis was put on rotation rates for which the two rotating cylinders perform self-propelled motion as a coupled body.

The following conclusions can be drawn:

1. Numerical algorithms and computer codes have been developed and validated.
2. For moderate values of Re in the steady flow regime (*e.g.*, $5 \leq Re \leq 40$), and for a gap spacing, $g = 1$, the flow around the two cylinders shows similar behavior to the flow around a single rotating cylinder: C_L increases with increasing α . The lift forces acting on the cylinders mostly result from the pressure force. As α increases, both the pressure drag and friction drag coefficients decrease, resulting in a net decrease of the total drag force. For $\alpha > \alpha_{crit}$, C_D becomes negative. (In the case of a single cylinder, as α increases, the pressure drag decreases, with increasing friction drag).
3. In the case $\alpha = \alpha_{crit}$ the self-propelled motion of two cylinders as a coupled body occurs. In the self-propelled regime ($Re = 10, 20$) there is a region which encloses both cylinders and which consists of two subregions of closed

streamlines. These subregions are connected along the axis of symmetry.

4. The critical rotation speed α_{crit} depends on the Reynolds number and gap spacing, for example, for gap spacing $g = 1$, $\alpha_{crit} \simeq 1.65, 1.74$ and 1.755 for $Re = 10, 20$ and 40 , respectively. For a fixed Reynolds number, the value of α_{crit} depends on the gap spacing, for example, if $Re = 20$ $\alpha_{crit} = 1.245, 1.74$ and 2.32 for $g = 0.5, 1.0$ and 1.5 respectively.
5. For $Re = 10, g = 1$ the self-propelled regime occurs for the drag coefficient $C_D = 0$ because $C_{D_p} = -C_{D_f} \approx 0.33$. For $Re = 20, g = 1$ the self-propelled regime corresponds to $C_D = 0$ due to $C_{D_p} \approx C_{D_f} \approx 0$. In the case of $Re = 40, g = 1$ the self-propelled regime corresponds to $C_{D_p} \approx -C_{D_f} = 0.141$.

The numerical investigations presented in this thesis suggest that it is possible to study flow past two cylinders of different radii which rotate with different angular velocities and to also study the case in which cylinders are in a tandem arrangement. Future work should include simulations for the cases of higher Reynolds number, $Re > 45$.

REFERENCES

REFERENCES

- Badr, T., Dennis, S.C.R., Young, P.J.S., (1989). Steady and unsteady flow past a rotating circular cylinder at low Reynolds numbers, **Computers & Fluids**, 17(4):579-609.
- Batchelor, G.K., (2000). **Introduction to Fluid Dynamics**, Cambridge University Press, Cambridge, UK, 615.
- Chorin, A.J., (1968). Numerical solution of the Navier-Stokes equations, **Mathematics of Computation**, 22(104):745-762.
- Chung, M-H., (2006). Cartesian cut cell approach for simulating incompressible flows with rigid bodies of arbitrary shape, **Computers & Fluids**, 35(6):607-623.
- Danielson, D.A, (1997). **Vectors and Tensors in Engineering and Physics**, 2nd ed. Perseus Books, Cambridge, MA, USA, 282
- Douglas, J., Rachford, H.H., (1956). On the numerical solution of heat conduction problem in two and three space variables, **Transactions of the American Mathematical Society**, 82(2):421-439.
- Douglas, J., Gunn, J.E., (1964). A general formulation of alternating direction methods, Part I. Parabolic and hyperbolic problems. **Numerische Mathematik**, 6:428-453.
- Elliot, L., Ingham, D.B. and Bashir, T.B.A.El, (1995). Stokes flow past two circular cylinders using a boundary element method, **Computers & Fluids**, 24(7):787-798.

- Finn, R., (1965). On the exterior stationary problem for the Navier-Stokes equations and associated perturbation problems, **Archive for Rational Mechanics and Analysis**, 19:363-406.
- Galdi, G.P., (1997). On the steady, translational self-propelled motion of a symmetric body in a Navier- Stokes fluid, **Quaderni di Matematica della II Universita di Napoli**, 1:97-169.
- Galdi, G.P., (1999). On the steady self-propelled motion of a body in a viscous incompressible fluid, **Archive for Rational Mechanics and Analysis**, 148:53-88.
- Ingham, D.B., (1983). Steady flow past a rotating cylinder, **Computer and Fluids**, 11(4):351-366.
- Ingham, D.B. and Tang, T., (1990). A numerical investigation into the steady flow past a rotating circular cylinder at low and intermediate Reynolds numbers, **Journal of Computational Physics**, 87:91-107.
- Izteleulov, M.I., (1985). Calculation of Momentumless Flow Past an Ellipsoid, **Problemy Dinamiki Vyazkoi Zidkosti, Novosibirsk, Russian**, 21-32.
- Jeffery, G.B., (1922). The Rotation of Two Circular Cylinders in a Viscous Fluid, **Proceedings of the Royal Society of London**, Series A; May 1, 1922; London, UK, Containing Papers of a Mathematical and Physical Character, 101(709):169-174.
- Kang, S., (2003). Characteristics of flow over two circular cylinders in a side-by-side arrangement at low Reynolds numbers, **Physics of Fluids**, 15(9):2486-2498.

- Khonichev, V.I. and Yakovlev, V.I., (1985). Ball moving into unbounded conducting liquid, caused by alternating magnetic dipole lying into the ball, **Zurnal Prikladnoi Mexaniki Technicheskoi Physiki**,1:22-28.
- Lugovtsov, A.A. and Lugovtsov, B.A., (1971). The example of viscous incompressible flow past a body with a moving boundary, **Dinamika Sploshnoi Sredy**, Novosibirsk, Russia, 8.
- Milne-Thomson, L.M., (1952). **Theoretical Aerodynamics**, Van Nostrandt Co., NY, USA.
- Moshkin, N.P., (1991). On certain example of numerical modeling of a steady flow past a self-propelled sphere, **Russian Journal of Theoretical and Applied Mechanics**, 1(2):111-125.
- Moshkin, N.P., Pukhnachov, V.V., Sennitskii, V.L., (1989). Numerical and analytical investigations of a stationary flow past a self-propelled body, **Fifth International Conference on Numerical Ship Hydrodynamics**, Part 1; 25-28 September 1989; Hiroshima, Japan, p.238-248.
- Nakanishi, M. and Kida, K., (1999). Unsteady low Reynolds number flow past two rotating circular cylinders by a vortex method, **Proceeding of the 3rd ASME/JSME Joint Fluid Engineering Conference**; July 18-23, 1999; San Frantsisco, California, USA.
- Pukhnacev, V.V., (1989). Asymptotics of a velocity field at considerable distances from a self-propelled body, **Journal of Applied Mechanics and Technical Physics**, 30:52-60.
- Pukhnacev, V.V., (1990). **The Problem of Momentumless Flow for the**

- Navier-Stokes Equations**, In: Lecture Notes in Mathematics, 1431, Springer-Verlag, New York, p. 87-94.
- Relf, E.F., (1913). **Reports and Memoranda**, Adv. Comm. for Aeronautics, (ACA), London, UK, 102.
- Samarskij and Aleksandr A., (1989). **Numerical Methods for Grid Equations**, Birkhauser Verlag Basel, 101.
- Sennitskii, V.L., (1973). Viscous incompressible fluid flow past rotating cylinders, **Dinamika Sploshnoi Sredy**, Novosibirsk, Russia, 14:71-88.
- Sennitskii, V.L., (1975a). Rotating cylinders in a viscous liquid, Part 1., **Dinamika Sploshnoi Sredy**, Novosibirsk, Russia, 21:70-83.
- Sennitskii, V.L., (1975b). Rotating cylinders in a viscous liquid, Part 2., **Dinamika Sploshnoi sredy**, Novosibirsk, Russia, 23: 169-181.
- Sennitskii, V.L., (1978). Liquid flow around a self-propelled body, **Journal of Applied Mechanics and Technical Physics**, 3:15-27.
- Sennitskii, V.L., (1980). On the propelling of a pair of rotating circular cylinders in a liquid, **Dinamika Sploshnoi Sredy**, Novosibirsk, Russia, 47:145-153.
- Sennitskii, V.L., (1981). On the drag force acting on a pair of circular cylinders streamed by water, **Dinamika Sploshnoi Sredy**, Novosibirsk, Russia, 52:178-182.
- Sennitskii, V.L., (1984). An example of axisymmetric fluid flow around a self-propelled body, **Journal of Applied Mechanics and Technical Physics**, 4:31-36.

- Sennitskii, V.L., (1990). Self-propulsion of a body in a fluid, **Journal of Applied Mechanics and Technical Physics**, 31:266- 272.
- Shatrov, V.I and Yakovlev V.I., (1985). Hydrodynamic drag of a ball containing a conduction-type source of electromagnetic fields, **Journal of Applied Mechanics and Technical Physics**, 26:19-24.
- Silvestre, A.L., (2002a). On the self-propelled motion of a rigid body in a viscous liquid and on the attainability of steady symmetric self-propelled motions, **Journal of Mathematical Fluid Mechanics**, 4:285-326.
- Silvestre, A.L., (2002b). On the slow motion of a self-propelled rigid body in a viscous incompressible fluid, **Journal of Mathematical Analysis and Applications**, 274:203-227.
- Smith, S.H., (1991). **The rotation of two circular cylinders in a viscous fluid**, *Mathematika*, 38(63).
- Stojkovic, D., Breuer, M., and Durst, F., (2002). Effect of high rotation rates on the laminar flow around a circular cylinder, **Physics of Fluids**, 4(9):3160-3178.
- Sumner, D., Wong, S.S.T., Price, S.J. and Paidoussis, M.P., (1999). Fluid behavior of side-by-side circular cylinders in steady cross-flow, **Journal of Fluids and Structures**, 13:309-338.
- Taneda, S. (1956). Experimental Investigation of the Wakes Behind Cylinders and Plates at Low Reynolds Numbers, **Journal of the Physical Society of Japan**, 11:302-307.
- Temam, R., (1991). Remark on the pressure boundary condition for the projection method, **Theory Compute Fluid Dynamics** 3:181-184.

- Tolstykh, A.I., (1992). **Algorithms for Calculating Incompressible Flows with Compact Third Order Approximations**, In : Modern problems in computational aerodynamics. CRC Press. Boca Raton, pp. 103-129.
- Tritton, D.J., (1959). Experiments on the flow past a circular cylinder at low Reynolds number, **Journal of Fluid Mechanics**, 6:547.
- Watson, E.J., (1995). **The rotation of two circular cylinders in a viscous fluid**, *Mathematika*, 42(1):105.
- Yanenko, N.N., (1971). **Method of Fractional Steps**, Gordon and Breach, NY, USA.
- Zdravkovich, M.M., (1997). **Flow Around Circular cylinders**, Fundamentals, Oxford University Press, NY, 1.

APPENDICES

APPENDIX A

TRANSFORMATION OF GOVERNING EQUATIONS TO CYLINDRICAL BIPOLAR COORDINATES

In this Appendix, we review the main definitions of tensor-vector calculus in curvilinear coordinate systems. We then derive a detailed transformation of the Navier-Stokes equations into the cylindrical bipolar coordinate system.

A.1 Definitions of Main Tensor Operations in the Curvilinear Coordinate System

Let $\Omega \subset \mathbb{R}^3(\vec{x})$ be an open set. A one-to-one and reciprocal continuously differentiable mapping from Ω to a subset of \mathbb{R}^3 is called a coordinate system. This mapping is defined by the formula

$$\vec{x} \rightarrow K(\vec{x}) = (K^1(\vec{x}), K^2(\vec{x}), K^3(\vec{x})).$$

The values of the functions $K^i(\vec{x})$ are called the coordinates (curvilinear coordinates) of the point \vec{x} . Let a point $\vec{x} \in \Omega$ be fixed. At this point there are vectors

$$\vec{e}_i = \frac{\partial \vec{x}}{\partial K^i}, \quad \vec{e}^i = \frac{\partial K^i}{\partial \vec{x}} = \nabla K^i, \quad (i = 1, 2, 3), \quad (\text{A.1})$$

which form a basis, \vec{e}_i , and cobasis, \vec{e}^i , in \mathbb{R}^3 . These bases are called a coordinate basis and cobasis of the coordinate system K at the point \vec{x} . A vector \vec{v} can be

decomposed along either basis or cobasis vectors

$$\vec{v} = v_i \vec{e}^i = v^i \vec{e}_i.$$

The components, v_i , are called covariant components of the vector, \vec{v} , and the v^i , are called contravariant components of the vector, \vec{v} .

A coordinate system is called orthogonal (at a point or on a set) if its basis is orthogonal (at the point or on the set).

$$\vec{e}_i \cdot \vec{e}_j = 0, \quad \vec{e}^i \cdot \vec{e}^j = 0, \quad (i \neq j).$$

The fundamental tensor and its inverse are defined by

$$g_{ij} = \vec{e}_i \cdot \vec{e}_j, \quad g^{ij} = \vec{e}^i \cdot \vec{e}^j. \quad (\text{A.2})$$

Coordinates of the fundamental tensor g with respect to an orthogonal coordinate system are

$$(g_{ij}) = \begin{bmatrix} g_{11} & 0 & 0 \\ 0 & g_{22} & 0 \\ 0 & 0 & g_{33} \end{bmatrix}, \quad (g^{ij}) = \begin{bmatrix} g^{11} & 0 & 0 \\ 0 & g^{22} & 0 \\ 0 & 0 & g^{33} \end{bmatrix},$$

where

$$g_{ii} = |\vec{e}_i|^2 = \left| \frac{\partial \vec{x}}{\partial K^i} \right|^2, \quad g^{ii} = |\vec{e}^i|^2 = |\nabla K^i|^2, \quad i = 1, 2, 3; \quad |g| = [\vec{e}_1 \cdot (\vec{e}_2 \times \vec{e}_3)]^2.$$

The derivatives of the basis and cobasis vectors with respect to curvilinear coordinates can be represented in terms of the basis $\{\vec{e}_i\}$ and cobasis $\{\vec{e}^i\}$, respectively

$$\frac{\partial \vec{e}_i}{\partial K^j} = \Gamma_{ij}^s \vec{e}_s, \quad \frac{\partial \vec{e}^i}{\partial K^j} = -\Gamma_{js}^i \vec{e}^s,$$

where the coefficients Γ_{ij}^s are called Christoffel symbols of second order. The Christoffel symbols are related to the derivatives of the fundamental tensor

$$\Gamma_{ij}^l = \frac{1}{2} \left(\frac{\partial g_{is}}{\partial K^j} + \frac{\partial g_{js}}{\partial K^i} - \frac{\partial g_{ij}}{\partial K^s} \right) g^{ls}. \quad (\text{A.3})$$

Covariant derivatives are expressed in terms of partial derivatives with respect to corresponding coordinates, Christoffel symbols and components of a tensor. The simplest are covariant derivatives of a scalar field, F , which coincide with the usual partial derivatives

$$F_{,i} = \frac{\partial F}{\partial K^i}.$$

The covariant derivatives of the covariant and contravariant components of a second order tensor Φ are

$$\Phi_{ij,l} = \frac{\partial \Phi_{ij}}{\partial K^l} - \Gamma_{li}^s \Phi_{sj} - \Gamma_{lj}^s \Phi_{is}, \quad \Phi^{ij}_{,l} = \frac{\partial \Phi^{ij}}{\partial K^l} + \Gamma_{ls}^i \Phi^{sj} + \Gamma_{ls}^j \Phi^{is}, \quad (\text{A.4})$$

Similarly, the covariant derivatives of the mixed components are

$$\Phi_{i,l}^j = \frac{\partial \Phi_{i,l}^j}{\partial K^l} - \Gamma_{li}^s \Phi_{s,l}^j + \Gamma_{ls}^j \Phi_{i,l}^s, \quad \Phi^j_{,i,l} = \frac{\partial \Phi^j_{,i}}{\partial K^l} - \Gamma_{li}^s \Phi^j_{,s} + \Gamma_{ls}^j \Phi^s_{,i}, \quad (\text{A.5})$$

In the above equations and everywhere below, a comma with an index in a subscript denotes covariant differentiation. A derivative of the vector field, \vec{v} , is the second order tensor which is denoted by the symbol, $\left(\frac{\partial \vec{v}}{\partial \vec{x}}\right)$. Covariant and mixed coordinates of the $\left(\frac{\partial \vec{v}}{\partial \vec{x}}\right)$ are

$$\left(\frac{\partial \vec{v}}{\partial \vec{x}}\right)_{ij} = \frac{\partial v_i}{\partial K^j} - \Gamma_{ij}^s v_s = v_{i,j}; \quad \left(\frac{\partial \vec{v}}{\partial \vec{x}}\right)^{ij} = \frac{\partial v^i}{\partial K^j} + \Gamma_{js}^i v_s = v^i_{,j}. \quad (\text{A.6})$$

The divergence of a vector field, \vec{v} , is a scalar. Divergence can be expressed in terms of the covariant derivatives of the contravariant components of vector field, \vec{v} ,

$$\text{div } \vec{v} = v^i_{,i} = \frac{\partial v^i}{\partial K^i} + \Gamma_{is}^i v^s = \frac{\partial v^i}{\partial K^i} + \frac{v^i}{\sqrt{|g|}} \frac{\partial \sqrt{|g|}}{\partial K^i} = \frac{1}{\sqrt{|g|}} \frac{\partial}{\partial K^i} \left(\sqrt{|g|} v^i \right). \quad (\text{A.7})$$

The vector

$$\nabla F = \frac{\partial F}{\partial \vec{x}} = \frac{\partial F}{\partial K^i} \vec{e}^i,$$

is called a gradient of the scalar function F . Covariant components of the gradient vector are

$$(\nabla F)_i = F_{,i} = \frac{\partial F}{\partial K^i}. \quad (\text{A.8})$$

The scalar

$$\Delta F = \text{div} (\nabla F) = ((\nabla F)^i)_{,i} = (g^{is}(\nabla F)_s)_{,i} = g^{is} \left[\frac{\partial^2 F}{\partial K^s \partial K^i} - \Gamma_{is}^\alpha \frac{\partial F}{\partial K^\alpha} \right],$$

is called the Laplace operator of the scalar function F . We can rewrite this formula in the following form

$$\Delta F = \frac{1}{\sqrt{|g|}} \frac{\partial}{\partial K^i} \left(\sqrt{|g|} g^{is} \frac{\partial F}{\partial K^s} \right). \quad (\text{A.9})$$

A *curl* of a vector field, \vec{v} , is a vector field. In a right-handed basis, $\varepsilon_{123} = \vec{e}_1 \cdot (\vec{e}_2 \times \vec{e}_3) = \sqrt{|g|}$, the contravariant components of *curl* \vec{v} are

$$\begin{aligned} (\text{curl } \vec{v})^1 &= \frac{1}{\sqrt{|g|}} \left(\frac{\partial v_3}{\partial K^2} - \frac{\partial v_2}{\partial K^3} \right), & (\text{curl } \vec{v})^2 &= \frac{1}{\sqrt{|g|}} \left(\frac{\partial v_1}{\partial K^3} - \frac{\partial v_3}{\partial K^1} \right), \\ (\text{curl } \vec{v})^3 &= \frac{1}{\sqrt{|g|}} \left(\frac{\partial v_2}{\partial K^1} - \frac{\partial v_1}{\partial K^2} \right). \end{aligned} \quad (\text{A.10})$$

The divergence of a tensor field is a vector. The s -th contravariant component of this vector is

$$(\text{div } P)^s = P^{sj}{}_{,j} = \text{div} (\overline{P}^s) + \Gamma_{j\alpha}^s P^{j\alpha}, \quad (\text{A.11})$$

where $\overline{P}^s = (P^{s1}, P^{s2}, P^{s3})$ is s -th row of a matrix which represents second order tensor P and $\text{div} (\overline{P}^s) = \frac{\partial P^{sj}}{\partial K^j} + \Gamma_{j\alpha}^j P^{s\alpha}$.

The Laplace operator of a vector field is a vector field and the contravariant components of this vector are

$$\begin{aligned} (\Delta \vec{v})^l &= g^{ij} \left(\left(\frac{\partial \vec{v}}{\partial \vec{x}} \right)_{,j}^l \right)_{,i} = g^{ij} (v^l_{,i})_{,j} = g^{ij} \left[\frac{\partial v^l_{,i}}{\partial K^j} - \Gamma_{ji}^s v^l_{,s} + \Gamma_{js}^l v^s_{,i} \right] \\ &= g^{ij} \left[\left(\frac{\partial^2 v^l}{\partial K^j \partial K^i} + \frac{\partial \Gamma_{is}^l}{\partial K^j} v^s + \Gamma_{is}^l \frac{\partial v^s}{\partial K^j} \right) - \Gamma_{ji}^s \left(\frac{\partial v^l}{\partial K^s} + \Gamma_{s\alpha}^l v^\alpha \right) + \Gamma_{js}^l \left(\frac{\partial v^s}{\partial K^i} + \Gamma_{i\alpha}^s v^\alpha \right) \right]. \end{aligned}$$

After regrouping one has

$$(\Delta \vec{v})^l = (\Delta v^l) + 2g^{ij} \Gamma_{is}^l \frac{\partial v^s}{\partial K^j} + g^{ij} \left(\frac{\partial \Gamma_{is}^l}{\partial K^j} - \Gamma_{ji}^\alpha \Gamma_{\alpha s}^l + \Gamma_{j\alpha}^l \Gamma_{i\alpha}^s \right) v^s, \quad (\text{A.12})$$

where $(\Delta v^l) = g^{ij} \left[\frac{\partial^2 v^l}{\partial K^j \partial K^i} - \Gamma_{ji}^s \frac{\partial v^l}{\partial K^s} \right]$ is the Laplace operator of scalar function v^l .

The covariant and contravariant components of the acceleration of a vector field, \vec{v} , are

$$\left(\frac{d\vec{v}}{dt}\right)_i = \frac{\partial v_i}{\partial t} + v^s v_{i,s} = \frac{\partial v_i}{\partial t} + v^s \frac{\partial v_i}{\partial K^s} - \Gamma_{is}^j v^s v_j, \quad (\text{A.13})$$

$$\left(\frac{d\vec{v}}{dt}\right)^i = \frac{\partial v^i}{\partial t} + v^s v^{i,s} = \frac{\partial v^i}{\partial t} + v^s \frac{\partial v^i}{\partial K^s} + \Gamma_{js}^i v^j v^s.$$

If vectors of coordinate bases and cobases are not normed, then components of tensors have different numerical values in different bases even if directions of basis vectors coincides. Numerical values of tensor components divided by the length of corresponding basis or cobasis vectors, which define these components are called physical components of the tensor. For example, if $a_i = \vec{a} \vec{e}_i$ are covariant coordinates of a vector \vec{a} , then the physical components are

$$\tilde{a}_i = \frac{a_i}{|\vec{e}_i|}, \quad (\text{A.14})$$

the covariant components of a tensor, L_{ij} , related with the physical components as

$$\tilde{L}_{ij} = \frac{L_{ij}}{(|\vec{e}_i| |\vec{e}_j|)}. \quad (\text{A.15})$$

A.2 The Cylindrical Bipolar Coordinate System

Let \vec{e}_i be a fixed right-handed orthonormal Cartesian basis in \mathbb{R}^3 . A vector $\vec{x} \in \mathbb{R}^3$ has components $\vec{x} = (x, y, z); (x = \vec{x} \vec{e}_1, y = \vec{x} \vec{e}_2, z = \vec{x} \vec{e}_3)$ in this basis. Curvilinear coordinates are a transformation from \mathbb{R}^3 to a subset of \mathbb{R}^3

$$K(\vec{x}) = (K^1(x, y, z), K^2(x, y, z), K^3(x, y, z)).$$

For the cylindrical bipolar coordinates we use the notation

$$\xi = K^1(x, y, z), \eta = K^2(x, y, z), z = K^3(x, y, z).$$

The cylindrical bipolar coordinate system can be defined by the inverse transformation K^{-1}

$$x = \frac{a \sinh \eta}{\cosh \eta - \cos \xi}, \quad y = \frac{a \sin \xi}{\cosh \eta - \cos \xi}, \quad z = z, \quad (\text{A.16})$$

where $\xi \in [0, 2\pi)$, $\eta \in (-\infty, \infty)$, $z \in (-\infty, \infty)$, a is a characteristic length in the cylindrical bipolar coordinate system which is positive. The following identities show that curves of constant ξ and η are circles in xy -space

$$\begin{aligned} x^2 + (y - a \cot \xi)^2 &= a^2 \csc^2 \xi, \\ (x - a \coth \eta)^2 + y^2 &= a^2 \operatorname{csch}^2 \eta. \end{aligned} \quad (\text{A.17})$$

The coordinate surface $\eta = \text{const}$ corresponds to a family of nonintersecting cylinders whose centers lie along the x -axis. The value $\eta = 0$ is a cylinder of infinite radius and equivalent to the entire plane $x = 0$. Figure A.1 shows the sketch of the cylindrical bipolar coordinate system. If two cylinders are chosen to be $\eta = \eta_1$ (with $\eta_1 > 0$) and $\eta = \eta_2$ (with $\eta_2 < 0$) then cylinders radii r_1 and r_2 as well as the distances of their centers from the origin d_1 and d_2 are given by

$$r_i = a \operatorname{csch} |\eta_i|, \quad d_i = a \coth |\eta_i|, \quad i = 1, 2. \quad (\text{A.18})$$

The center to center distance between the cylinders equals $d = d_1 + d_2$. If r_1, r_2 and d are given, one can find a , η_1 and η_2 from the relations (A.16) – (A.18) to be as follows

$$\eta_1 = \ln \left(\cosh \eta_1 + \sqrt{\cosh^2 \eta_1 - 1} \right) \quad (\text{A.19})$$

$$\eta_2 = \ln \left(\cosh \eta_2 - \sqrt{\cosh^2 \eta_2 - 1} \right) \quad (\text{A.20})$$

$$a = \sqrt{\frac{d^4 - 2d^2(r_1^2 + r_2^2) + (r_1^2 - r_2^2)^2}{4d^2}} \quad (\text{A.21})$$

Using the main definitions of vector-tensor operations given above, we now demonstrate the detailed transformation of the Navier-Stokes equations into cylindrical bipolar coordinates:

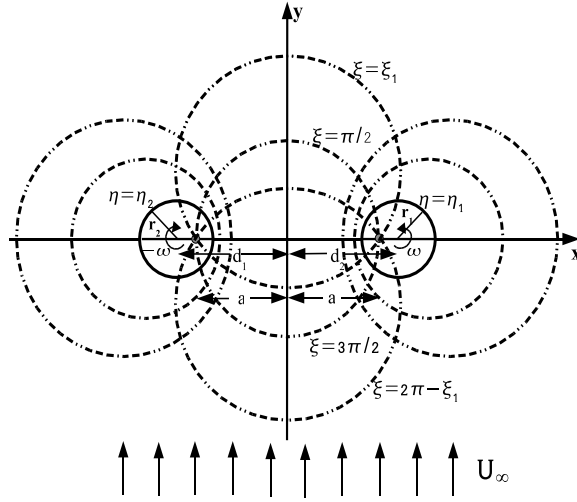


Figure A.1 Geometrical sketch of the cylindrical bipolar coordinates.

The bases and cobases of the cylindrical bipolar coordinate system are orthogonal and consist of the vectors

$$\begin{aligned}
 \vec{e}_1 &= \frac{\partial \vec{x}}{\partial K^1} = \left(\frac{\partial x}{\partial \xi}, \frac{\partial y}{\partial \xi}, \frac{\partial z}{\partial \xi} \right) = \frac{a}{(\cosh \eta - \cos \xi)^2} (-\sinh \eta \sin \xi, \cos \xi \cosh \eta - 1, 0), \\
 \vec{e}_2 &= \frac{\partial \vec{x}}{\partial K^2} = \left(\frac{\partial x}{\partial \eta}, \frac{\partial y}{\partial \eta}, \frac{\partial z}{\partial \eta} \right) = \frac{a}{(\cosh \eta - \cos \xi)^2} (1 - \cosh \eta \cos \xi, -\sin \xi \sinh \eta, 0), \\
 \vec{e}_3 &= \frac{\partial \vec{x}}{\partial K^3} = \left(\frac{\partial x}{\partial z}, \frac{\partial y}{\partial z}, \frac{\partial z}{\partial z} \right) = (0, 0, 1), \\
 \vec{e}^1 &= \left(\frac{\partial K^1}{\partial x}, \frac{\partial K^1}{\partial y}, \frac{\partial K^1}{\partial z} \right) = \frac{1}{a} (-\sinh \eta \sin \xi, \cos \xi \cosh \eta - 1, 0), \\
 \vec{e}^2 &= \left(\frac{\partial K^2}{\partial x}, \frac{\partial K^2}{\partial y}, \frac{\partial K^2}{\partial z} \right) = \frac{1}{a} (1 - \cosh \eta \cos \xi, -\sin \xi \sinh \eta, 0), \\
 \vec{e}^3 &= \left(\frac{\partial K^3}{\partial x}, \frac{\partial K^3}{\partial y}, \frac{\partial K^3}{\partial z} \right) = (0, 0, 1).
 \end{aligned} \tag{A.22}$$

$$\text{and } |\vec{e}_1| = |\vec{e}_2| = h = \frac{a}{\cosh \eta - \cos \xi}, \quad |\vec{e}^1| = |\vec{e}^2| = \frac{1}{h}, \quad |\vec{e}_3| = |\vec{e}^3| = 1.$$

The fundamental tensor can be written as follows

$$(g_{ij}) = \begin{bmatrix} h^2 & 0 & 0 \\ 0 & h^2 & 0 \\ 0 & 0 & 1 \end{bmatrix}, \quad (g^{ij}) = \begin{bmatrix} \frac{1}{h^2} & 0 & 0 \\ 0 & \frac{1}{h^2} & 0 \\ 0 & 0 & 1 \end{bmatrix}, \quad |g| = h^4. \tag{A.23}$$

The Christoffel symbols (A.3) for the cylindrical bipolar coordinate system are

$$\begin{aligned} \Gamma_{11}^1 &= \Gamma_{12}^2 = \Gamma_{21}^2 = -h \frac{\sin \xi}{a}, & \Gamma_{11}^2 &= h \frac{\sinh \eta}{a}, \\ \Gamma_{12}^1 &= \Gamma_{21}^1 = -h \frac{\sinh \eta}{a}, & \Gamma_{22}^1 &= h \frac{\sin \xi}{a}, & \Gamma_{22}^2 &= -h \frac{\sinh \eta}{a}, \end{aligned} \quad (\text{A.24})$$

with all other components being equal to zero.

Let (v_ξ, v_η, v_z) be the physical component of the velocity vector, \vec{v} , in the cylindrical bipolar coordinate system. Then the tensor components of \vec{v} are

$$(v^1, v^2, v^3) = \left(\frac{1}{h} v_\xi, \frac{1}{h} v_\eta, v_z \right), \quad (v_1, v_2, v_3) = (h v_\xi, h v_\eta, v_z). \quad (\text{A.25})$$

If the physical components of a tensor T are

$$(T) = \begin{pmatrix} T_{\xi\xi} & T_{\xi\eta} & T_{\xi z} \\ T_{\eta\xi} & T_{\eta\eta} & T_{\eta z} \\ T_{z\xi} & T_{z\eta} & T_{zz} \end{pmatrix}, \quad (\text{A.26})$$

then the contravariant and covariant components of the tensor T are

$$(T^{ij}) = \begin{pmatrix} \frac{1}{h^2} T_{\xi\xi} & \frac{1}{h^2} T_{\xi\eta} & \frac{1}{h} T_{\xi z} \\ \frac{1}{h^2} T_{\eta\xi} & \frac{1}{h^2} T_{\eta\eta} & \frac{1}{h} T_{\eta z} \\ \frac{1}{h} T_{z\xi} & \frac{1}{h} T_{z\eta} & T_{zz} \end{pmatrix}, \quad (T_{ij}) = \begin{pmatrix} h^2 T_{\xi\xi} & h^2 T_{\xi\eta} & h T_{\xi z} \\ h^2 T_{\eta\xi} & h^2 T_{\eta\eta} & h T_{\eta z} \\ h T_{z\xi} & h T_{z\eta} & T_{zz} \end{pmatrix}. \quad (\text{A.27})$$

The covariant and contravariant coordinates of the gradient of a scalar function p are

$$\begin{aligned} (\nabla p)_1 &= \frac{\partial p}{\partial \xi}, & (\nabla p)_2 &= \frac{\partial p}{\partial \eta}, & (\nabla p)_3 &= \frac{\partial p}{\partial z} \\ (\nabla p)^1 &= g^{11} (\nabla p)_1 = \frac{1}{h^2} \frac{\partial p}{\partial \xi}, & (\nabla p)^2 &= g^{22} (\nabla p)_2 = \frac{1}{h^2} \frac{\partial p}{\partial \eta}, \\ (\nabla p)^3 &= g^{33} (\nabla p)_3 = \frac{\partial p}{\partial z}. \end{aligned} \quad (\text{A.28})$$

A matrix of the covariant derivatives of a vector field can be written as follows

$$v^i_{,j} = \frac{\partial v^i}{\partial K^j} + \Gamma^i_{js} v^s.$$

Thus we have a matrix of covariant derivatives in terms of physical components of vector \vec{v}

$$(v^i{}_{,j}) = \begin{pmatrix} \frac{1}{h} \frac{\partial v_\xi}{\partial \xi} - \frac{\sinh \eta}{a} v_\eta & \frac{1}{h} \frac{\partial v_\xi}{\partial \eta} + \frac{\sin \xi}{a} v_\eta & \frac{1}{h} \frac{\partial v_\xi}{\partial z} \\ \frac{1}{h} \frac{\partial v_\eta}{\partial \xi} + \frac{\sinh \eta}{a} v_\xi & \frac{1}{h} \frac{\partial v_\eta}{\partial \eta} - \frac{\sin \xi}{a} v_\xi & \frac{1}{h} \frac{\partial v_\eta}{\partial z} \\ \frac{\partial v_z}{\partial \xi} & \frac{\partial v_z}{\partial \eta} & \frac{\partial v_z}{\partial z} \end{pmatrix}. \quad (\text{A.29})$$

The divergence of a vector field, \vec{v} , (A.7) can be expressed in terms of physical components of the vector \vec{v} as follows

$$\text{div} \vec{v} = \frac{1}{h^2} \left[\frac{\partial(hv_\xi)}{\partial \xi} + \frac{\partial(hv_\eta)}{\partial \eta} \right] + \frac{\partial v_z}{\partial z}. \quad (\text{A.30})$$

The i – th contravariant components of the convective derivative are defined by

$$[(\vec{v} \cdot \nabla) \vec{v}]^i = v^l v^i{}_{,l},$$

or in term of physical components as follows

$$\begin{aligned} [(\vec{v} \cdot \nabla) \vec{v}]^1 &= \frac{1}{h^2} \left[v_\xi \frac{\partial v_\xi}{\partial \xi} + v_\eta \frac{\partial v_\xi}{\partial \eta} \right] + \frac{1}{h} v_z \frac{\partial v_\xi}{\partial z} - \frac{1}{h} \left[\frac{\sinh \eta}{a} v_\xi v_\eta - \frac{\sin \xi}{a} (v_\eta)^2 \right], \\ [(\vec{v} \cdot \nabla) \vec{v}]^2 &= \frac{1}{h^2} \left[v_\xi \frac{\partial v_\eta}{\partial \xi} + v_\eta \frac{\partial v_\eta}{\partial \eta} \right] + \frac{1}{h} v_z \frac{\partial v_\eta}{\partial z} + \frac{1}{h} \left[\frac{\sinh \eta}{a} (v_\xi)^2 - \frac{\sin \xi}{a} v_\xi v_\eta \right], \\ [(\vec{v} \cdot \nabla) \vec{v}]^3 &= \frac{1}{h} \left[v_\xi \frac{\partial v_z}{\partial \xi} + v_\eta \frac{\partial v_z}{\partial \eta} \right] + v_z \frac{\partial v_z}{\partial z}. \end{aligned} \quad (\text{A.31})$$

The Laplace operator of a scalar function p , (see equation (A.9)) is

$$\Delta p = \frac{1}{h^2} \left[\frac{\partial^2 p}{\partial \xi^2} + \frac{\partial^2 p}{\partial \eta^2} \right] + \frac{\partial^2 p}{\partial z^2}. \quad (\text{A.32})$$

The contravariant components of the vorticity vector, $\text{curl} \vec{v} = \nabla \times \vec{v}$, (see equation (A.10)) are

$$\begin{aligned} \omega^1 &= \frac{1}{h^2} \frac{\partial v_z}{\partial \eta} - \frac{1}{h} \frac{\partial v_\eta}{\partial z}, & \omega^2 &= \frac{1}{h} \frac{\partial v_\xi}{\partial z} - \frac{1}{h^2} \frac{\partial v_z}{\partial \xi}, \\ \omega^3 &= \frac{1}{h} \left(\frac{\partial v_\eta}{\partial \xi} - \frac{\partial v_\xi}{\partial \eta} \right) - \frac{\sin \xi}{a} v_\eta + \frac{\sinh \eta}{a} v_\xi \end{aligned} \quad (\text{A.33})$$

The divergence of a tensor T (see equation (A.11)) is a vector with the contravariant components

$$\begin{aligned} (\operatorname{div} T)^1 &= \operatorname{div}(\bar{T}^1) + \frac{1}{h} \left(\frac{\sin \xi}{a} (T_{\eta\eta} - T_{\xi\xi}) - \frac{\sinh \eta}{a} (T_{\xi\eta} + T_{\eta\xi}) \right), \\ (\operatorname{div} T)^2 &= \operatorname{div}(\bar{T}^2) + \frac{1}{h} \left(\frac{\sinh \eta}{a} (T_{\xi\xi} - T_{\eta\eta}) - \frac{\sin \xi}{a} (T_{\xi\eta} + T_{\eta\xi}) \right), \end{aligned} \quad (\text{A.34})$$

$$(\operatorname{div} T)^3 = \operatorname{div}(\bar{T}^3),$$

where

$$\begin{aligned} \bar{T}^1 &= \left(\frac{1}{h^2} T_{\xi\xi}, \frac{1}{h^2} T_{\xi\eta}, \frac{1}{h} T_{\xi z} \right), & \bar{T}^2 &= \left(\frac{1}{h^2} T_{\eta\xi}, \frac{1}{h^2} T_{\eta\eta}, \frac{1}{h} T_{\eta z} \right), \\ \bar{T}^3 &= \left(\frac{1}{h} T_{z\xi}, \frac{1}{h} T_{z\eta}, \frac{1}{h} T_{zz} \right). \end{aligned}$$

The Laplace operator of a vector field, \vec{v} , (see equation (A.12)) is the vector with the contravariant components

$$\begin{aligned} (\Delta \vec{v})^1 &= \frac{1}{h^2} \left[\frac{1}{h} \left(\frac{\partial^2 v_\xi}{\partial \xi^2} + \frac{\partial^2 v_\xi}{\partial \eta^2} \right) - \frac{2}{a} \left(\sinh \eta \frac{\partial v_\eta}{\partial \xi} - \sin \xi \frac{\partial v_\eta}{\partial \eta} \right) \right] - \\ &\quad - \frac{1}{h^2} \left(\frac{\cosh \eta + \cos \xi}{a} \right) v_\xi + \frac{1}{h} \frac{\partial^2 v_\xi}{\partial z^2}, \\ (\Delta \vec{v})^2 &= \frac{1}{h^2} \left[\frac{1}{h} \left(\frac{\partial^2 v_\eta}{\partial \xi^2} + \frac{\partial^2 v_\eta}{\partial \eta^2} \right) + \frac{2}{a} \left(\sinh \eta \frac{\partial v_\xi}{\partial \xi} - \sin \xi \frac{\partial v_\xi}{\partial \eta} \right) \right] - \\ &\quad - \frac{1}{h^2} \left(\frac{\cosh \eta + \cos \xi}{a} \right) v_\eta + \frac{1}{h} \frac{\partial^2 v_\eta}{\partial z^2}, \end{aligned} \quad (\text{A.35})$$

$$(\Delta \vec{v})^3 = \frac{1}{h^2} \left[\frac{\partial^2 v_z}{\partial \xi^2} + \frac{\partial^2 v_z}{\partial \eta^2} \right] + \frac{\partial^2 v_z}{\partial z^2}.$$

The acceleration has the components

$$\begin{aligned} \left(\frac{d\vec{v}}{dt} \right)^1 &= \frac{1}{h} \left[D(v_\xi) + \frac{\sin \xi}{a} v_\eta v_\eta - \frac{\sinh \eta}{a} v_\xi v_\eta \right], \\ \left(\frac{d\vec{v}}{dt} \right)^2 &= \frac{1}{h} \left[D(v_\eta) - \frac{\sin \xi}{a} v_\eta v_\xi + \frac{\sinh \eta}{a} v_\xi v_\xi \right], \end{aligned} \quad (\text{A.36})$$

$$\left(\frac{d\vec{v}}{dt} \right)^3 = D(v_z),$$

where $D(f) = \frac{\partial f}{\partial t} + \frac{1}{h}v_\xi \frac{\partial f}{\partial \xi} + \frac{1}{h}v_\eta \frac{\partial f}{\partial \eta} + v_z \frac{\partial f}{\partial z}$.

With the use of above formulae, one can transform the Navier-Stokes equations into the cylindrical bipolar coordinates (ξ, η, z) and obtain

$$\begin{aligned} & \frac{\partial v_\xi}{\partial t} + \frac{1}{h} \left(v_\xi \frac{\partial v_\xi}{\partial \xi} + v_\eta \frac{\partial v_\xi}{\partial \eta} \right) + v_z \frac{\partial v_\xi}{\partial z} - \frac{1}{a} (\sinh \eta (v_\xi v_\eta) - \sin \xi (v_\eta)^2) \\ &= -\frac{1}{h} \frac{1}{\rho} \frac{\partial p}{\partial \xi} + \nu \frac{\partial^2 v_\xi}{\partial z^2} + \frac{\nu}{h} \left\{ \frac{1}{h} \left(\frac{\partial^2 v_\xi}{\partial \xi^2} + \frac{\partial^2 v_\xi}{\partial \eta^2} \right) \right. \\ & \left. - \frac{2}{a} \left(\sinh \eta \frac{\partial v_\eta}{\partial \xi} - \sin \xi \frac{\partial v_\eta}{\partial \eta} \right) - \left(\frac{\cosh \eta + \cos \xi}{a} \right) v_\xi \right\}, \end{aligned} \quad (\text{A.37})$$

$$\begin{aligned} & \frac{\partial v_\eta}{\partial t} + \frac{1}{h} \left(v_\xi \frac{\partial v_\eta}{\partial \xi} + v_\eta \frac{\partial v_\eta}{\partial \eta} \right) + v_z \frac{\partial v_\eta}{\partial z} + \frac{1}{a} (\sinh \eta (v_\xi)^2 - \sin \xi (v_\xi v_\eta)) \\ &= -\frac{1}{h} \frac{1}{\rho} \frac{\partial p}{\partial \eta} + \nu \frac{\partial^2 v_\eta}{\partial z^2} + \frac{\nu}{h} \left\{ \frac{1}{h} \left(\frac{\partial^2 v_\eta}{\partial \xi^2} + \frac{\partial^2 v_\eta}{\partial \eta^2} \right) \right. \\ & \left. + \frac{2}{a} \left(\sinh \eta \frac{\partial v_\xi}{\partial \xi} - \sin \xi \frac{\partial v_\xi}{\partial \eta} \right) - \left(\frac{\cosh \eta + \cos \xi}{a} \right) v_\eta \right\}, \end{aligned} \quad (\text{A.38})$$

$$\begin{aligned} & \frac{\partial v_z}{\partial t} + \frac{1}{h} \left(v_\xi \frac{\partial v_z}{\partial \xi} + v_\eta \frac{\partial v_z}{\partial \eta} \right) + v_z \frac{\partial v_z}{\partial z} \\ &= -\frac{1}{\rho} \frac{\partial p}{\partial z} + \nu \left\{ \frac{1}{h^2} \left(\frac{\partial^2 v_z}{\partial \xi^2} + \frac{\partial^2 v_z}{\partial \eta^2} \right) + \frac{\partial^2 v_z}{\partial z^2} \right\}, \end{aligned} \quad (\text{A.39})$$

$$\frac{1}{h^2} \left[\frac{\partial(hv_\xi)}{\partial \xi} + \frac{\partial(hv_\eta)}{\partial \eta} \right] + \frac{\partial v_z}{\partial z} = 0, \quad (\text{A.40})$$

where v_ξ , v_η , and v_z are the physical components of velocity vector $v = (v_\xi, v_\eta, v_z)$,

p is the pressure, $\nu = \frac{\mu}{\rho}$ is the coefficient of kinematic viscosity.

APPENDIX B

THE METHOD OF STABILIZING CORRECTIONS

In this research we use the iterative method of stabilizing corrections (Yanenko (1971)) for computing the finite difference equation (3.21) for pressure. The method of stabilizing corrections, which was introduced by Douglas and Rachford (1956) and formulated in its general form by Douglas and Gunn (1964), is a very general and effective method for the construction of schemes with fractional steps. We present here the general iterative scheme of stabilizing corrections for elliptic equations. In our explanation, we follow Yanenko (1970).

For the elliptic equation

$$Lu + f = \sum_{i,j=1}^m a_{ij} \frac{\partial^2 u}{\partial x_i \partial x_j} + f = 0. \quad (\text{B.1})$$

the parallel between the iterative schemes and integration schemes of the corresponding parabolic equation

$$\frac{\partial u}{\partial t} = \sum_{i,j=1}^m a_{ij} \frac{\partial^2 u}{\partial x_i \partial x_j} + f. \quad (\text{B.2})$$

is always valid, i.e., the solution of the unsteady problem (B.2) approaches the solution of the steady problem with the same boundary conditions, regardless of the choice of initial data. The scheme of stabilizing corrections is

$$\begin{aligned}
\frac{u^{n+1/m} - u^n}{\tau} &= \Lambda_{11}u^{n+1/m} + (\Omega - \Lambda_{11})u^n, \\
\frac{u^{n+2/m} - u^{n+1/m}}{\tau} &= \Lambda_{22}(u^{n+2/m} - u^n), \\
&\dots \\
\frac{u^{n+1} - u^{n+(m-1)/m}}{\tau} &= \Lambda_{mm}(u^{n+1} - u^n),
\end{aligned} \tag{B.3}$$

where $\Omega = \sum_{i,j=1}^n \Lambda_{ij}$. After eliminating fractional steps, the equivalent scheme in whole steps is

$$\begin{aligned}
\frac{u^{n+1} - u^n}{\tau} &= \Lambda u^{n+1} + (\Omega - \Lambda)u^n - \tau \sum_{i < j} \Lambda_{ii} \Lambda_{jj} (u^{n+1} - u^n) + \\
&\quad + \tau^2 \sum_{i < j < k} \Lambda_{ii} \Lambda_{jj} \Lambda_{kk} (u^{n+1} - u^n) + \dots \\
&\quad + (-1)^{m-1} \Lambda_{11} \dots \Lambda_{mm} \tau^{m-1} (u^{n+1} - u^n), \\
\Lambda &= \sum_{i=1}^m \Lambda_{ii}, \quad i, j, k = 1, \dots, m.
\end{aligned} \tag{B.4}$$

From (B.4) complete consistency follows at any m . Scheme (B.3) is strongly stable. The main idea of the scheme of stabilizing correction is to solve at each fractional step the system of algebraic equations only with tridiagonal matrix. Next we give a short description of the ‘‘sweep’’ method of solution of three-point equations and the cyclic elimination method for three-point equations. The three-point equations arise from three-point difference schemes designed to find periodic solutions of second-order ordinary differential equation and also when approximating the solutions of equations with partial derivatives in cylindrical bipolar coordinates.

B.1 The Elimination Method for Three-Point Equations (Samarskij (1989))

Suppose we must solve the following system of three-point equations

$$\begin{aligned} c_0 y_0 - b_0 y_1 &= f_0, & i = 0, \\ -a_i y_{i-1} + c_i y_i - b_i y_{i+1} &= f_i, & 1 \leq i \leq N-1, \\ -a_N y_{N-1} + c_N y_N &= f_N, & i = N, \end{aligned} \tag{B.5}$$

or, in vector form,

$$\mathbf{A}Y = F \tag{B.6}$$

where $Y = (y_0, y_1, \dots, y_N)^T$ is the vector of unknowns, $F = (f_0, f_1, \dots, f_N)^T$ is the right hand side vector, and A is the square $(N+1) \times (N+1)$ matrix with real or complex coefficients.

$$\mathbf{A} = \begin{pmatrix} c_0 & -b_0 & 0 & 0 & \cdots & 0 & 0 & 0 & 0 \\ -a_1 & c_1 & -b_1 & 0 & \cdots & 0 & 0 & 0 & 0 \\ 0 & -a_2 & c_2 & -b_2 & \cdots & 0 & 0 & 0 & 0 \\ \cdot & \cdot & \cdot & \cdot & \cdots & \cdot & \cdot & \cdot & \cdot \\ 0 & 0 & 0 & 0 & \cdots & -a_{N-2} & c_{N-2} & -b_{N-2} & 0 \\ 0 & 0 & 0 & 0 & \cdots & 0 & -a_{N-1} & c_{N-1} & -b_{N-1} \\ 0 & 0 & 0 & 0 & \cdots & 0 & 0 & -a_N & c_N \end{pmatrix}$$

Systems of the form (B.5) arise from a three-point approximation to a boundary-value problem for second-order ordinary differential equations with constant and variable coefficients, and also when realizing difference schemes for equations with partial derivatives.

Following the idea of Gauss' method, we carry out the elimination of the unknown in (B.5). We introduce the notation $\alpha_1 = b_0/c_0, \beta_1 = f_0/c_0$ and write

(B.5) in the following form

$$\begin{aligned}
y_0 - \alpha_1 y_1 &= \beta_1, & i = 0, \\
-a_i y_{i-1} + c_i y_i - b_i y_{i+1} &= f_i, & 1 \leq i \leq N-1, \\
-a_N y_{N-1} + c_N y_N &= f_N, & i = N,
\end{aligned} \tag{B.7}$$

Take the first two equations of the system (B.7)

$$y_0 - \alpha_1 y_1 = \beta_1, \quad -a_1 y_0 + c_1 y_1 - b_1 y_2 = f_1.$$

Multiply the first equation by a_1 and add it to the second equation. We get

$(c_1 - a_1 \alpha_1) y_1 - b_1 y_2 = f_1 + \alpha_1 \beta_1$ or, after dividing by $c_1 - a_1 \alpha_1$

$$y_1 - \alpha_2 y_2 = \beta_2, \quad \alpha_2 = \frac{b_1}{c_1 - \alpha_1 a_1}, \quad \beta_2 = \frac{f_1 + \alpha_1 \beta_1}{c_1 - \alpha_1 a_1}.$$

All the remaining equations of the system (B.7) do not contain y_0 , therefore this stage of the elimination process is completed. As a result we obtain a new “reduced” system

$$\begin{aligned}
y_1 - \alpha_2 y_2 &= \beta_2, & i = 1, \\
-a_i y_{i-1} + c_i y_i - b_i y_{i+1} &= f_i, & 2 \leq i \leq N-1, \\
-a_N y_{N-1} + c_N y_N &= f_N, & i = N,
\end{aligned} \tag{B.8}$$

which does not contain the unknown y_0 and which has a structure analogous to (B.7). When this system has been solved, the unknown y_0 is found from the formula $y_0 = \alpha_1 y_1 + \beta_1$. We can apply the above described elimination procedure to system (B.8). At the second stage, the unknown y_1 is eliminated, at the third y_2 , and so forth. At the end of the l^{th} stage we obtain a system for the unknowns y_l, y_{l+1}, \dots, y_N

$$\begin{aligned}
y_l - \alpha_{l+1} y_{l+1} &= \beta_{l+1}, & i = l, \\
-a_i y_{i-1} + c_i y_i - b_i y_{i+1} &= f_i, & l+1 \leq i \leq N-1, \\
-a_N y_{N-1} + c_N y_N &= f_N, & i = N,
\end{aligned} \tag{B.9}$$

and formulas for finding y_i for $i \leq l - 1$

$$y_i = \alpha_{i+1}y_{i+1} + \beta_{i+1}, \quad i = l - 1, l - 2, \dots, 0. \quad (\text{B.10})$$

The coefficients α_i and β_i , clearly, are found from the formulas

$$\alpha_{i+1} = \frac{b_i}{c_i - \alpha_i a_i}; \quad \beta_{i+1} = \frac{f_i + a_i \beta_i}{c_i - \alpha_i a_i}; \quad i = 1, 2, \dots,; \quad \alpha_1 = \frac{b_0}{c_0}, \quad \beta_1 = \frac{f_0}{c_0}.$$

Substituting $l = N - 1$ in (B.9), we obtain a system for y_N and y_{N-1}

$$y_{N-1} - \alpha_N y_N = \beta_N, \quad -a_N y_{N-1} + c_N y_N = f_N \quad (\text{B.11})$$

from which we find $y_N = \beta_{N+1}$, $y_{N-1} = \alpha_N y_N + \beta_N$.

Combining these equations with (B.10) ($l = N - 1$), we obtain the final formulas for finding the unknowns

$$\begin{aligned} y_i &= \alpha_{i+1}y_{i+1} + \beta_{i+1}, & i = N - 1, N - 2, \dots, 0, \\ y_N &= \beta_N + 1, \end{aligned} \quad (\text{B.12})$$

where α_i and β_i are found from the recurrence formulas

$$\begin{aligned} \alpha_{i+1} &= \frac{b_i}{c_i - a_i \alpha_i}, & i = 1, 2, \dots, N - 1, & \quad \alpha_i = \frac{b_0}{c_0}, \\ \beta_{i+1} &= \frac{f_i + a_i \beta_i}{c_i - a_i \alpha_i}, & i = 1, 2, \dots, N, & \quad \beta_i = \frac{f_0}{c_0}. \end{aligned} \quad (\text{B.13})$$

Thus, the formulas (B.12) and (B.13) describe Gauss' method which, when applied to the system (B.5), is given a special name - the *elimination method*. The coefficients α_i and β_i are called the *elimination coefficients*, formulas (B.13) describe the *forward elimination path*, and (B.12) the *backward path*. Since the values y_i are found sequentially in reverse order, the formulas (B.12) and (B.13) are sometimes called the *right-elimination formulas*.

An elementary count of the arithmetic operations in (B.12) and (B.13) shows that realizing the elimination method using these formulas requires $3N$ multiplications, $2N + 1$ divisions and $3N$ additions and subtractions. If there is no

difference between arithmetic operations, the total number of operations required for the elimination method is $Q = 8N + 1$. Of this total, $3N - 2$ operations are used for computing α_i , and $5N + 3$ operations for computing β_i and y_i .

Notice that the coefficients α_i do not depend on the right-hand side of the system (B.5), but are determined solely by the coefficients a_i, b_i, c_i of the difference equations. Therefore, if we must solve a series of problems (B.5) with different right-hand sides, but with the same matrix \mathbf{A} , then the elimination coefficients α_i are only computed for the first problem of the series. Thus solving the first problem in the series costs $Q = 8N + 1$ operations, but solving each of the remaining problems only costs $5N + 3$ operations.

In conclusion we indicate the order of the computations for the formulas of the elimination method. Beginning with α_1 and β_1 , we calculate and store α_i and β_i using (B.13). Then the solutions y_i are found using (B.12).

B.2 The Cyclic Elimination Method (Samarskij (1989))

Let us consider the following system

$$-a_i y_{i-1} + c_i y_i - b_i y_{i+1} = f_i, i = 0, \pm 1, \pm 2, \dots, \quad (\text{B.14})$$

the coefficients and right-hand side of which are periodic with period N :

$$a_i = a_{i+N}, b_i = b_{i+N}, c_i = c_{i+N}, f_i = f_{i+N}. \quad (\text{B.15})$$

Systems of the type (B.14) and (B.15) arise, for example, from three-point difference schemes designed to find periodic solutions of second-order ordinary differential equations, and also when approximating the solutions of equations with partial derivatives in Cylindrical bipolar coordinate,

A solution of system (B.14) satisfying the conditions (B.15) will, if it exists,

also be periodic with period N , i.e.,

$$y_i = y_{i+N}. \quad (B.16)$$

Therefore it is sufficient to find the solution at, for example, $i = 0, 1, \dots, N - 1$.

In this case, the problem (B.14) – (B.16) can be written as:

$$\begin{aligned} -a_0 y_{N-1} + c_0 y_0 - b_0 y_1 &= f_0, & i = 0 \\ -a_i y_{i-1} + c_i y_i - b_i y_{i+1} &= f_i, & 1 \leq i \leq N - 1, \end{aligned} \quad (B.17)$$

$$y_N = y_0. \quad (B.18)$$

We appended the condition (B.18) to the system (B.17) so that the equations for $i = N - 1$ would not include y_N , it having been replaced by y_0 . This allows us to retain a unique form for the equations (B.17) for $i = 1, 2, \dots, N - 1$.

If we introduce the vector of unknowns $Y = (y_0, y_1, \dots, y_{N-1})^T$ and the right-hand side $F = (f_0, f_1, \dots, f_{N-1})^T$, then (B.17) and (B.18) can be written in the vector form $\mathbf{A}Y = F$ where

$$\mathbf{A} = \begin{pmatrix} c_0 & -b_0 & 0 & 0 & \cdots & 0 & 0 & -a_0 \\ -a_1 & c_1 & -b_1 & 0 & \cdots & 0 & 0 & 0 \\ 0 & -a_2 & c_2 & -b_2 & \cdots & 0 & 0 & 0 \\ \cdot & \cdot & \cdot & \cdot & \cdots & \cdot & \cdot & \cdot \\ 0 & 0 & 0 & 0 & \cdots & c_{N-3} & -b_{N-3} & 0 \\ 0 & 0 & 0 & 0 & \cdots & -a_{N-2} & c_{N-2} & -b_{N-2} \\ -b_{N-1} & 0 & 0 & 0 & \cdots & 0 & -a_{N-1} & c_{N-1} \end{pmatrix}$$

is the matrix of the system (B.17) and (B.18). The presence of non-zero coefficients a_0 and b_{N-1} in (B.17) does not allow us to solve this system using the elimination method described in the previous section. To find the solution of the system (B.17) and (B.18) we construct a variant of the elimination method called *the cyclic elimination method*

The solution of the problem (B.17) and (B.18) will be found in the form of a linear combination of the grid functions u_i and v_i

$$y_i = u_i + y_0 v_i, \quad 0 \leq i \leq N, \quad (\text{B.19})$$

where u_i is the solution of the non-homogeneous three-point boundary-value problem

$$\begin{aligned} -a_i u_{i-1} + c_i u_i - b_i u_{i+1} &= f_i, & 1 \leq i \leq N-1, \\ u_0 &= 0, \quad u_N = 0 \end{aligned} \quad (\text{B.20})$$

with homogeneous boundary conditions, and v_i is the solution of the homogeneous three-point boundary-value problem

$$\begin{aligned} -a_i v_{i-1} + c_i v_i - b_i v_{i+1} &= f_i, & 1 \leq i \leq N-1, \\ v_0 &= 1, \quad v_N = 1 \end{aligned} \quad (\text{B.21})$$

with non-homogeneous boundary conditions.

We now find under what conditions y_i from (B.19) is the desired solution. Multiplying (B.21) by y_0 , adding it to (B.20), and taking into account (B.19), we find that the equations in (B.17) can be satisfied for $i = 1, 2, \dots, N-1$. From the boundary conditions for u_i and v_i it follows that (B.18) will be satisfied. Thus, if y_i satisfied the remaining unused equation at $i = 0$ in (B.17), the problem would be solved. Substituting (B.19) in this equation, we obtain

$$-a_0 u_{N-1} - a_0 y_0 v_{N-1} + c_0 y_0 - b_0 u_1 - b_0 y_0 v_1 = f_0. \quad (\text{B.22})$$

Thus, if we choose y_0 from the formula

$$y_0 = \frac{f_0 - a_0 u_{N-1} + b_0 u_1}{c_0 - a_0 v_{N-1} - b_0 v_1}, \quad (\text{B.23})$$

then (B.22) will be satisfied, and consequently the solution of the problem (B.17), (B.18) can be found from (B.19).

We are left with solving (B.20) and (B.21). They are particular cases of the three-point systems of equations solved in the previous section using the elimination method. For (B.20) and (B.21), the elimination formulas have the following form:

$$\begin{aligned} u_i &= \alpha_{i+1}u_{i+1} + \beta_{i+1}, & i &= N-1, N-2, \dots, 1, & u_N &= 0, \\ v_i &= \alpha_{i+1}v_{i+1} + \gamma_{i+1}, & i &= N-1, N-2, \dots, 1, & v_N &= 1, \end{aligned} \quad (\text{B.24})$$

where the elimination coefficients α_i, β_i and γ_i are found from the following formulas

$$\alpha_{i+1} = \frac{b_i}{c_i - a_i\alpha_i}, \quad i = 1, 2, \dots, N, \quad \alpha_1 = 0, \quad (\text{B.25})$$

$$\beta_{i+1} = \frac{f_i + a_i\beta_i}{c_i - a_i\alpha_i}, \quad i = 1, 2, \dots, N, \quad \beta_1 = 0, \quad (\text{B.26})$$

$$\gamma_{i+1} = \frac{a_i\gamma_i}{c_i - a_i\alpha_i}, \quad i = 1, 2, \dots, N, \quad \gamma_1 = 1, \quad (\text{B.27})$$

Let us transform (B.23). From (B.24) we obtain $u_{N-1} = \alpha_N u_N + \beta_N = \beta_N, v_{N-1} = \gamma_N + \alpha_N$. We substitute these expressions in (B.23) and take into account (B.15), (B.25) – (B.27) :

$$y_0 = \frac{f_N + a_N\beta_N + \beta_N u_1}{c_N - a_N\alpha_N - a_N\gamma_N - b_N v_1} = \frac{\beta_{N+1} + \alpha_{N+1}u_1}{1 - \gamma_{N+1} - \alpha_{N+1}v_1}.$$

We have constructed an algorithm for solving problem (B.17) and (B.18) called the method of cyclic elimination:

$$\begin{aligned} \alpha_2 &= b_1/c_1, & \beta_2 &= f_1/c_1, & \gamma_2 &= a_1/c_1, \\ \alpha_{i+1} &= \frac{b_i}{c_i - a_i\alpha_i}, & \beta_{i+1} &= \frac{f_i + a_i\beta_i}{c_i - a_i\alpha_i}, & \gamma_{i+1} &= \frac{a_i\gamma_i}{c_i - a_i\alpha_i}, \quad i = 2, 3, \dots, N; \\ u_{N-1} &= \beta_N, & v_{N-1} &= \gamma_N + \alpha_N, \\ u_i &= \alpha_{i+1}u_{i+1} + \beta_{i+1}, & v_i &= \alpha_{i+1}v_{i+1} + \gamma_{i+1}, & i &= N-2, N-3, \dots, 1; \\ y_0 &= \frac{\beta_{N+1} + \alpha_{N+1}u_1}{1 - \gamma_{N+1} - \alpha_{N+1}v_1}, & y_i &= u_i + y_0v_i, & i &= 1, 2, \dots, N-1. \end{aligned} \quad (\text{B.28})$$

An elementary computation indicates that the algorithm requires $6(N-1)$ multiplications, $5N-3$ additions and subtractions, and $3N+1$ divisions. If no dis-

inction is made among arithmetic operations, the total number is $Q = 14N - 8$.

CURRICULUM VITAE

NAME: Surattana Sungnul.

SEX: Female.

NATIONALITY: Thai.

DATE OF BIRTH: February 1, 1974.

MARITAL STATUS: Married.

EDUCATIONAL BACKGROUND:

- B.Sc. 2nd Class Honors in Applied Mathematics, King Mongkut's Institute of Technology North Bangkok, Bangkok, Thailand, 1995.
- M.Sc. in Applied Mathematics, Mahidol University, Bangkok, Thailand, 2000.

WORK EXPERIENCE:

- Lecturer in Mathematics Department, King Mongkut's Institute of Technology North Bangkok, Bangkok, Thailand since 1997.
- Visitor, Department of Mathematics and Statistics, Curtin University of Technology, Perth, WA, Australia, February 2004 - May 2004.

PUBLICATIONS:

- S. Sungnul, "On the representation of the Navier-Stokes equations in cylindrical bipolar coordinate system", The 9th Annual National Symposium on Computational Science and Engineering, 2004, Mahidol University.
- S. Sungnul, N.P. Moshkin, "Numerical simulation of flow over two rotating self-moving circular cylinders", The International Workshop on Computational Science and Its Education, 2005, Capital Normal University, Beijing, China.
- N.P. Moshkin, S. Sungnul, "Numerical Simulation of flow over two rotating circular cylinders", The 31st Congress on Science and technology of Thailand, 2005,

Suranaree University of Technology, Nakornratchasima, Thailand.

- N.P. Moshkin, S. Sungnul, “Numerical simulation of flow past two rotating circular cylinders”, The 10th Annual National Symposium on Computational Science and Engineering, 2005, Chiangmai University, Chiangmai, Thailand.

- S. Sungnul, N.P. Moshkin, “Numerical simulation of steady viscous flow past two rotating circular cylinders”, Suranaree Journal of Science and Technology, 2006, Suranaree University, Nakornratchasima, Thailand.

SCHOLARSHIPS:

- The Ministry of University affairs of Thailand (MUA), 2001-2003.